Engineering Properties, Micro- and Nano-Structure of Bentonite-Sand Barrier Materials in Aggressive Environments of Deep Geological Repository for Nuclear Wastes

Submitted by

Asmaa Shehata

In partial fulfillment of the requirements for the degree of

Master of Science

In

Civil Engineering

_____

Prof. M. Fall (Thesis supervisor)

Prof. C. Detellier (Thesis co-supervisor)

Contents

List of Figures

List of Tables

List of Symbols

a: cross-sectional area of the reservoir that contained the influent liquid, m^2

A: Cross-sectional area of specimen, m^2

Cm: Solution concentration or salinity

DW: Distilled water

h1: Hydraulic head at the beginning of the testing, m

h2: Hydraulic head at the end of the testing, m

K: Coefficient of permeability, m/s

L: Length of specimen, m

Md: Soil dry mass

Msalt: Mass of salt

Msol: Solution mass

Mw: Mass of water

t: Interval of time over which the flow has occurred, sec

t1: Time at start of permeation trial, date: hr: min: sec

t2: Time at end of permeation trial, date: hr: min: sec

TDS: Total mass of salt dissolved in the solution

W: Bulk water content

Wl: Liquid content

ρl: Solution density

ρd: Soil dry density

Acknowledgement

In the name of Allah, The Most Gracious and The Most Merciful.

First of all, I would like to thank Allah the Almighty and the Greatest of all for giving me the opportunity, determination and strength to successfully prepare, carry out and finish this master thesis.

This thesis appears in its current form due to the help, support and guidance of several people that I would like to thank. I would like to thank and express my deep and sincere gratitude to my supervisor, Dr. Mamadou Fall, for his continuous support, guidance and encouragement. I would also like to express my gratitude to my co-supervisor, Dr. Christian Detellier, for his valuable guidance and suggestions.

I owe everything to my family who has encouraged and helped me at every stage of my personal and academic life, and longed to see this achievement come true. I would to thank my mom for her endless support and motivation. I would like to thank my sincere and generous husband, Dr. Abdel Felfel, and my lovely daughters, Maryam Felfel, Halla Felfel, Janna Felfel and Rahman Felfel. I really appreciate their help and support all the time. I would also like to express my gratitude to my brothers, Mr. Ali Shehata and Mr. Mustafa Shehata.

I would like to thank my colleagues and friends for discussions, suggestions and criticism. Drs. Hana Adem, Omemah Glaih and Zaid Aldhafeer, Mr. Jean Claude Celestin, and Dr. Afshin Khoshand.

Abstract

Canada produces about one-third of the global supply of medical radioisotopes. The nuclear power reactors in Ontario, Quebec and New Brunswick have generated about 17 percent of the electricity in the country every year (NWMO, 2010; Noorden; 2013). Since the 1960s, more than 2 million used (or spent) fuel bundles (high-level radioactivity) and 75,000 m³ of low- and intermediate-level radioactive waste have been produced, which is increasing by 2000 to 3000 m³ every year after reducing the processed volume (Jensen et al., 2009).

More than 30 countries around the world, including Canada, have proposed construction of very deep geological repositories (DGRs) to store this nuclear waste for design periods 1,000,000 years. DGR concepts under development in Canada (the DGR is likely to be constructed in Ontario) are based on a multi-barrier system (NWMO, 2012). A crucial component of the multi-barrier system is the engineered barrier system (EBS), which includes a buffer, backfill, and tunnel sealing materials to physically, chemically, hydraulically and biologically isolate the nuclear waste. Bentonite-based material has been chosen for this critical use because of its high swelling capacity, low hydraulic conductivity, and for its good ability to retain radionuclides in the case of failed canisters.

However, the presence of bentonite-based material in DGRs, surrounded by an aggressive environment of underground saline water, nuclear waste heat decay, and corrosion products under confining stress, may lead to mineralogical changes. Consequently, the physical and physiochemical properties of bentonite-based materials may change, which could influence the performance of bentonite in an EBS as well as the overall safety of DGRs.

The objective of this research is to investigate the impact of the underground water salinity, heat generated by nuclear waste, and corrosion products of nuclear waste containers in Ontario on the engineering and micro-/nano-structural properties of bentonite-sand engineered barrier materials. Free-swelling, swelling pressure and hydraulic conductivity tests have been performed on bentonite-sand mixtures subjected to various chemical (groundwater chemistry; corrosion water with iron as a corrosion

product) and thermal (heat generated) conditions. Several techniques of micro- and nano-structural analyses, such as x-ray diffraction (XRD), X-Ray microanalysis (DES), surface area and pore size distribution analyses (BET, BJH) and differential gravimetric (TGA and DTG) analyses have also been conducted on the bentonite-sand materials. Valuable results have been obtained for better understanding the durability and performance of the bentonite-sand barrier for the DGR which may be located in Ontario. The obtained results have shown that the groundwater chemistry and corrosion products of the nuclear containers significantly deteriorate the swelling and permeability properties of the tested bentonite-sand barrier materials, while temperature has little or no effect.

Chapter 1- Introduction

1.1 Background and problem statement

Nowadays, nuclear technology has many applications in the medical, industrial, transportation and agricultural fields. Nuclear power produces about 11 percent of the electricity in the world, without releasing any greenhouse gases. However, this type of energy produces millions of spent fuel bundles and tons of radioactive waste every year. These nuclear wastes have the possibility of harming people as well as causing many environmental problems for hundreds or even thousands of years.

More than 30 countries, including Canada, have proposed the building of deep geological repositories (DGRs) that are 300 to 1000 m in depth for the disposal of these nuclear wastes in order to protect humans and their environment. DGR concepts under development in Canada are based on a multi-barrier system. A crucial component of the multi-barrier system is the engineered barrier system (EBS), which includes a buffer, backfill, and tunnel sealing materials to physically, chemically, hydraulically and biologically isolate nuclear waste. Bentonite-based material (bentonite-sand) has been chosen as a critical component of the EBS because of its excellent swelling capacity, low hydraulic conductivity, and good ability to retain radionuclides in the case of failed canisters.

However, the presence of bentonite-sand in DGRs, surrounded by an aggressive environment of high salinity with high underground temperature and under confining stress may cause mineralogical changes in bentonite-based materials and impact their physical and physiochemical properties. This would affect the bentonite performance in an EBS as well as the overall safety of the DGR. Thus, there is crucial need to understand the effect of the aforementioned aggressive environmental factors on the properties of bentonite-sand materials.

1.2 Objectives and scope

The overall objective of this research work is to characterize the engineering properties and micro-/nano-structure of MX-80 bentonite-sand based materials under different thermal conditions, and the underground water salinity and corrosion product conditions in Ontario, in order to acquire knowledge about the effectiveness and durability of bentonite-sand materials as a component of an EBS in a DGR in Ontario, this experimental study aims to:

- investigate the impact of high temperatures (T) on the engineering properties of bentonite-sand barrier materials;
- assess the effect of the underground water salinity (C) found in Ontario on the swelling capacity and permeability of bentonite-sand mixture;
- assess the coupled impact of water salinity and temperature on bentonite-sand based materials;
- understand the effect of iron (Fe) powder as a corrosion product of steel containers on the swelling capacity and mineralogical composition of bentonite-sand barrier materials;
- assess the combined effect of water salinity (C) and Fe on the engineering properties and mineralogical composition of bentonite-sand materials; and
- present a clear understanding of the triple effect of C, T and Fe on bentonite-sand durability and performance under aggressive conditions.

1.3 Research approach and methods

Three laboratory testing programs have been conducted to investigate the engineering and micro-/nano-structural properties of bentonite-sand mixtures (MX-80 bentonite-sand, mixing weight ratio of 30% and 70%, respectively) under different conditions, such as with variation in the T, C and Fe (Figure 1.1). Valuable results have been obtained with regards to the durability and performance of a bentonite-sand barrier for a DGR located in Ontario.

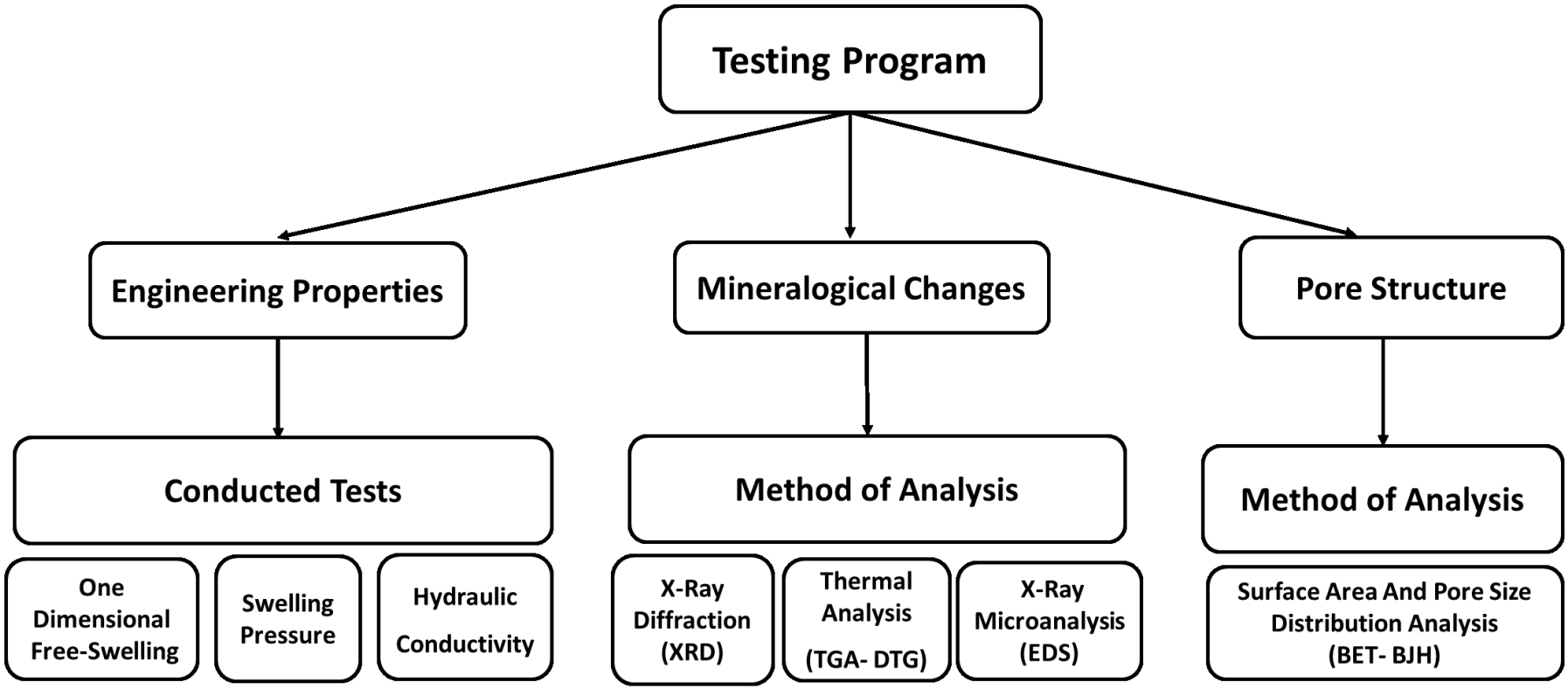

Figure 1.1 Testing Program flow chart

The first program investigates the engineering properties of the treated samples, including with the use of:

- one-dimensional free swell tests,
- swelling pressure tests, and
- hydraulic conductivity tests.

The second testing program is to assess the mineralogical changes by using:

- x-ray diffraction (XRD) analysis,
- thermo- and differential gravimetric analyses (TGA-DTG), and
- x-ray microanalysis (DES)

The third testing program is to evaluate the pore structure including the surface area analysis and to analyze the pore size distribution by using:

- the Brunauer, Emmett and Teller (BET) theory, and
- the Barrett-Joyner-Halenda (BJH) method, respectively.

1.4 Organization of the thesis

This thesis is organized in the form of five chapters.

- **Chapter 1** is the introduction, which provides some of the background information and the problem statement, thesis objectives, and the description of the thesis organization and testing program;
- **Chapter 2** provides the theoretical and technical background on bentonite based materials, DGR design, and properties of backfill and tunnel seals;
- **Chapter 3** presents Technical Paper I, which deals with the investigation of the impact of groundwater chemistry and temperature on the engineering, microstructural and nano-structural properties of bentonite-sand barriers,
- **Chapter 4** includes Technical Paper II which presents the experimental program and the results of the study of the effect of corrosion products on swelling

characteristics, and microstructural and nano-structural properties of bentonite-sand barriers in DGRs, and

- **Chapter 5** provides the conclusions of the present study and recommendations for future work.

1.5 References

Canadian Nuclear Safety Commission (CNSC) (2014) Nuclear Power Plants website nuclearsafety.gc.ca/eng/licenseesapplicants/powerplants/index.cfm

Jensen, M, Lam T., Luhowy D., McLay J., Semec B. and Frizzell R. (2009) Ontario Power Generation's Proposed L&ILW Deep Geologic Repository: An Overview of Geoscientific Studies. Nuclear Waste Management Organization, GeoHalifax2009/GéoHalifax2009

Jensen, M., Lam, T., Luhowy, D., McLay, J., Semec, B. and Frizzell, R. (2009) Ontario Power Generation's Proposed L&ILW Deep Geologic Repository: An Overview of Geoscientific Studies. Nuclear Waste Management Organization, GeoHalifax2009/GéoHalifax2009

Noorden, R. V. (2013) The medical testing crisis. Macmillan Publishers Limited 2 0 4 - Nature- Vol -5 0 4- 1 2 December news feature©.

NWMO (2010) Moving Forward Together: Process for Selecting a Site for Canada's Deep Geological Repository for Used Nuclear Fuel, Nuclear Waste Management Organization, May.

NWMO (2011) Regional hydrogeochemistry – Southern Ontario. Nuclear Waste Management Organization, NWMO DGR-TR-2011-12.

NWMO (2012) Newsletter, Nuclear Waste Management Organization, volume 10, issue 3 June.

Chapter 2- Theoretical and Technical Background

2.1 Introduction

The use of DGRs for the safe disposal of nuclear waste, such as high level nuclear waste (HLW) and spent fuel (SF), is one of the most discussed research topics in more than 30 countries, including Canada, the USA, Japan and France. These countries use nuclear technologies and produce millions of spent fuel bundles, and millions of tons of HLW and low and intermediate level radioactive wastes (L & ILW) every year (Pusch, 1982; Cho et al., 1998; Karnland et al., 2006; Quintessa, 2011). Numerous studies have been conducted to identify safe and durable designs and concepts for DGRs, and examine factors such as location and host rock specifications, EBS, and nuclear waste container materials.

Bentonite has been selected as an engineered barrier material in deep geological disposal repositories for nuclear waste in more than 30 countries in the world (Pusch, 1982; Cho et al., 1998; Karnland et al., 2006; Quintessa, 2011). The presence of bentonite in DGRs, surrounded by high salinized underground water, high temperature and confining stress conditions, may affect the mineralogical stability and performance of bentonite buffer-based material (Villar and Lloret, 2004; Karnland et al., 2007; Herbert et al., 2008; Cho et al., 2011).

In this chapter, a literature review on the physical and physiochemical properties of bentonite as well as the main factors that may affect the performance of a bentonite-based barrier in DGRs for radioactive waste will be presented. The concepts and design criteria for DGRs and the Canadian nuclear waste program will also be reviewed. A description of the Canadian DGR design concept and the expected aggressive conditions, such as heat and underground water salinity, is presented. This literature review will help to provide a better understanding of the experimental studies performed and the results obtained in this research.

2.2 Deep geological repository for nuclear waste

DGRs are permanent depositories that safely store radioactive waste for the long term at depths of 300 to 1000 m underground (NWMO, 2010; 2012). The main task of DGRs is to isolate nuclear waste inside a multi-barrier system to prevent radionuclide contamination (RWM, 2003), as illustrated in Figure 2.1. This multi-barrier system consists of a natural geological barrier (the host rock) and an EBS to provide a safe and secure place for nuclear waste for thousands of years in order to protect humans and their environment (RWM, 2003; NWMO, 2010).

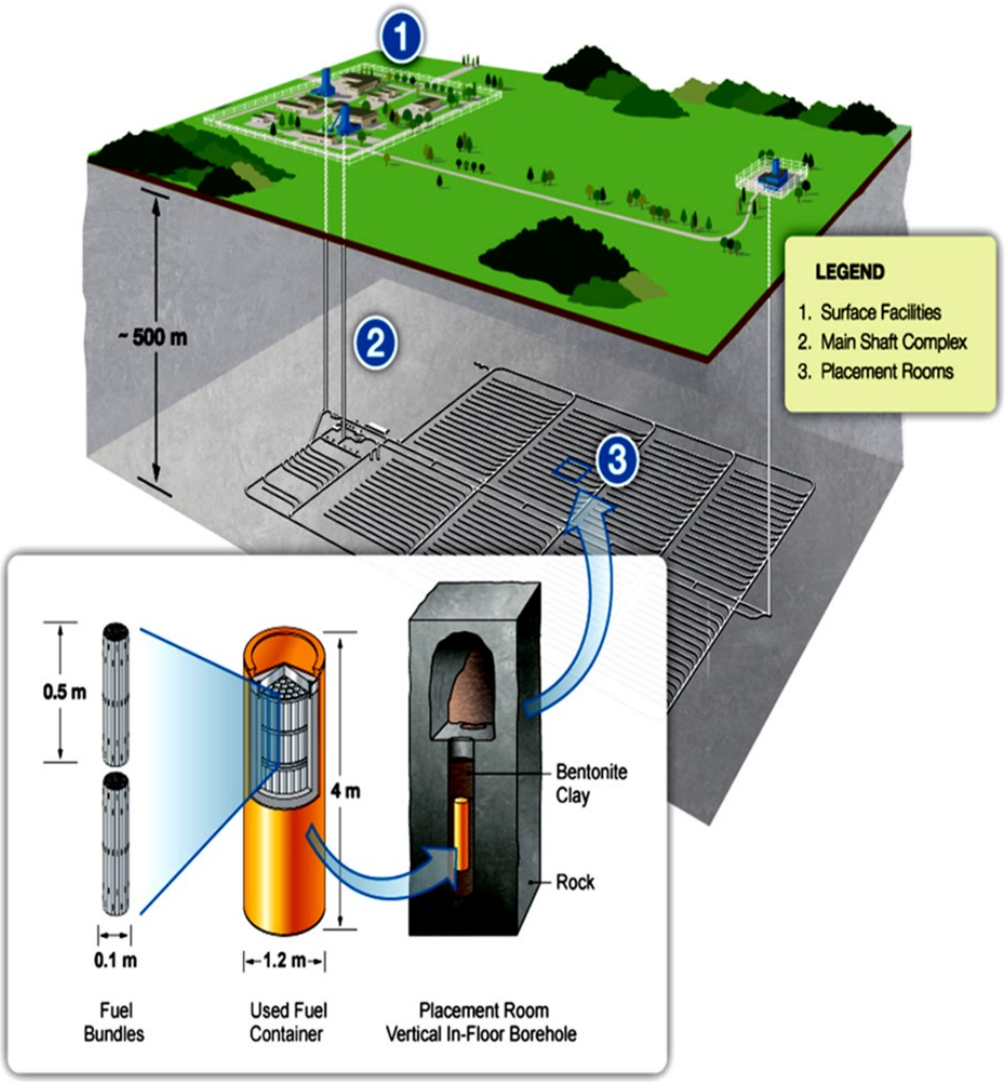

Figure 2.1 Deep geological repository design in crystalline rock (Villagran, 2012).

2.2.1 Types of nuclear wastes

I. **Low-level waste**

Low-level waste (LLW) is a common type of nuclear waste and about 90% by volume of all the accumulated nuclear waste in the world. It contains less than 1% radioactive waste (WNA, 2014). Low-level nuclear waste basically includes all items contaminated with radioactive materials, such as those found in medical supplies, protective cleaning tools, cooling water from nuclear reactors, and equipment used in uranium mining; for example: medical tubes, swabs, injection needles, syringes, shoe covers and clothing, wiping rags, mops, filters, and reactor water treatment residues (RWM, 2003; NWMO, 2010; NWA, 2014).

II. Intermediate-level waste

Intermediate-level waste (ILW) is about 7% by volume of the worldwide nuclear waste and it contains about 4% of the high radioactive waste (WNA, 2014). ILW refers to all contaminated materials from used reactor core components and comprises resins, chemical sludge, and cooling water filters. It requires special care, such as shielding protection, for handling and storage (NWMO, 2011; WNA, 2014).

III. High-level nuclear waste

HLW includes spent fuel bundles generated by nuclear fuel cycles and the isolation of fissile radionuclides from irradiated materials associated with nuclear weapon production (IAEA, 2007; WNA, 2014). They make up less than 1% in volume of the total nuclear waste worldwide; however, they comprise more than 95% of the total radioactivity of radioactive waste (WNA, 2014).

2.2.2 Multi-barrier systems

Multi-barrier systems include natural barriers, such as the host rock, and the EBS or human-made engineered materials.

2.2.2.1 Natural barrier systems

Natural geological barrier systems made of sedimentary or crystalline rock formation play a very important role in the selection of a DGR location. The properties of the host rock and underground water are among the major factors that control the site specifications. The host rock should have very low permeability to reduce underground water movement. Long-term stability and high strength are needed to sustain a stable geological environment for the safe and long-term storage of nuclear waste (Quintessa, 2011; NWMO, 2012).

2.2.2.2 Engineered barrier systems (EBS)

EBS include the waste form, waste canisters, buffer materials, backfill, and tunnel seals (RWM, 2003) as illustrated in Figure 2.1.

I. Waste form

The waste form is the first barrier and designed to keep the used nuclear pellets isolated and resist against leaching for a long period of time. It is made from a corrosion-resistant metal called Zircaloy (RWM, 2003; NWMO, 2011).

II. Waste canisters

Over the years, container materials have been the subject of investigation, and many countries, such as Canada and Korea, have proposed the use of carbon steel inside and copper or stainless steel outside of the containers (RWM, 2003). In addition, carbon and stainless steels, nickel-based and titanium-based alloys, and copper have been chosen as potential container materials for particular host rock formations (RWM, 2003; Kursten et al. 2004).

Waste containers/canisters are designed to:

- isolate nuclear waste,
- provide high corrosion resistance,
- withstand mechanical stresses during handling, storage, transport and facilitating of deposition, and;

- withstand shear loading and mechanical stresses caused by earthquakes and the overlying rock for a long period of time (RWM, 2003; NWMO, 2011).

III. Buffer

Highly compacted bentonite or bentonite/sand blocks are used as a buffer between the canisters themselves, and between the canisters and the host rocks. The buffer is designed to prevent radionuclides from being released in the case of canister failure and obstruct groundwater movement from the host rocks to the canisters. The buffer material is used to protect the canisters against mechanical stress and shear forces from the host rocks (Melamed and Pitkanen, 1996). The proposed thickness of the buffer material between the containers and the host rocks is a minimum of 35 cm (Villagran, 2012).

The desired properties of a highly compacted bentonite buffer, according to the Swedish KBS-3, are as follows (Laine and Karttunen, 2010; Quintessa, 2011):

- very low hydraulicity of less than 10^{-12} m/s,
- developing swelling pressure > 2 MPa,
- a density at water saturation that ranges between 1900 and 2050 kg/m^3 and
- maintaining a buffer temperature of under 100ºC.

IV. Backfill and tunnel sealing

Bentonite or bentonite/crushed rock mixtures are considered in HLW repositories as backfill, hole and shaft sealing materials. Backfill and tunnel sealing are used to eliminate underground contamination and prevent interaction between nuclear disposal areas (Quintessa, 2011). The desired properties of the backfill materials according to Quintessa (2011) include:

- very low hydraulicity < 10^{-10} m/s, and
- developing an adequate swelling pressure of > 0.1 MPa.

2.2.2.3 Bentonite based barriers in deep geological repositories for nuclear waste

Bentonite has been studied for more than 30 years and it has been chosen as buffer based materials in EBS in many countries, such as Canada, Germany, Sweden, Switzerland and France for DGRs of nuclear waste (Pusch, 1982; Cho et al., 1998; Karnland et al., 2006; Quintessa, 2011).

Bentonite satisfies all of the requirements of an EBS for nuclear waste repositories according to Cho et al. (1999), Karnland et al. (2006) and Quintessa (2011) due to the following reasons:

- adsorption of radionuclides and chemotaxis materials in the case of canister failure which prevents radioactive contamination,
- minimization or prevention of groundwater movement from the host rock to the radioactive canisters,
- sealing of cracks and fractures that may have occurred in the surrounding areas and the host rocks,
- provision of short term and long term stability without being affected by elevated temperatures generated by the HLW radioactive decay heat, groundwater salinity or pH,
- has a high swelling pressure that isolates and protects the canisters by creating good contact between the buffer and host rock on one side, and between the buffer and the canisters on the other side, and
- available where large amounts of barrier materials are needed to construct repositories. This is why there are plans for a repository in Sweden, which will store 6,000 copper canisters and require about 130,000 metric tons of buffer materials, as well as twice this amount for the backfill (Karnland et al., 2006).

2.2.3 Nuclear waste disposal and design concepts of deep geological repositories

There are many design concepts and standards for the EBS of DGRs and the DGRs of nuclear waste. Each country has its own research program and design standards according to several studies (RWM, 2003; Hicks et al., 2009; Rebak, 2011). Some examples are as follows:

- oxygen availability: e.g. design concepts in the USA construct nuclear waste depositories above the water table because they take into account the presence of oxygen, while others will use deep repositories (Rebak, 2011),
- the materials of containers have been studied for many years, and many different types of container materials have been suggested accordingly, such as those made of carbon and stainless steels, nickel- and titanium-based alloys, and copper (RWM, 2003; Kursten et al. 2004), as illustrated in Table 2.1,
- the container lifetime varies from more than 100,000 to millions of years, depending on the composition of the container materials and corrosion rate resultant of the anticipated amount of salt from the environment that surrounds the container, as shown in Table 2.2,
- there are temperature requirements for bentonite when it is used as a buffer in DGRs, and also for the container surface, as many countries, such as Canada, Finland, Sweden and Japan, stipulate the need to maintain container surface and buffer temperatures below 100ºC. In Japan, the buffer or interface temperature of the inner liner is expected to be 50ºC, while in the USA, the design requirement is less than 350°C (RWM, 2003; Hicks et al., 2009), and
- buffer and sealing materials vary among the use of bentonite or bentonite-sand based materials as the buffer, or backfill, concrete lining and bentonite buffer with metal disposal tubes.

Table 2.1. Deep geological repository design standards of different countries (RWM, 2003)

Country/Program	Waste type	Waste matrix	Container/ overpack	Buffer/ backfill	Other
Belgium	HLW.	Borosilicate glass	304 stainless steel container, 316L stainless steel overpack	FoCa clay, 60% calcium bentonite, 35% quartz sand, 5% graphite	Disposal tube, tunnel lining
	Spent fuel	-	-		-
Canada	Spent fuel	UO_2	Carbon steel inner container with copper outer shell	Bentonite buffer, bentonite/sand buffer, clay/crushed rock backfill	Tunnel and shaft seals
Czech Republic	ILW.	Concrete	Steel	Bentonite buffer	Clay seals
	Spent fuel	UO_2			
	HLW.	Glass			
France	Type B (ILW)	Wide variety	Stainless steel and concrete containers	Concrete lining	Bentonite and/or concrete seals
	Type C (HLW)	Borosilicate glass	Stainless steel containers, steel overpack	Optional bentonite buffer	Bentonite seals
	Spent fuel	UO_2 and MOX	Stainless steel with metal insert	Bentonite buffer with metal disposal tube	Bentonite seals

Table 2.2. Comparison of predictions of long-term corrosion behaviour and canister lifetime from various international programs (Kursten et al., 2004).

Country	General Corrosion	Localised Corrosion	Microbially Influenced Corrosion	Stress Corrosion Cracking (SCC)	Predicted lifetime
Sweden/ Finland*1	0.35 mm in 10^6 yrs	0.35 mm in 10^6 yrs (realistic). 1.4 mm in 10^6 yrs (conservative).	SRB assumed to reduce $SO4^{-2}$ to HS	Maximum possible nitrite concentration below threshold for SCC	>10^6 yrs
Sweden/ Finland*1	0.33 mm in 10^6 yrs	0.33 mm in 10^6 yrs (realistic) 1.3 mm in 10^6 yrs (conservative)	SRB assumed to reduce $SO4^{-2}$ to HS in tunnel and groundwater only	SCC does not occur based on threshold potential and concentrations of SCC agent, and because creep is faster than SCC	>10^6 yrs
Canada*2	0.011 mm in 10^6 yrs	6 mm in 10^6 yrs	limited impact: maximum additional wall loss of 1 mm in 10^6 yrs	SCC not included because of limited period of stress, absence of SCC agents, general lack of oxidant and inhibitive effects of Cl-	>10^6 yrs
Japan	9-13 mm in 10^3 yrs, depending on repository design	18-26 mm in 10^3 yrs based on pitting factor of 3 2 mm in 10^3 yrs based on extreme value analysis	SRB assumed to reduce SO4 2- to HS	Maximum concentrations of ammonia, nitrite and acetate less than threshold concentration	None given

1) Reference wall canister thickness of 50 mm
2) Reference wall canister thickness of 25 mm

2.2.4 Canadian nuclear waste program

Nuclear power reactors in Ontario (as shown in Figure 2.2), Quebec and New Brunswick generate about 17 percent of the electricity in Canada every year. These reactors have produced more than 2 million used SF bundles since the 1960s according to the Canadian Nuclear Safety Commission (CNSC) and Nuclear Waste Management Organization (NWMO, 2010).

Figure 2.2. Ontario nuclear generating station (http://assystem.files.wordpress.com)

2.2.4.1 High-level radioactive waste

The used fuel bundles are HLW; such chemically toxic waste could harm people and cause many environmental problems for hundreds, or even thousands of years. However, currently, used fuel bundles are being safely stored in nuclear power plants, under strict conditions (NWMO, 2010), until it is possible to move them to a permanent DGR, see Figure 2.3.

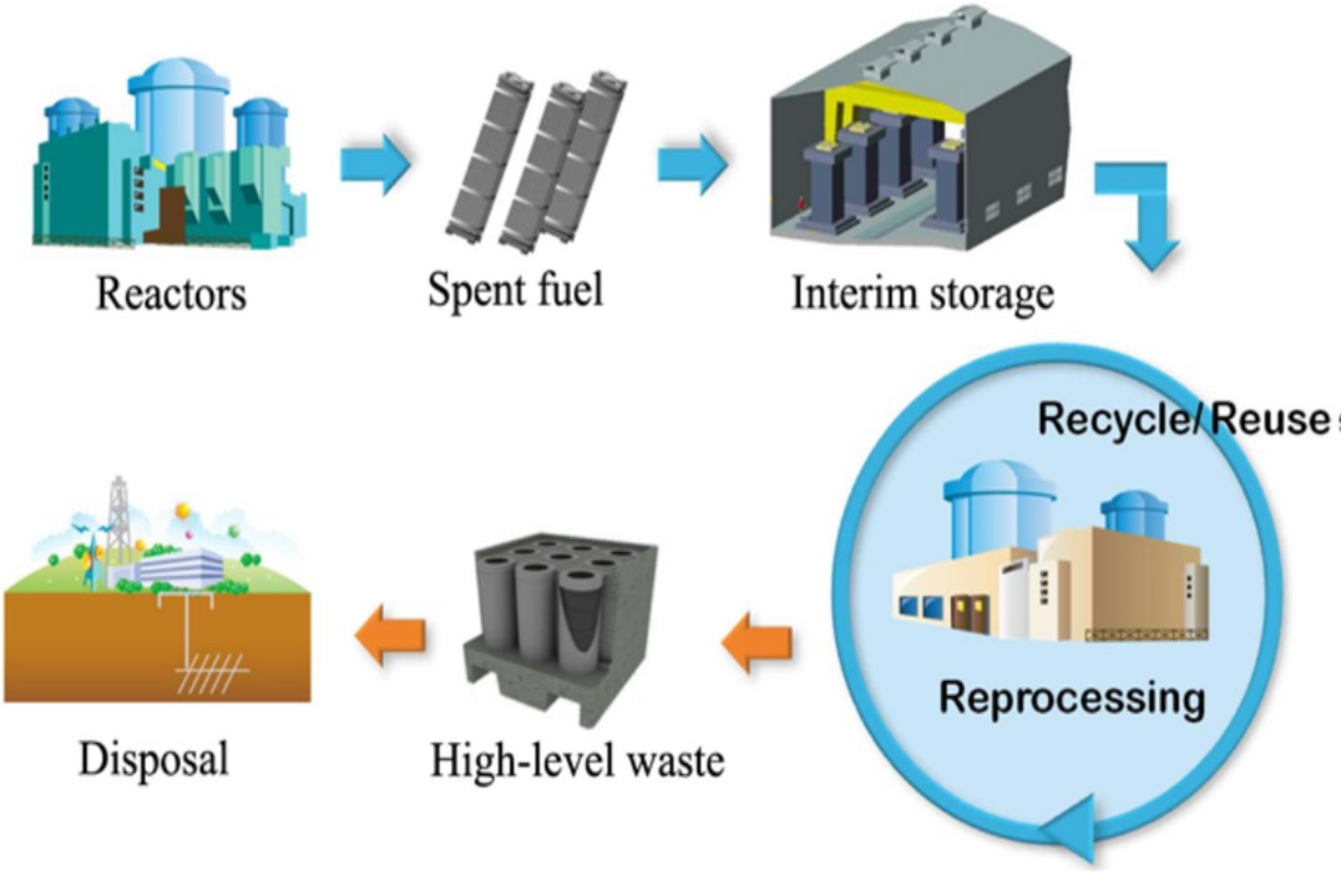

Figure 2.3. Nuclear waste (spent fuel) cycle (Kim et al., 2011)

2.2.4.2 Low and intermediate level radioactive waste

In addition, more than 75,000 m³ of low and intermediate level (L& IL) radioactive waste have been accumulated over a time period of 30 years. The amount of this type of waste has increased by 2000 to 3000 m³ due to the volume of additional stored waste after processing every year (Jensen et al., 2009). L & IL waste have been stored in Ontario waste management engineered facilities; these would be transferred to the proposed permanent DGR in Kincardine, Ontario (NWMO, 2011) after construction of the facilities is completed, see Figure 2.4.

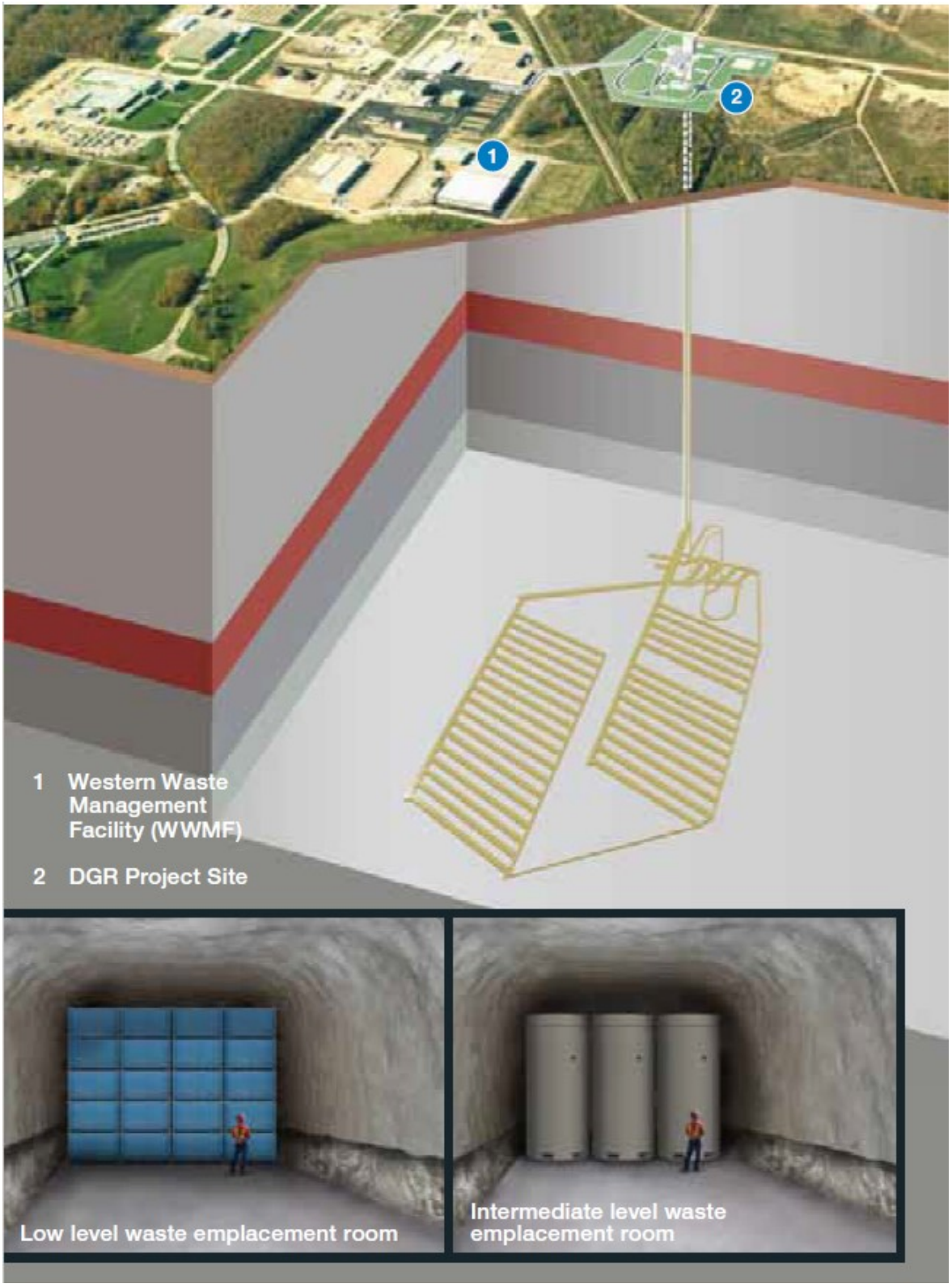

Figure 2.4. Deep geological repository for L & IL waste in Municipality of Kincardine, Ontario, as proposed by Ontario Power Generation (NWMO, 2011).

2.2.5 Canadian nuclear waste disposal and concepts of DGR

The NWMO has proposed the construction of a DGR to bury used nuclear fuel waste in Canada at a depth that varies between 300 and 700 m from the underground surface. The NWMO (2012) is currently investigating sixteen locations in Ontario and three in Northern Saskatchewan to construct the DGR, see Figure 2.5. The design standards of the Canadian Nuclear Fuel Waste Management Program for DGRs of SF are different from those of other countries, see Table 2.1. The Canadian design standards include the following.

- The Canadian program takes into consideration a carbon steel inner container with a copper outer shell of 25 mm in thickness. This container will be placed inside the DGR. In addition, the target lifetime of the container is more than 100,000 years (RWM, 2003; Rebak, 2011). However, King et al. (1994) estimated that the lifetime of a copper container with a thickness of 25 mm will be longer than 1,000,000 years.
- A significant depth is required for the DGR and the bentonite buffer, which will limit the availability of oxygen on the copper surface, therefore reducing the redox potential (Rebak, 2011). The total corrosion on the copper container would be less than 7 mm after 1,000,000 years since the redox potential will be very small (King et al., 1994).
- Radionuclide flow from the EBS is estimated to occur after 1,000,000 years (RWM, 2003), as illustrated in Table 2.1.
- The EBS consists of a bentonite buffer or bentonite/sand mixture buffer and clay/crushed rock mixture backfill. The initial unsaturated engineered barrier will be placed in the DGR, and once it comes into contact with the host rocks, it will adsorb the groundwater at a very slow rate due to the low permeability and very small pore size from the developing swelling pressure and sufficient confinement (Man et al., 2010; Delage et al., 2010; Quintessa, 2011).
- Typically, the container surface and bentonite buffer temperatures will be under 100ºC (RWM, 2003; Hicks et al., 2009).

Figure 2.5. Proposed locations for Canadian deep geological repository (NWMO, 2012).

2.2.6 Conditions in a Canadian deep geological repository

2.2.6.1 High temperature

HLW decay can raise the canister-bentonite interface peak temperature up to 95ºC in 40 years and then this temperature will decrease. However, according to Steefel et al. (2010), the bentonite-host rock interface temperature increases to about 80ºC, as evidenced by TOUGH-FLAC simulation results of a repository model for a Swiss nuclear waste disposal repository in Opalinus clay at a depth of 500 m, see Figure 2.6.

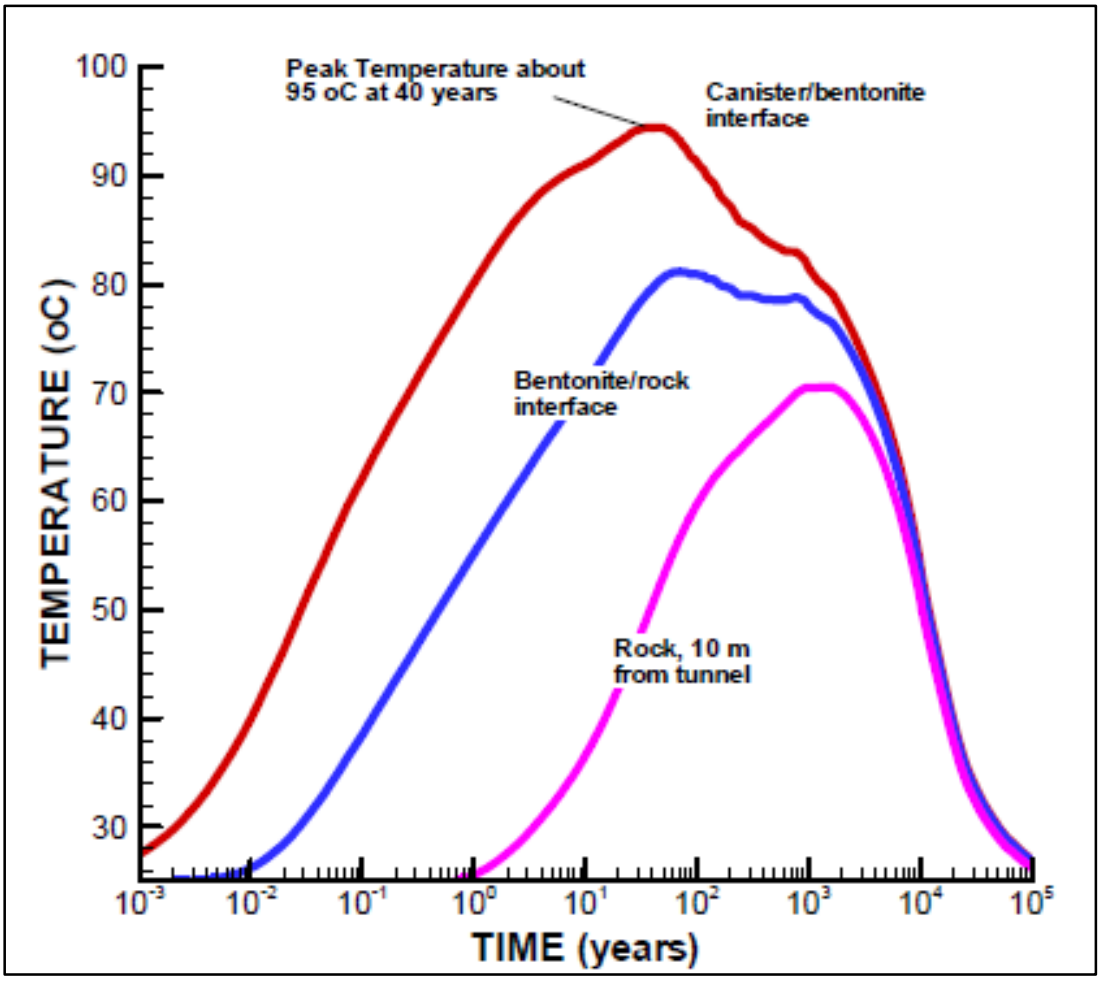

Figure 2.6. Elevated temperature from simulation results of deep geological repository (Steefel et al., 2010).

Moreover, the maximum temperature expected in the center of the canisters of the spent nuclear fuel repository in Olkiluoto, Finland at a depth of 400 m is 65ºC plus the host rock temperature of 10.5ºC. That is an overall temperature of 75.5ºC in the case of full saturation after 20 years and up to 87.5ºC in the case of unsaturated bentonite. While the corners of the canisters increase in temperature up to 52ºC, and in addition, there is the host rock temperature of 10.5ºC which equals to 62.5ºC, the temperature of the rock edge is expected to be around 40ºC according to Pastina and Hellä (2006), as shown in Figure 2.7.

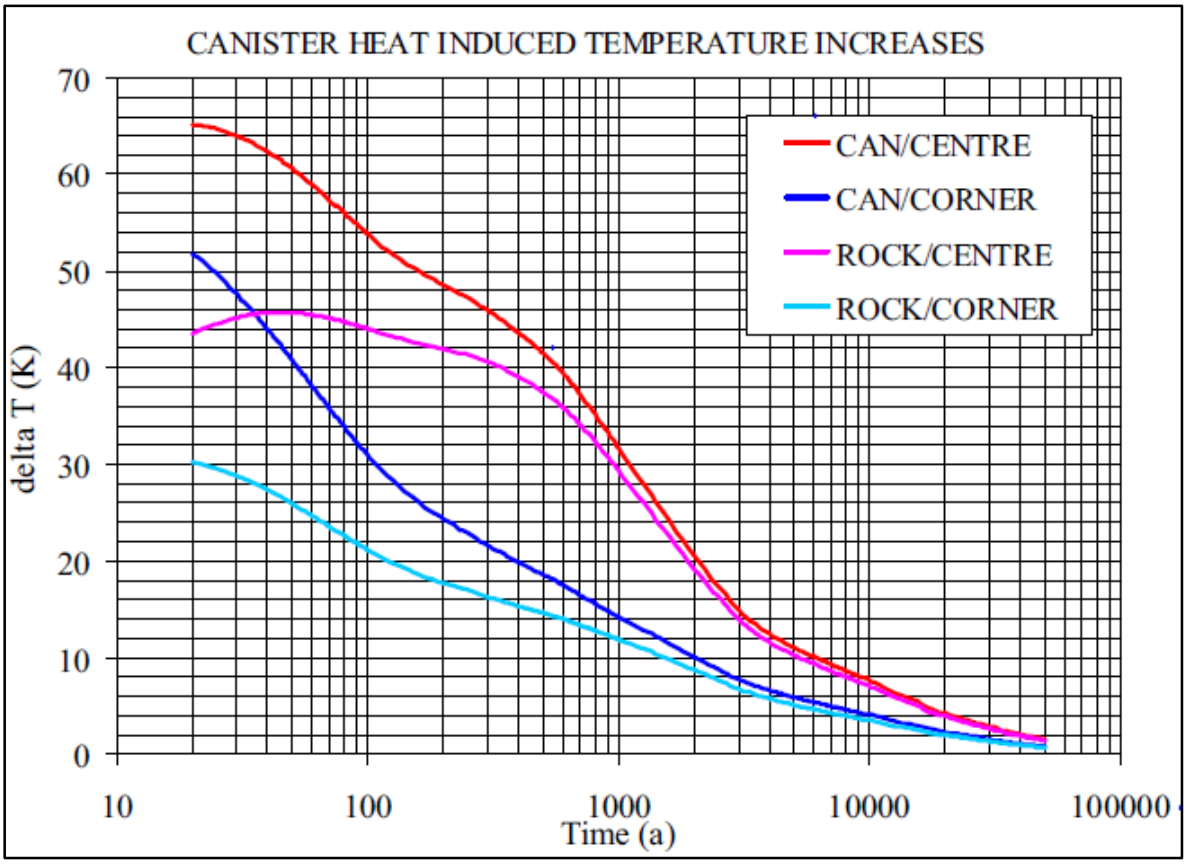

Figure 2.7. Canister and bentonite buffer temperature increases in repository post-closure and before the next glaciation (Pastina and Hellä, 2006).

2.2.6.2 Deep groundwater salinity

The Canadian DGR for HLW is proposed to be constructed in one of the sixteen chosen areas in Ontario or any of the other three chosen regions in Saskatchewan at a depth of about 650 m (NWMO, 2012). The geochemical nature of the underground water, within the sedimentary formations that underlie to the southwest at a depth of more than 200 m, falls within that of an intermediate to deep geological system (Dollar, 1988; NWMO, 2011a), as shown in Figure 2.8.

An intermediate to deep geological system is characterized by a very high salinity sedimentary formation. It contains Na-Ca-Cl or Ca-Na-Cl type of water, and the total dissolved solids (TDS) range from 200,000 to 400,000 mg/L (Dollar, 1988; NWMO, 2011a; 2012).

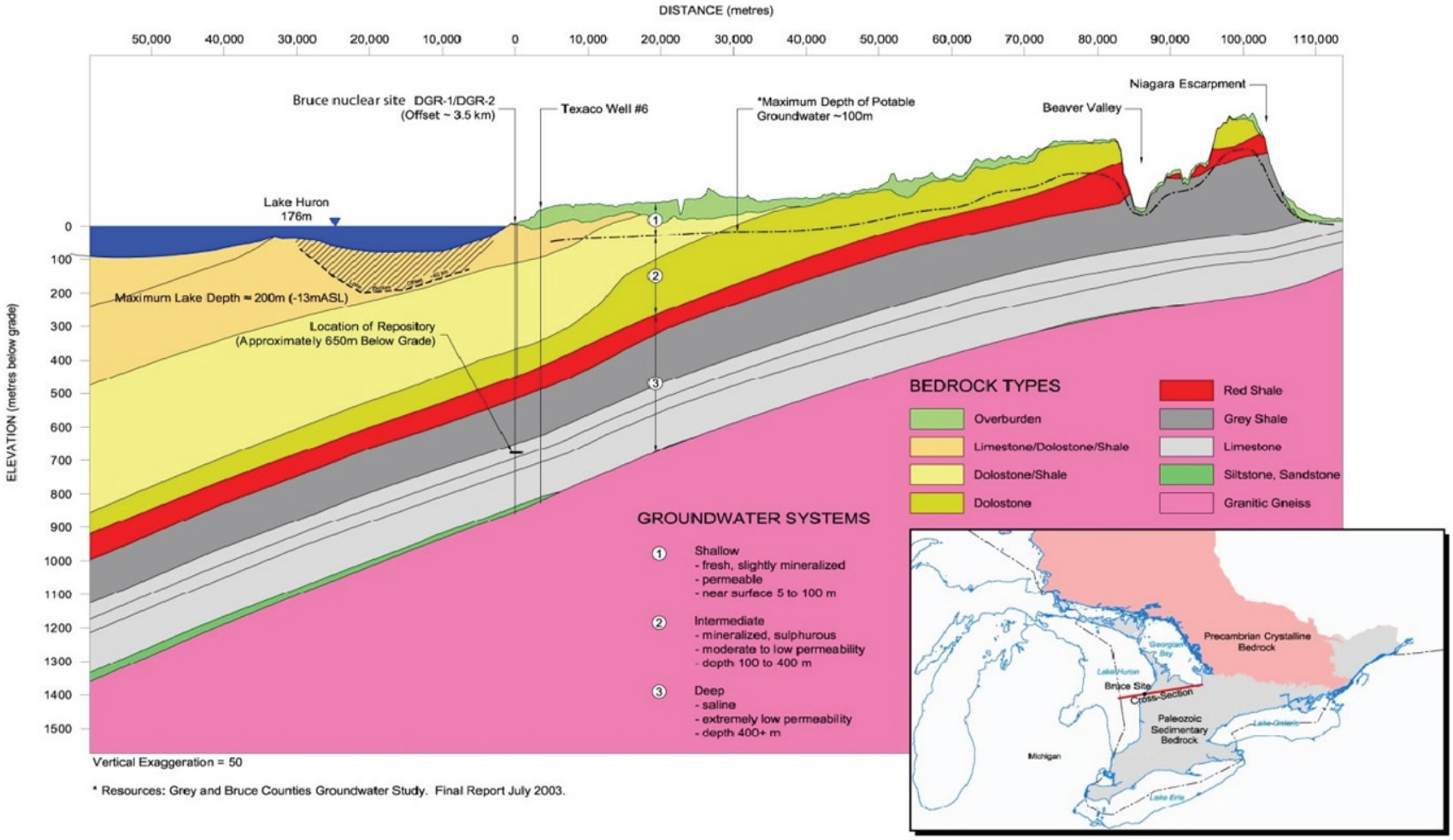

Figure 2.8. Geochemical regimes present in the sedimentary formations that underlie southwestern Ontario (NWMO, 2011a)

2.3 Background information on bentonite

Bentonite is colloidal plastic clay that is naturally formed from volcanic ash alteration millions to hundreds of millions of years ago. Bentonite is a member of the smectite group with 2:1 clay minerals, and mainly consists of montmorillonite and other accessory minerals, such as quartz, feldspar, calcite, pyrite and gypsum (Melamed and Pitkanen, 1996). It also has excellent swelling ability, high adsorption and cation exchange capacities, low permeability and thermal conductivity, high plasticity and self-sealing properties (Pusch, 1982; Mitchell et al., 1993; Melamed and Pitkanen, 1996; Quintessa, 2011).

Furthermore, bentonite is desirable for many industrial and environmental applications, such as in drilling muds, construction backfill, stabilizing agents in oil-water systems, water treatment, pipe jacking, water proofing, paper technologies, rubber, paint, food, pelletizing, detergents, and catalysts (Grim and Güven, 1978; Mitchell et al., 1993; IMA-NA, 2009). Moreover, compacted bentonite has been studied for more than three decades as part of the EBS of DGRs for nuclear waste (Karnland, 2006).

2.3.1 Types of Bentonites

There are mainly two natural types of bentonites: one is Na-bentonite, which was composited millions of years ago when volcanic ash was deposited into salt water rich with sodium Na^{+}. The second is Ca-bentonite, which formed when volcanic ash was deposited into fresh water rich with calcium (Ca^{2+}) (Athanassopoulos, 2011). These two types of bentonites have different properties, industrial applications, and in some cases, mixed together with a certain percentage to form a compound with specific properties.

Bentonite properties vary from one kind to another depending on the availability of montmorillonite and the major exchangeable cations. Na-bentonite has higher compressibility than Ca-bentonite (Grim and Güven, 197); however, Ca-bentonite has relatively higher permeability than Na-bentonite with the equivalent dry density (Grim and Güven, 1978). Furthermore, Na-bentonite has a very high swelling capacity which

exceeds the swelling capacity of Ca-bentonite several times (Grim and Güven, 1978; Mitchell et al., 1993; Liu et al., 2011).

There are many different commercial types of bentonites depending on its deposition location and the percentage of montmorillonite. The quality of bentonite increases with increasing fraction of its swelling component (montmorillonite). Mx-80 Wyoming, FEBEX and Asha bentonites, as well as bentonite from the island of Milo, contain high fractions of montmorillonite, and their use in EBS for nuclear waste have been studied (Karnland et al., 2006; Rautioaho and Korkiala-Tanttu, 2009).

2.3.1.1 Mx-80 bentonite

Mx-80 bentonite was deposited in Wyoming, USA hundreds of millions of years ago. It contains 80% to 85% montmorillonite and 4% to 12% accessory minerals, such as quartz, 5 to 8% feldspar, and traces of cristobalite, calcite, pyrite, gypsum, illite and amphibole (Pusch, 1982; Mitchell et al., 1993; Carlson, 2004). Mx-80 bentonite has excellent swelling ability, adsorption capacity, permeability, low thermal conductivity, high plasticity and self-sealing properties (Pusch, 1982; Mitchell et al., 1993; Melamed and Petteri, 1996; Quintessa, 2011).

MX-80 bentonite has a very high cation-exchange capacity, which varies from 80 to 120 milliequivalents (meq)/100 g of clay (Carlson, 2004; Meunier, 2005). The major exchangeable cations are Na (61 meq/100 g), Ca (10 meq/100 g) and Mg (3 meq/100 g). Grain size analyses have demonstrated that 86% of the grains of Mx-80 bentonite are smaller than 2 μm. It also has an average specific gravity of 2.58, a liquid limit of 530%, and a plastic limit of 52%. An Mx-80 bentonite sample is shown in Figure 2.9.

Figure 2.9. MX-80 bentonite sample (Carlson, 2004).

2.3.1.2 FEBEX bentonite

The FEBEX bentonite deposits that are found in Spain originate from the hydrothermal alteration of acid volcanic rocks millions of years ago. FEBEX bentonite has been studied for more than 30 years as a component of EBS and chosen as a buffer material in a Spanish DGR for nuclear waste. It contains more than 92% montmorillonite and accessory minerals, such as quartz, plagioclase, cristobalite, potassic feldspar, calcite, and trydimite (García-Gutiérrez et al, 2011) It has high cation exchange capacity (CEC), which varies from 96 to 102 meq/100 g. The predominant exchangeable cations are Ca (35 to 42 meq/100 g), Mg (31 to 32 meq/100 g), Na (24 to 27 meq/100 g), and K (2 to 3 meq/100 g) (Rautioaho and Korkiala-Tanttu, 2009).

2.3.1.3 Friedland bentonite

Friedland bentonite was deposited 35 to 57 million years ago into a shallow marine basin near the town of Neubrandenburg, NE Germany (Karnland et al., 2006). It contains about 45% montmorillonite, 24% quartz, 13% mica, 11% chlorite, 5% feldspar, and 2% carbonate (Karnland et al., 2006; Rautioaho and Korkiala-Tanttu, 2009). It has a CEC that ranges from 35 to 45 meq/100 g. Sodium is the predominant exchangeable cation. The Friedland bentonite has a low liquid limit of 126%, and low hydraulic conductivity and swelling capacity compared to the Mx-80 bentonite (Johannesson and Börgesson, 2002). A sample of the Friedland bentonite is shown in Figure 2.10.

Figure 2.10. Friedland bentonite sample (Carlson, 2004).

2.3.2 Bentonite mineralogy

The structure of smectite group minerals consists of an aluminum octahedral sheet between two silica tetrahedral sheets. The aluminum octahedral unit is composed of one aluminum atom bound with six hydroxyl atoms in the composition of $Al_2(OH)_6$ or the gibbsite mineral. In the case of clay minerals, the crystals are based on an octahedral or gibbsite sheet and have a thickness of 5.05 Å (Grim, 1968), as shown in Figure 2.11.a. While the silica tetrahedral unit is composed of one silica atom bound with four oxygen atoms in the composition of $(Si_4O_{10})^{4-}$, these units are connected together in a hexagonal structure sheet with a thickness of 4.63 Å (Grim, 1968), as shown in Figure 2.11.b.

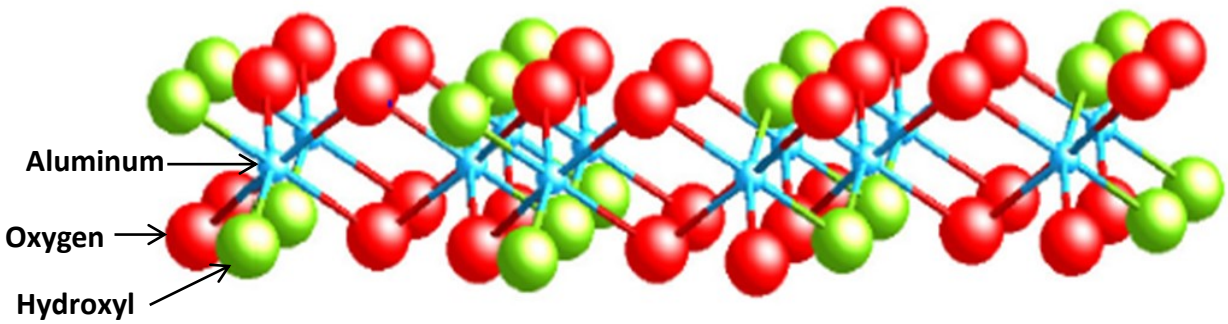

(a) Octahedral unit and octahedral structure

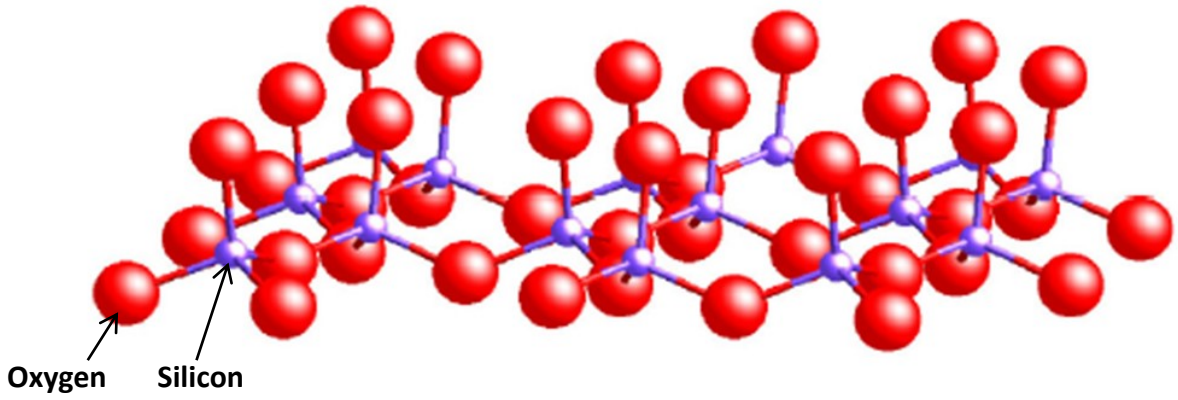

(b) Silicon tetrahedron and tetrahedral structure

Figure 2.11. Clay mineral structure: a) octahedral unit and octahedral structure, b) silicon tetrahedron and tetrahedral structure (source: Quintessa, 2011).

2.3.2.1 Structure

Montmorillonite has a very small crystal size of less than 0.002 mm (2 μm) in the long direction. These crystals are arranged as very thin platelets or layers of about 0.98 nm (9.8 Å) in thickness. Montmorillonite layers extend from 10 to 100 Å in both directions; length and width (Saito and Murata, 2003). A montmorillonite crystal consists of an aluminum octahedral sheet between two silica tetrahedral sheets arranged in a three direction structure, as shown in Figure 2.12.

The silica tetrahedral sheets connect with the aluminum octahedral sheet through a very strong bond of the primary valence, which results from the ionic bonds (Mitchell et al., 1993). In contrast, montmorillonite layers connect together by van der Waals forces and exchangeable cations, which are weak and easily disconnect when in contact with water or any other polar liquids or cleavage (Mitchell et al., 1993).

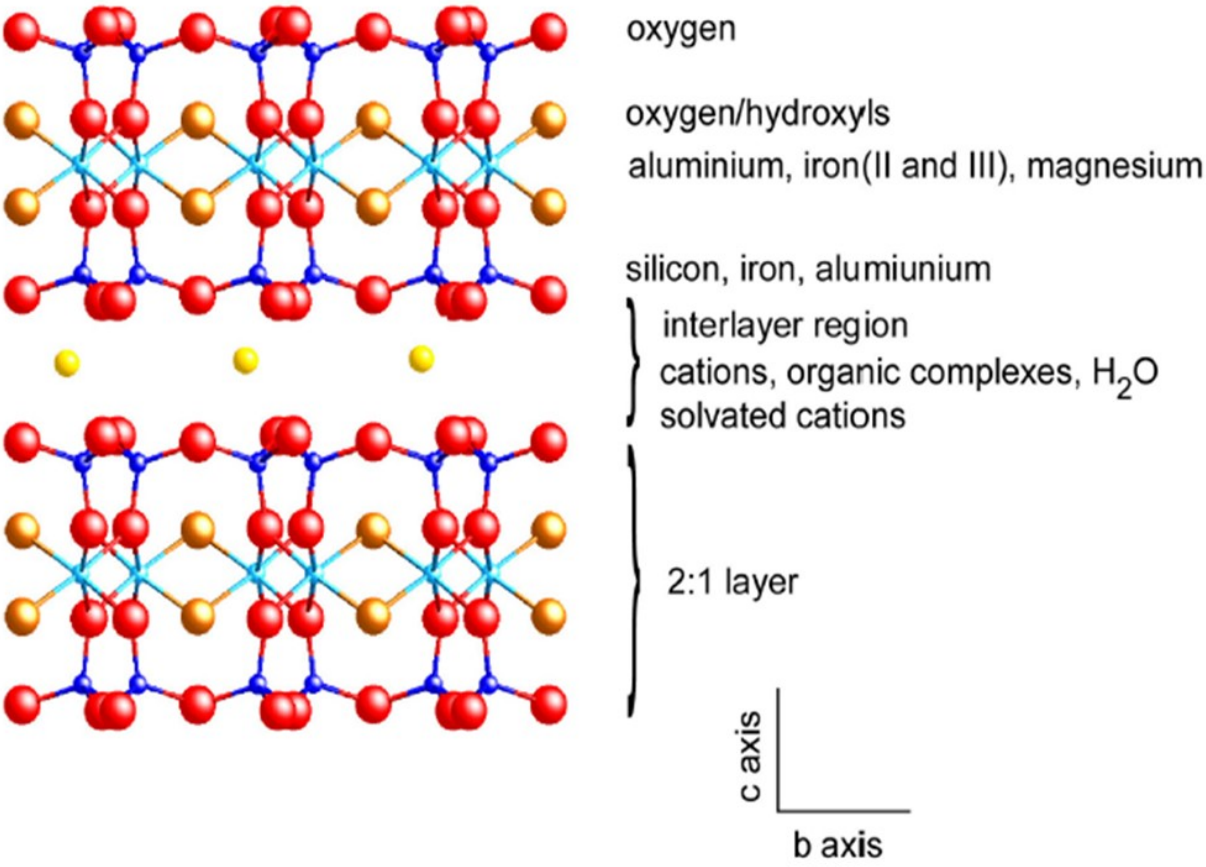

Figure 2.12. Sketch of montmorillonite structure (source: Quintessa, 2011)

2.3.2.2 Bentonite microstructure

In order to understand the mechanical behavior of bentonite, it is important to understand the clay and bentonite microstructures. There are primarily two types of structures for clay.

- The macrostructure of clay consists of an aggregate arrangement, and there is space between the aggregates (inter-aggregate pore or macropores) as shown in Figure 2.13.a. The inter-aggregate pores range between 10 and 40 μm in diameter, depending on the compaction dry density. For example, when the bentonite is heavily compacted to a dry density of ρ_d = 1.8 Mg/m³, the macropores are reduced to 10 μm, as opposed to when the bentonite is lightly compacted to a dry density of ρ_d = 1.5 Mg/m³, there are larger spaces between the aggregates of

up to 40 μm (Lloret et al., 2003). The macrostructure of clay can also be affected by compaction loads and external forces (Gens and Alonso, 1992).

- The microstructure of clay consists of elementary particle arrangements that connect face–to-face, face–to-edge, and edge-to-edge to form aggregates (Gens and Alonso, 1992; Meniere, 2005) as shown in Figure 2.13.b. The spaces between the elementary particles inside the aggregate are called intra-aggregate pores (micropores), and about 10 nm in diameter (Lloret et al., 2003). The microstructure is considered saturated even if the soil is in an unsaturated state, and responsible for the physico-chemical activities at the clay particle level (Gens and Alonso, 1992; Meunier, 2005). Microstructure deformation is completely reversible, and not only independent of the macrostructure state, but also affects the macrostructure (Gens and Alonso, 1992; Lloret et al., 2003).

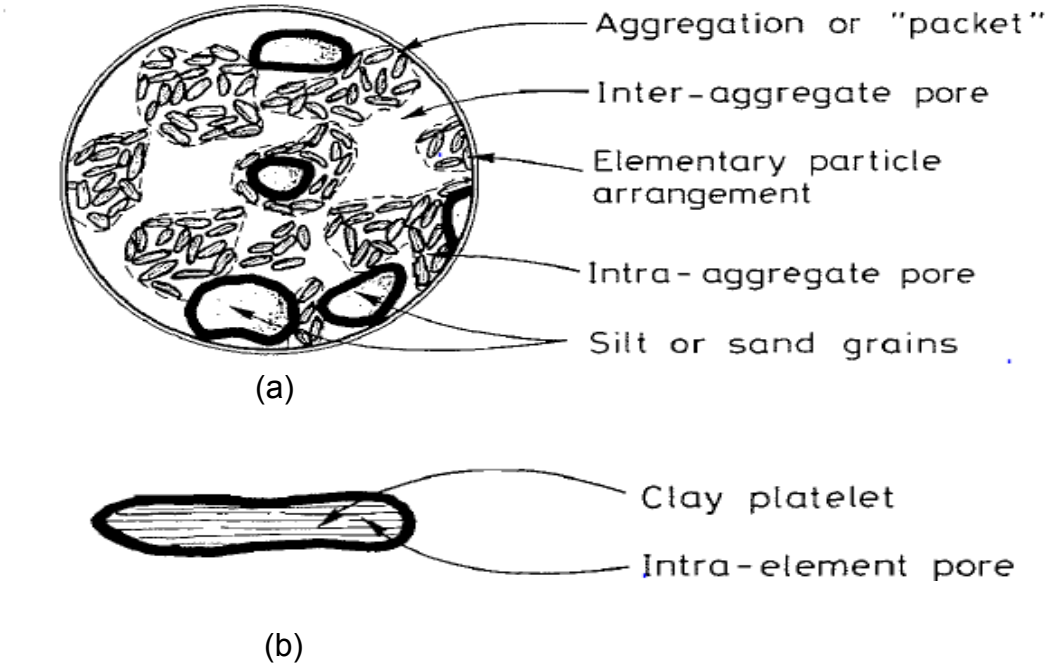

Figure 2.13. Clay structure: a) macrostructure of a clay that predominantly consists of aggregations of elementary particle arrangements, b) microstructure of clay that consists of elementary particle arrangements (Gens and Alonso, 1992)

2.3.3 Water adsorption

Water molecules interact with clay surfaces and penetrate the innercrystalline structure thus causing innercrystalline swelling and osmotic swelling (Savage, 2005). When water molecules penetrate the innercrystalline structure of dry Na-montmorillonite, an increase in the d-space (d_{001}) occurs between the innercrystalline from 9.60 to 12.5 Å with two water layers, or even to 18.8 Å, in the case of three water layers (Meunier, 2005) as shown in Figure 2.14. This changes the physical and physicochemical properties of the clay minerals (Mitchell et al., 1993; Meunier, 2005).

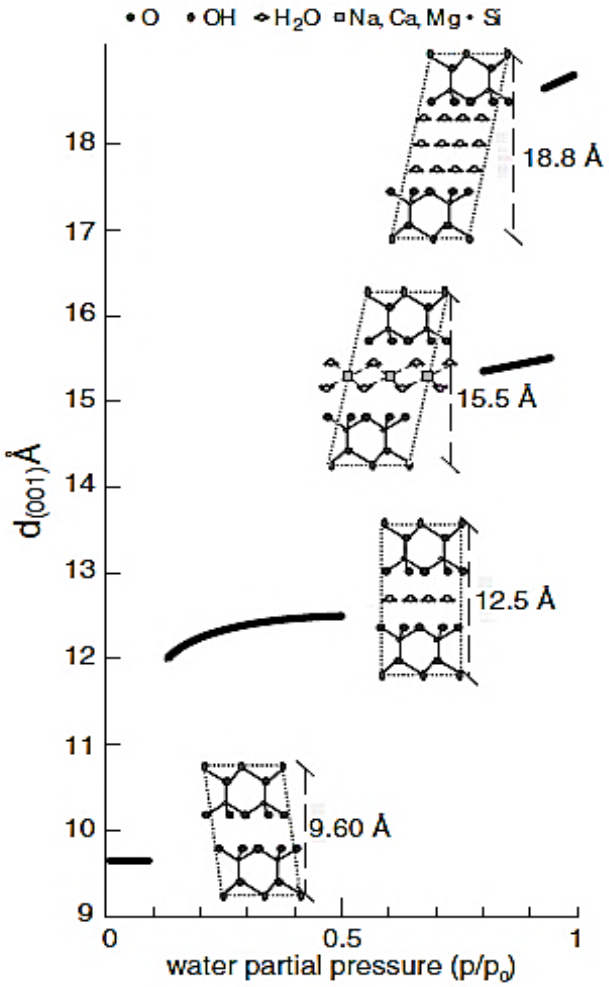

Figure 2.14. Water molecules penetrate innercrystalline structure of Na-montmorillonite and increase d-space (Meunier, 2005).

2.3.3.1 Water adsorption mechanism

The water adsorption mechanism can be explained by the fact that montmorillonite consists of 2:1 silica to alumina. Therefore, montmorillonite has a net negative surface charge, resulting from the isomorphic substitution of Al^{3+} for Si^{4+} and Mg^{2+} for Al^{3+} in the tetrahedral layer and the Al octahedral layer, respectively. This net negative charge ranges from 0.4 to 1.2 unit charge per $O_{20}(OH)_{4-}$ unit. The tetrahedral charge is smaller than the octahedral charge (Karnland et al. 2006). The montmorillonite formula can be written as the following composition (Karnland et al. 2006):

Si8–x Alx	Al4–yMgy (Fe)	O_{20}(OH)4	cx+yn(H2O)	(x < y) and
Tetrahedral	octahedral	anions	interlayer	0.4 < x+y > 1.2

where n refers to the number of water molecules; c refers to the interlayer space cations; and x and y are the octahedral and tetrahedral substitutions, respectively. The cations between the interlayers balance the layer of negative charge and n water molecules adsorbed between the montmorillonite layers (Karnland et al. 2006), as shown in Figure 2.15. Mitchell et al. (1993) concluded that montmorillonite particles could attract water molecules by:

- developing hydrogen bonds between the negative layer of oxygen on the clay surface and the positive hydrogen side of the bipolar water molecule or between the layer of positive hydroxyls on the clay surface and the negative oxygen from water, as shown in Figure 2.16.a.,
- the hydration of the interlayer cations between the Al octahedral sheet and the two Si tetrahedral sheets, as shown in Figure 2.16.b.,
- osmosis attraction, which results from increasing ion concentration between the clay surface and porewater, as shown in Figure 2.16.c., and

- dipole attraction due to the large net negative charge on the montmorillonite particle surface which attracts the positive poles of the water molecules. Therefore, water orients with its positive poles towards the clay surface and connects with other water molecules, thus forming several layers of water dipoles, as shown in Figure 2.16.d.

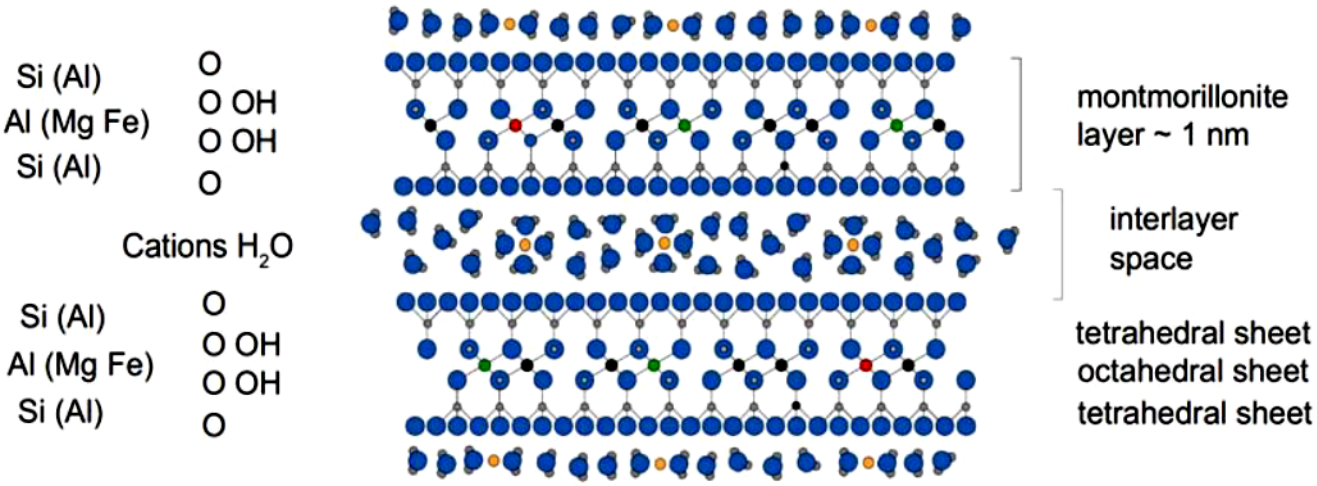

Figure 2.15. Two montmorillonite layers with interlayer cations and water molecules (Karnland et al., 2006).

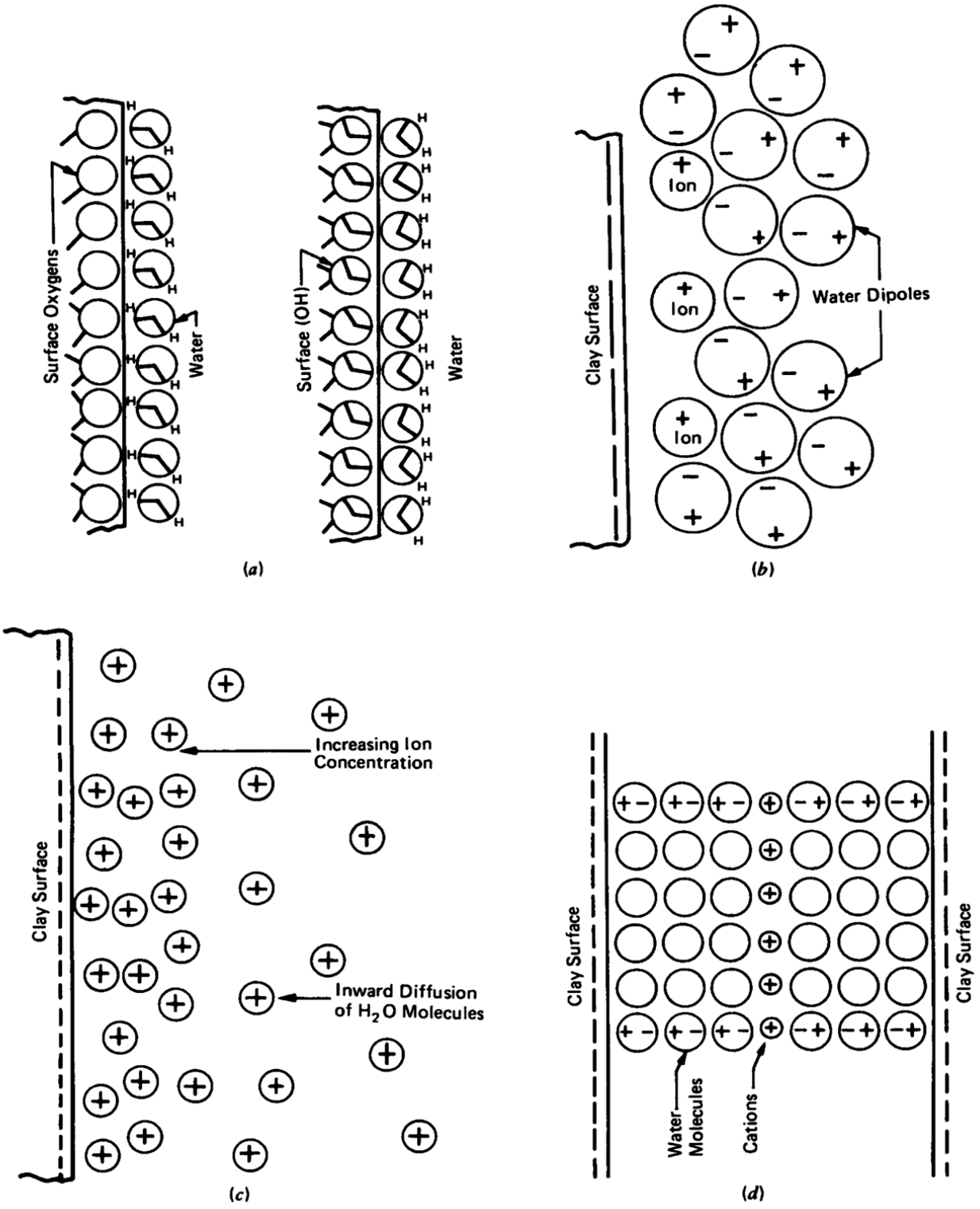

Figure 2.16. Clay – water interaction: a) hydrogen bonding, b) ion hydration, c) attraction by osmosis, and d) dipole attraction (Mitchell et al., 1993).

2.3.4 Cation- exchange capacity

CEC refers to the number of positive ions adsorbed on the surface of clay particles to balance the permanent negative charges. CEC depends on the presence of unbalanced substitutions in the montmorillonite, temperature, pressure, chemical and biological compositions, and the pH of the surrounding solutions (Mitchell at al., 1993). CEC is usually expressed in meq per 100 g of clay at a pH of 7 (Meunier, 2005).

Montmorillonite has a very high cation-exchange capacity, which varies from 80 to 120 meq/100 g of clay (Meunier, 2005). In spite of the fact that cation exchange does not normally influence the structure of the montmorillonite particles, it does have a great impact on their physical and physicochemical properties (Mitchell et al., 1993). CEC is a function of the valence and ion size, where high power cations replace low power cations (Mitchell et al., 1993) as follows:

$$Na^{+} < Li^{+} < K^{+} < Rb^{+} < Cs^{+} < Mg^{2+} < Ca^{2+} < Ba^{2+} < Cu^{2+} < Al^{3+} < Fe^{3+} < Th^{4+}$$

However, this series can be reversed by mass action in highly concentrated solutions where low power ions replace high power ions (Mitchell et al., 1993).

The CEC of montmorillonite can be determined by theoretical calculations and from experimental work. Meunier (2005) determined the internal CEC ($CEC_{permanent\ charges}$) of montmorillonite from the following relation:

$$CEC_{permanent\ charges} = (charge/\ mass) *1000 * 100 \quad (PH7)$$

$CEC = CEC_{variable\ charges} + CEC_{permanent\ charges}$.

Where the half-unit cell formula of montmorillonite is: $Si_4O_{10}\ Al_{1.7}\ M_{o.3}\ (OH)_2\ Na_{o.3}$ and the mass of the half unit cell = 367 g and the charge = 0.33 so

$CEC_{permanent\ charges}$ = (0.33 / 367) * 1000 *100 = 89.9 meq/100 g

Therefore, 89.9 meq/100 g is the exchange capacity of the interlayer sites, and the external exchange capacity of the crystal surface (CEC variable charges) should be determined to obtain the total CEC of montmorillonite, as shown in Table 2.3.

Table 2.3.Total CEC values of the main clay mineral species (Meunier, 2005).

Mineral	CEC (meq/100 g)
Kaolinite	5-15
Illite	25-40
Vermiculite	100-120
Montmorillonite	80-120
Chlorite	5-15

2.3.5 Main factors that affect performance of bentonite-based engineered barrier material

Bentonite has often been chosen for use as an engineered barrier material due to its high swelling capacity, low hydraulic conductivity, and good ability to retain radionuclides in the event of a failed canister (Melamed and Pitkanen, 1996; Cho et al., 1999, 2011; Quintessa, 2011). However, the initial dry density of bentonite, initial water content, presence of many solvents and salts in the groundwater under confining stress, and high temperature may affect the physical and physiochemical properties of bentonite; thus these influence the bentonite performance as an engineered barrier (Villar and Lloret, 2004; Karnland et al., 2007; Herbert et al., 2008; Cho et al., 2011). The impact of underwater salinity and high temperature will be discussed in more detail below.

2.3.5.1 Dry density

The dry density of compacted bentonite has a great impact on the performance of bentonite as an engineered barrier material. The hydraulic conductivity of compacted bentonite decreases with increasing dry density (Cho et al. 2009), while the swelling pressure increases with increasing dry density. The “maximum swelling strain is directly proportional to the initial dry density for all bentonite” (Komine, 2004).

Villar and Lloret (2008) conducted a swelling test on FEBEX bentonite that contained a very high montmorillonite fraction (more than 90%). The bentonite materials, with an initial water content of 13.2±1.2%, were compacted to 36–38 mm in diameter with a height of 12 mm. The specimens had dry densities of 1.50, 1.60 and 1.70 Mg/m³ under static uniaxial compaction. The test results showed that the swelling pressure significantly increases with increases in the dry density, as shown in Figure 2.17.

Furthermore, Delage et al. (2010) investigated the impact of dry density on the swelling pressure of three different kinds of bentonites: MX80 Wyoming, Kunigel from Japan, and Foca7 from France. The test results confirmed that the swelling pressure of all three kinds of bentonites increases with increases in the dry density of the specimens, as shown in Figure 2.18

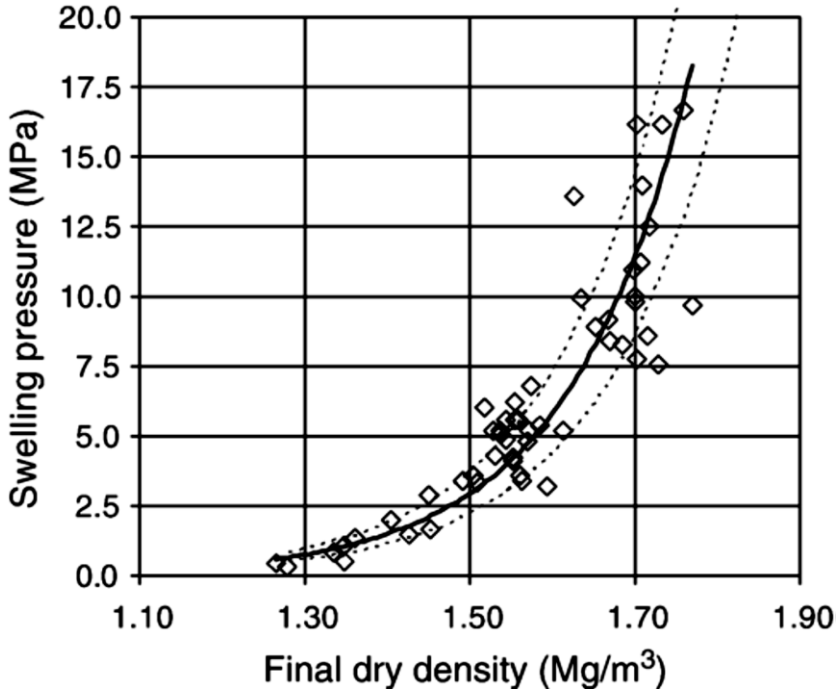

Figure 2.17. Increases in swelling pressure with increasing dry density (Villar and Lloret, 2008).

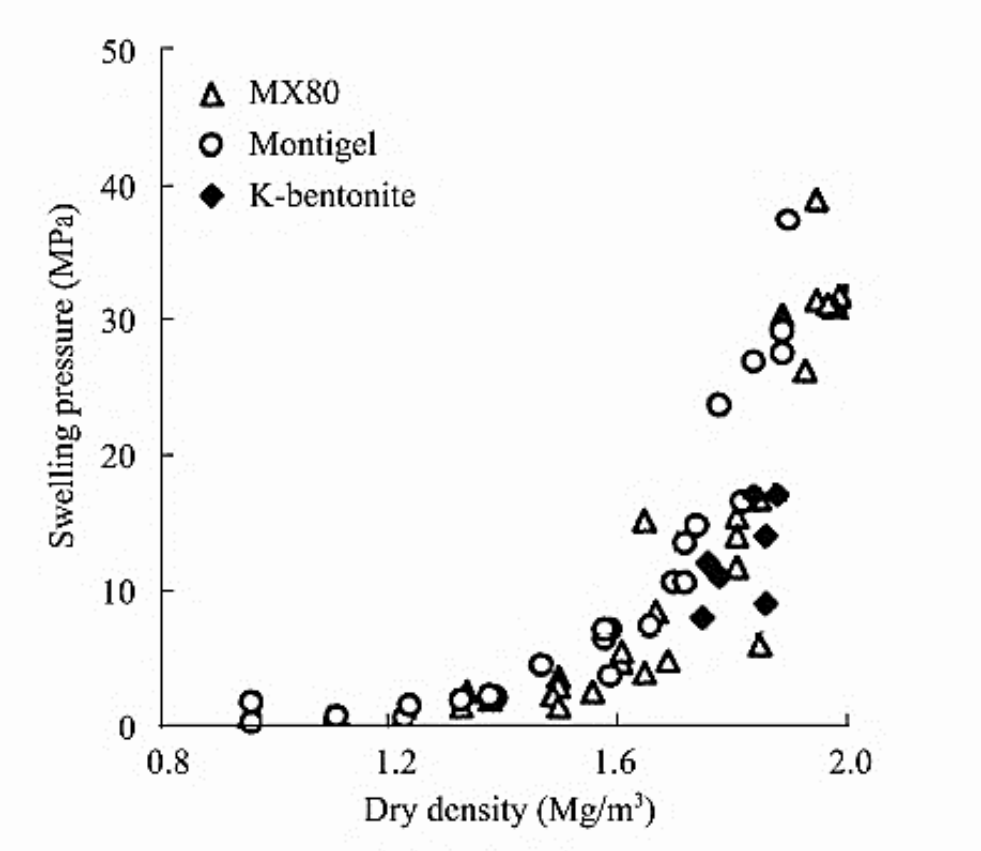

Figure 2.18. Swelling pressure of various bentonites as a function of the compacted sample dry density (Delage et al., 2010).

Cho et al. (2009) measured the hydraulic conductivity of Kyungju Ca-bentonite, which was chosen as the buffer material based on the Korean reference repository concept. The bentonite specimens were compacted in a stainless steel cylindrical cell with an inner diameter of 50 mm and a height of 25 mm or 10 mm to dry densities of 1.4 Mg/m³, 1.6 Mg/m³ and 1.8 Mg/m³ at a temperature of 25 ^{O}C. The test results demonstrated that the hydraulic conductivity decreases with increasing dry density of the bentonite, as shown in Figure 2.19.

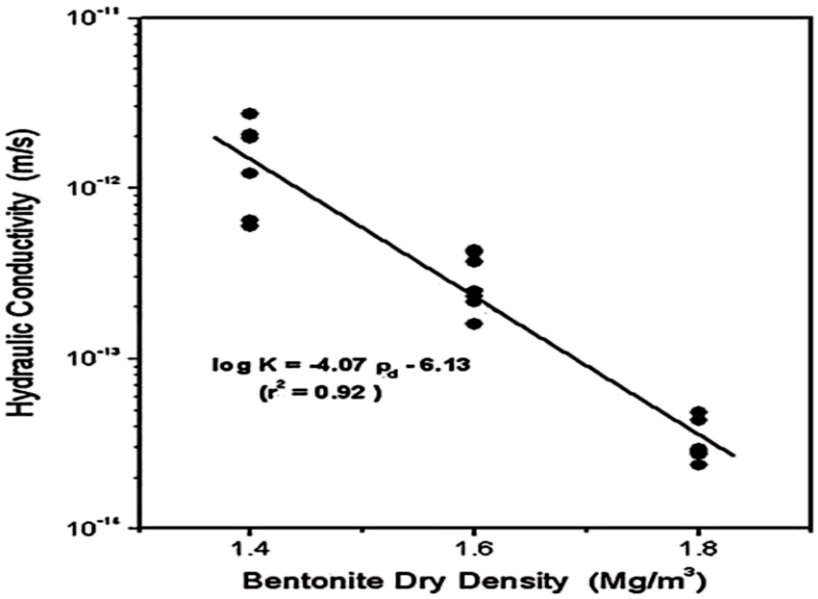

Figure 2.19. Influence of compaction of bentonite on hydraulic conductivity (Cho et al. 2009).

2.3.5.2 Initial water content

The initial water content has remarkable influence on the swelling pressure of compacted bentonite with a high dry density; however, it could be neglected for compacted bentonite with a low dry density (Villar and Lloret, 2008). Villar and Lloret (2008) investigated the impact of the initial water content on the swelling strain of compacted FEBEX bentonite under different testing conditions. The test results indicated that the impacts of the initial water content on the swelling strain of compacted FEBEX bentonite are reduced with increases in the vertical stress, as shown in Figure 2.20.a. Moreover, the swelling strain of highly compacted FEBEX bentonite specimens is significantly decreased with increasing initial water content, as shown in Figure 2.20.b.

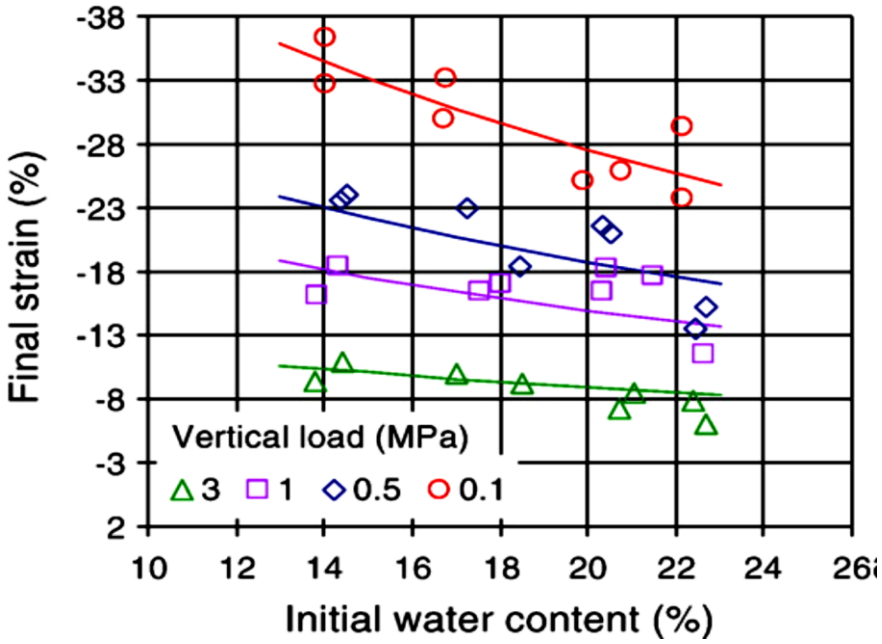

(a)

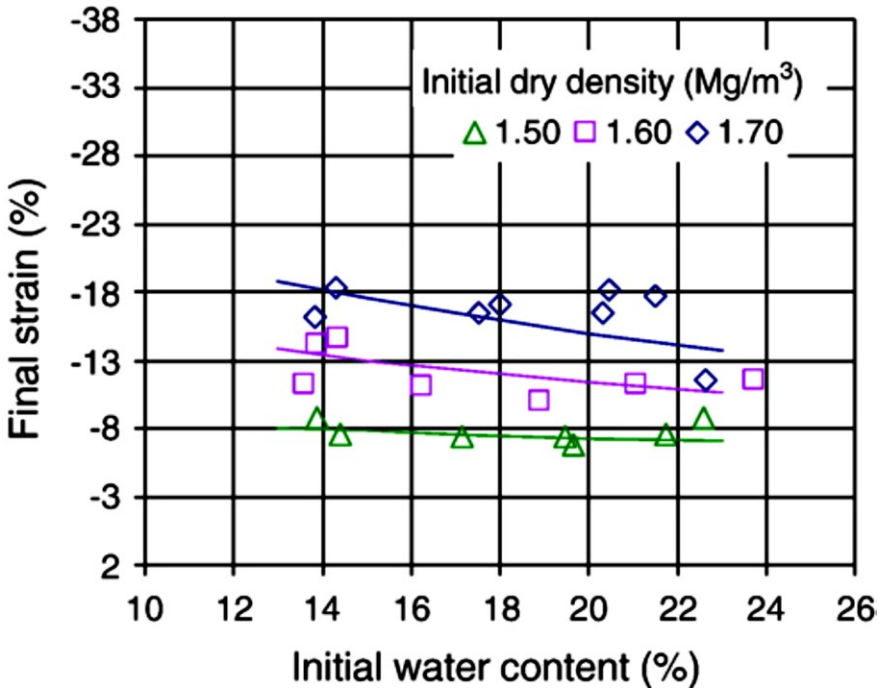

(b)

Figure 2.20. Impact of initial water content of bentonite on swelling properties of various specimens under: a) different vertical stresses, and b) different dry densities (Villar and Lloret, 2008).

2.3.5.3 Sand content

It has been shown that mixing bentonite with a specific amount of sand gives a mixture with new properties that satisfies all of the physical and chemical specifications of a buffer as well as improves the buffer performance and durability (RWM, 2003; Cho et al., 2011; Quintessa, 2011).

The hydraulic conductivity and swelling pressure of a bentonite-sand mixture depends on the sand content ratio and dry density of the mixture (Cho et al., 2000; 2011; Cui et al., 2012). The maximum swelling pressure increases with increasing dry density and decreases with increasing the sand content according to the experimental results of Cui et al. (2012) on GMZ Na-bentonite (Figure 2.21), whereas the hydraulic conductivity and void ratio were found to increase with increases in the sand content, according to the experimental results of Cho et al. (2000; 2011) on Kyungju Ca-bentonite (Figure 2.22). It has been also shown that a bentonite-sand mixture has advantages and disadvantages, according to Pusch (2008) and Quintessa (2011).

The advantages are summarized as follows - bentonite-sand mixture:

- increases the thermal conductivity when bentonite is mixed with silica sand that has high thermal conductivity (increases the ability of the buffer (media) to transfer heat);
- reduces the impact of groundwater salinity on the hydraulic conductivity and swelling capacity of the buffer;
- reduces the risk of increasing the swelling pressure more than anticipated which leads to an increase in the mechanical stress on the canisters and the host rocks; and
- is cheaper than pure bentonite.

The disadvantages are summarized as follows - bentonite-sand mixture:

- increases the hydraulic conductivity (but this can be controlled by increasing the dry density);
- reduces the swelling capacity (but still in an acceptable range).

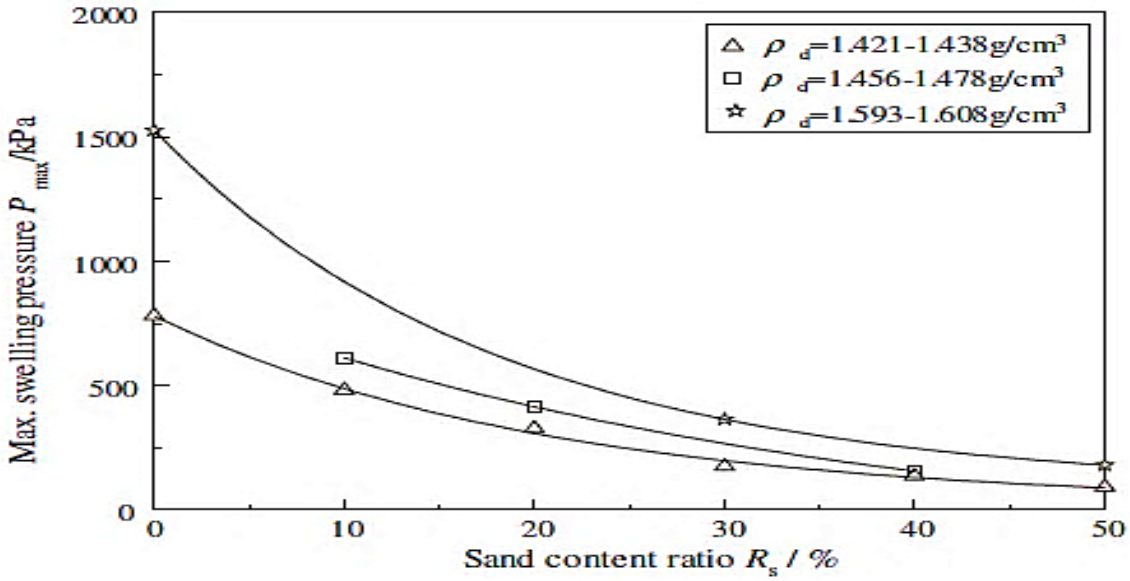

Figure 2.21. Maximum swelling pressure vs. sand content ratio (Cui et al., 2012)

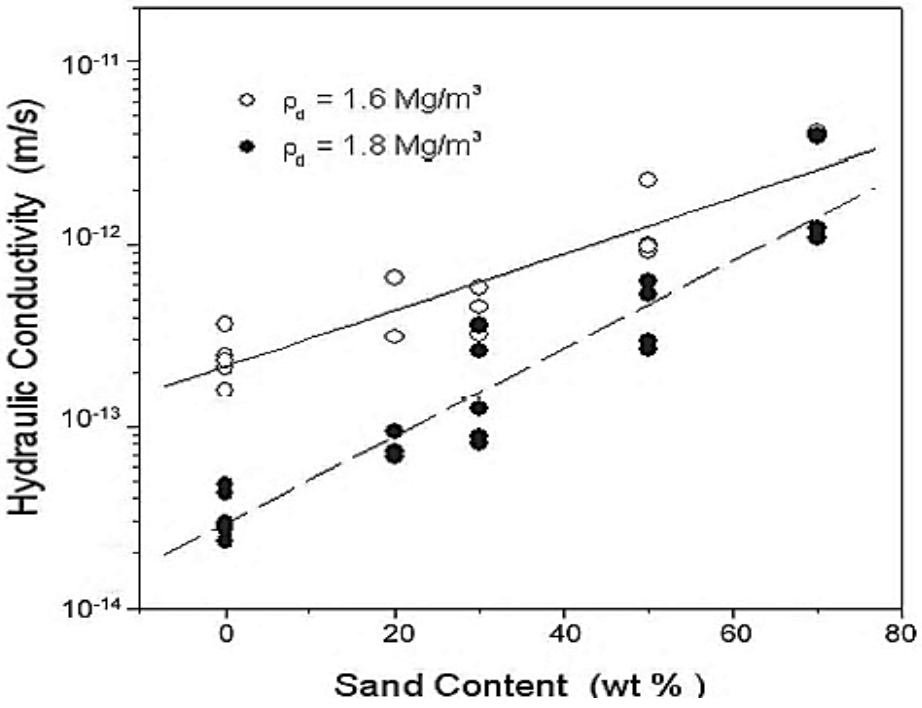

a)

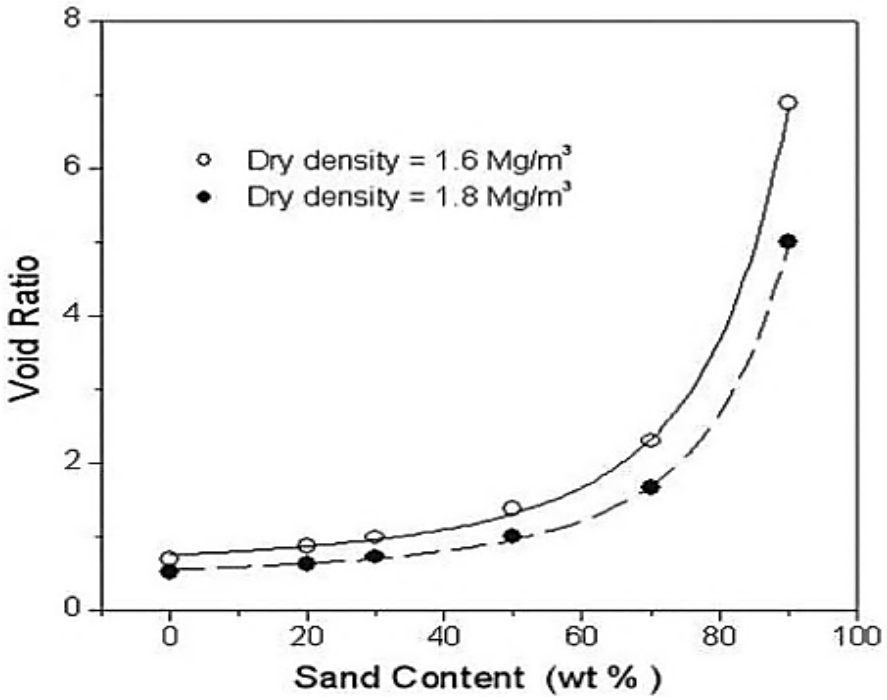

b)

Figure 2.22. Sand content of bentonite-sand mixture versus: a) hydraulic conductivity, and b) void ratio (Cho et al., 2011)

2.3.5.3.1 Bentonite –sand mixing ratio

The mixing of Na-smectite-rich materials with round shaped grains of glacial sediment (silica sand) has been investigated to reduce buffer swelling capacity and avoid mechanical stress on canisters and host rocks. The minimum acceptable mixing weight ratio is 30% Na-bentonite to 70% ballast to form a homogeneous and dense buffer mixture with low hydraulic conductivity and reasonable amount of swelling pressure, especially in the case of high groundwater salinity (Pusch and Yong, 2006; Quintessa, 2011) as illustrated in Table 2.4.

Table 2.4. Physical properties of pure MX-80 and MX-80 – crushed rock mixture (Pusch, 2002; Quintessa, 2011)

Buffer % Clay	**Density (at water saturation)** kg/m^3	**Hydraulic conductivity** (dist. water) m/s^{-l}	**Swelling pressure** (dist. water) MPa
100% MX-80	2000	4.00E-13	7.3
50% MX-80	2100	1.00E-12	2.0
30% MX-80	1950	1.00E-11	0.2

2.4 Effect of pore water chemistry on properties of bentonite based materials

The presence of many chemical substances or solutes in the groundwater under confining stress and high temperatures may affect the physical and physiochemical properties of bentonite and the bentonite performance (Villar and Lloret ,2004; Karnland et al., 2007; Herbert et al., 2008; Cho et al., 2011). Therefore, it is important to determine the impact of solutes in the pore water on the bentonite properties, such as swelling pressure and hydraulic conductivity. A literature review of key previous studies on the impact of solutes in the pore water on the bentonite properties is provided below.

2.4.1 Swelling capacity

Many studies have been conducted that investigate the impact of different electrolyte solutions of different salinities and pHs on the bentonite swelling capacity (Pusch, 1982; Melamed and Pitkanen, 1996; Karnland et al., 2007; Batenipour, 2008; Herbert et al., 2008, Man et al., 2010; Liu et al., 2011).

Pusch (1982) conducted more than 90 experiments at laboratory temperature (23 ^{O}C) by using a swelling pressure oedometer (1981) to measure the swelling pressure of MX-bentonite saturated with distilled water (DW), 0.6 M NaCl solution, and 0.3 M $CaCl_2$ solution under different bulk densities. The results showed that the swelling pressure increases with increasing bulk density in the three cases. In addition, at the same bulk density, the average swelling pressure, in the case of MX- bentonite saturated with 0.6 M NaCl, is less than the average swelling pressure of the MX- bentonite saturated with 0.3 M $CaCl_2$ as well as less than the average swelling pressure of the MX-bentonite saturated with DW. These test results fall in good agreement with the experimental results of Karnland et al. (2007) on highly compacted MX-bentonite that contained 83% montmorillonite by mass. The compacted bentonite was saturated with four solutions: de-ionized water, 1.0 M NaCl, 1.0 M NaOH, and 1.0 M NaCl which was replaced with 1.0 M NaOH after 15 days, as shown in Figure 2.23. The samples treated with de-ionized water showed higher swelling pressures compared to the samples treated with NaCl, high ionic strength NaOH, and NaCl-NaOH solutions. The swelling pressure of MX-bentonite differs from one solution to another with regards to the ionic strength. It also varies from one chemical concentration to another for the same solution (Karnland et al., 2007).

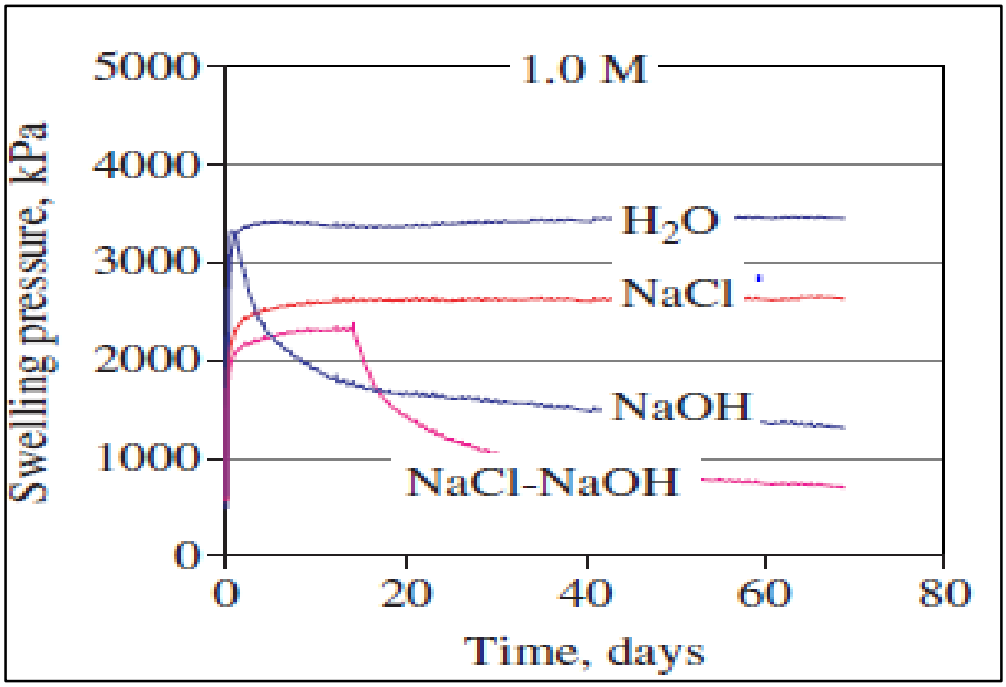

Figure 2.23. Swelling pressure response in four individual MX-80 samples (Karnland et al., 2007).

Karnland et al. (2007) conducted swelling pressure tests on three highly compacted MX-bentonite specimens. The specimens were initially saturated with de-ionized water for five days then replaced with 0.1, 0.3 and 1 M NaCl solutions, and finally after 60 days, replaced with 0.1 M NaOH (pH 12.9), 0.3 M NaOH (pH 13.3), and 1.0 M NaOH (pH 13.8), respectively. The test results showed that these specimens record maximum swelling pressures that exceed the recorded 3700 kPa in the H_2O solution after the first 5 days. Then the swelling pressure was significantly decreased when H_2O was replaced with the 1.0 M NaCl solution and significantly decreased in the 0.3 M NaCl solution. For the sample treated with the 0.1 M NaCl solution, the swelling pressure is slightly increased even after 60 days when the NaCl was replaced with NaOH, as shown in Figure 2.24.

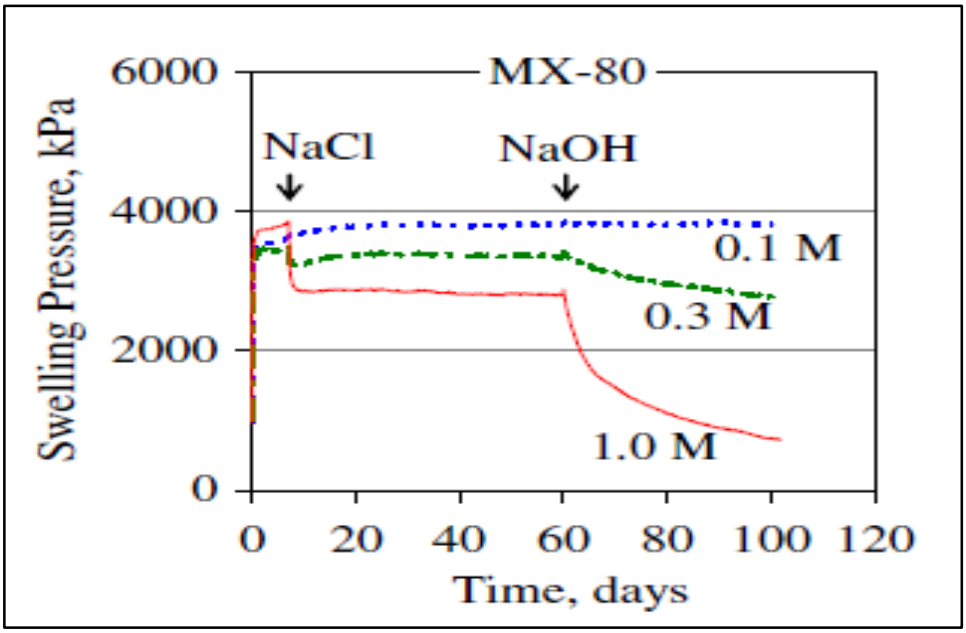

Figure 2.24. Swelling pressure of MX-80 bentonite samples exposed to 0.1, 0.3 and 1.0M NaCl/NaOH, respectively (Karnland et al., 2007).

2.4.2 Hydraulic conductivity

The hydraulic conductivity of bentonite is defined the rate of the water that flows through the fine-grained particles. It depends on the montmorillonite content, dry density, swelling pressure, void ratio, groundwater salinity, and temperature. The pore water chemistry and dry density have significant impacts on the hydraulic conductivity of bentonite. The hydraulic conductivity increases with increasing ionic strength of the surrounding groundwater and decreases with increasing dry density (Pusch, 2001; Batenipour, 2008; Cho et al., 2011).

Batenipour (2008) conducted a series of one-dimensional compression experiments on MX-bentonite that contained 75 wt. % montmorillonite. The experiments were performed with four different chemical solutions: DW, 100 g/L $CaCl_2$, 250 g/L $CaCl_2$ and constrained 250 g/L $CaCl_2$ under different effective montmorillonite dry densities (EMDDs). The test results confirmed that the hydraulic conductivity increases with increasing solution salinity, whereas the hydraulic conductivity (K) for the experiments with the 100 g/l $CaCl_2$ is several times higher than that of fresh water but less than that of the tests that used

250 g/l $CaCl_2$ for specimens with the same dry density. Furthermore, the hydraulic conductivity decreases with increasing EMDD, as shown in Figure 2.25.

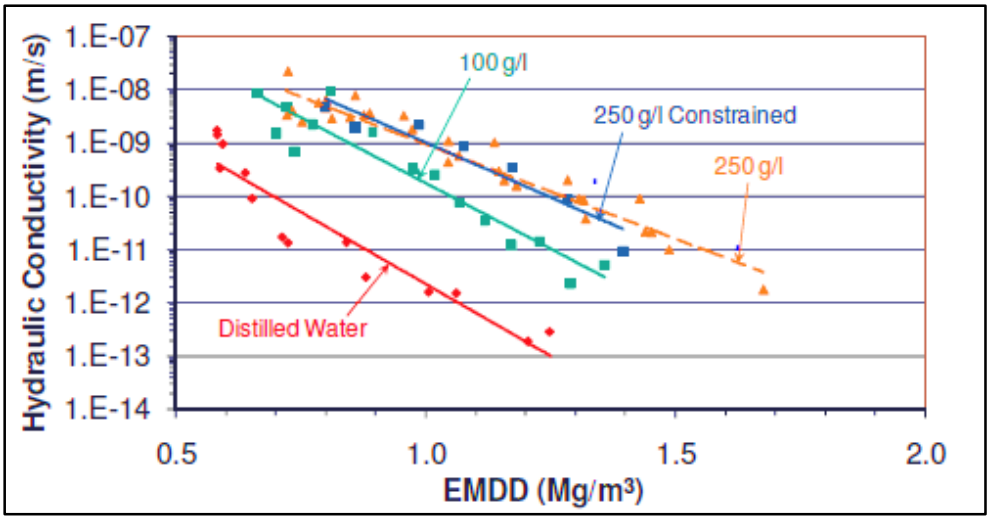

Figure 2.25. Hydraulic conductivity versus effective montmorillonite dry densities (EMDD) for loading paths (Batenipour, 2008).

Moreover, Cho et al. (2011) investigated the influence of water salinity on the hydraulic conductivity of compacted bentonite by using calcium bentonite, which contained 70% montmorillonite by mass. The experimental results demonstrated that the hydraulic conductivity for low dry density bentonite (1.0 Mg/m³), saturated with a 0.4 M NaCl solution, increases up to 7 times higher than that of the fresh water experiments. However, the hydraulic conductivity for bentonite with a dry density of 1.4 Mg/m³, saturated in the same solution (0.4 M NaCl) under the same conditions, is increased only 3 times greater than that of the fresh water experiments, as shown in Figures 2.26.a and 2.26.b. Furthermore, the hydraulic conductivity does not change with increases to the dry density of bentonite to more than 1.46 Mg/m³. It was reported that the test results of the compacted bentonite samples with a dry density of 1.6 and 1.8 Mg/m³, saturated in 0.0 to 0.4 M NaCl solutions, provide almost the same hydraulic conductivity values (Cho et al., 2011), as shown in Figures 2.26.c and 2.26.d. It can be observed that the hydraulic

conductivity of low dry density compacted bentonite decreases with increasing swelling pressure. When the compacted bentonite was saturated with water, several layers of the water molecules adsorbed on the montmorillonite surface and penetrated the innercrystalline structure. These adsorbed water particles caused expansion in the thickness of the double layer and innercrystalline swelling (Meunier, 2005). Therefore, the pore size is reduced as well as the flow rate.

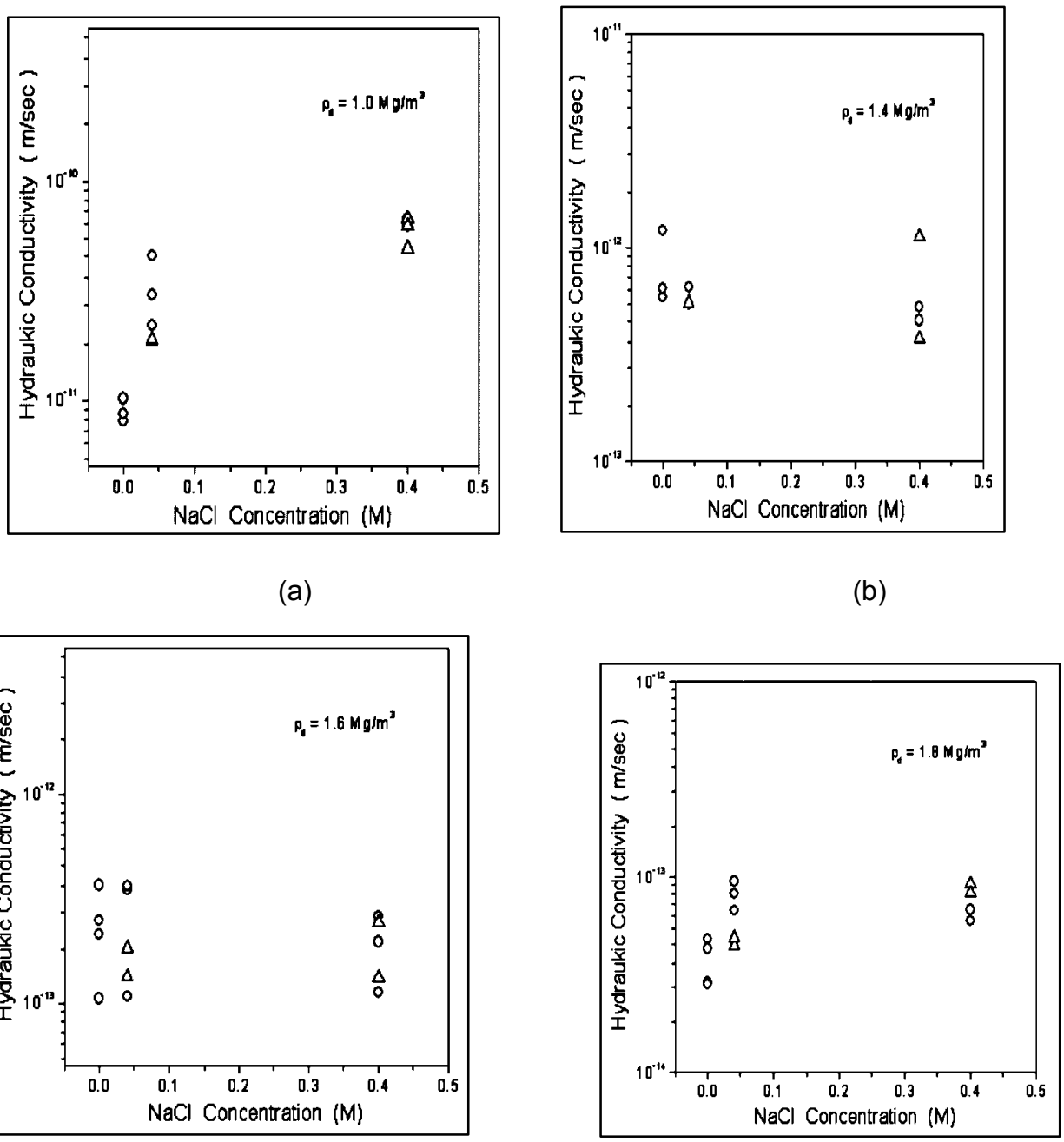

Figure 2.26. Hydraulic conductivity of compacted bentonite with a dry density of (a) 1.0 Mg/m^3 ; (b) 1.4 Mg/m^3; (c) 1.8 Mg/m^3 and (d) 1.8 Mg/m^3, at different salinities (Cho et al., 2011).

2.5 Effect of temperature on properties of bentonite based materials

The radioactive decay of HLW induces heat and raises the temperature on the container surface and of the bentonite buffer. Elevated temperature could dry out the inner part of the buffer which surrounds the canisters, thus inducing water vapor migration which increases the water movement from the inner part of the buffer to the host rock, as shown in Figure 2.27 (Quintessa, 2011). Moreover, high temperatures in the inner part of the buffer may cause the bentonite microstructure to fail, thus causing disordered lamellae of the smectite which then causes partial saturation of the bentonite. Therefore, elevated temperature has an impact on the engineering properties of compacted bentonite, such as the hydraulic conductivity and the swelling pressure. As a result, water movement increases and may also increase radionuclide release (Cho et al., 1999). Thus, it is very important to determine the impact of temperature changes on the hydraulic conductivity and swelling potential of compacted bentonite to ensure a safe performance of the DGR and durability of nuclear waste disposal means in the long term.

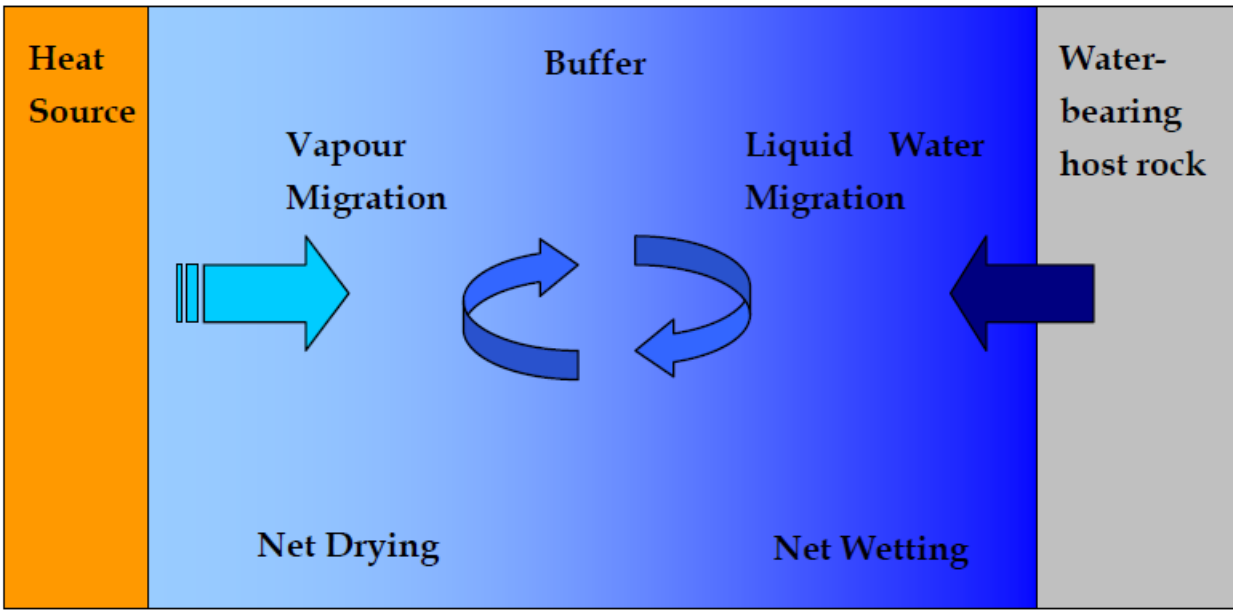

Figure 2.27. Migration of water vapor from the inner part of the buffer to the host rock (Quintessa, 2011).

2.5.1 Swelling pressure

Many studies have been conducted to gain a better understanding of the impact of temperature changes on the swelling pressure of compacted bentonite (Villar and Lloret, 2004; Villar et al., 2010; Ye et al., 2013). The impact of elevated temperature on the swelling pressure of Na-bentonite differs from that on Ca-bentonite depending on the prevalent exchangeable cations. The swelling pressure of Na-bentonite increases with increasing temperature, while the swelling pressure of Ca-bentonite decreases with increasing temperature (Pusch et al., 1990; Ye et al., 2013). Villar and Lloret (2004) performed several tests on FEBEX bentonite with prevalent exchangeable cations (Ca 42%, Mg 33%, Na 23% and K 2%) and a dry density of 1.58 g/cm^3. The tests results confirmed that the swelling pressure of Ca-bentonite decreases with increasing temperature from 20ºC to 90ºC and the swelling pressure might decrease to 2 MPa at 100ºC, as shown in Figure 2.28.

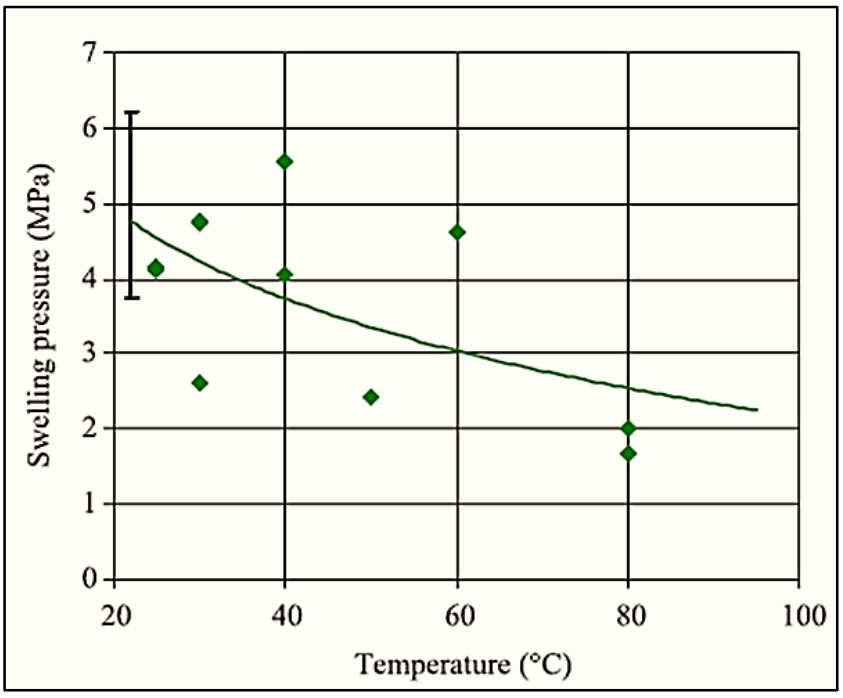

Figure 2.28. Swelling pressure as a function of temperature for FEBEX (Ca-bentonite) with average dry density of 1.58 g/cm (Villar and Lloret, 2004)

Moreover, Villar et al. (2010) determined the swelling pressure as a function of temperature for FEBEX bentonite at different dry densities by using high-pressure oedometer equipment. The experimental results confirmed that the swelling pressure of the saturated compacted Ca-bentonite with all dry densities significantly decreases when the temperature is increased up to 90ºC, as shown in Figure 2.29. It can be observed that the swelling pressure of the sample with a high dry density (1.7 Mg/m^3) is significantly reduced while the swelling pressure of the sample with a low dry density (1.5 Mg/m^3) is slightly reduced when the temperature is increased from 20ºC to 90ºC.

In addition, Villar et al. (2010) conducted saturated infiltration tests on compacted FEBEX bentonite with a dry density of 1.5 Mg/m^3 at temperatures that varied from 30ºC to 80ºC. The test results showed that the swelling pressure sharply increased at the beginning of the tests, but after a short time, the swelling pressure slowly increased. The sample tested at a low temperature (30ºC) recorded a swelling pressure of more than 3.1 kPa, while the sample tested at a higher temperature (80ºC) recorded a swelling pressure of less than 1.5 kPa, as shown in Figure 2.30.

Furthermore, Shariatmadari and Saeidijam (2011) conducted tests on the free swelling pressure, under a constant vertical load of 15 kPa on a Na-bentonite and silica sand mixture, with a ratio of 1:1 and a dry density of 1500 kg/m^3, under three temperatures (25ºC, 55ºC and 90ºC). The test results demonstrated that the swelling capacity of the bentonite-sand mixture decreases by 20% when the temperature is increased from 25ºC to 90ºC within 10,000 minutes, as shown in Figure 2.31.

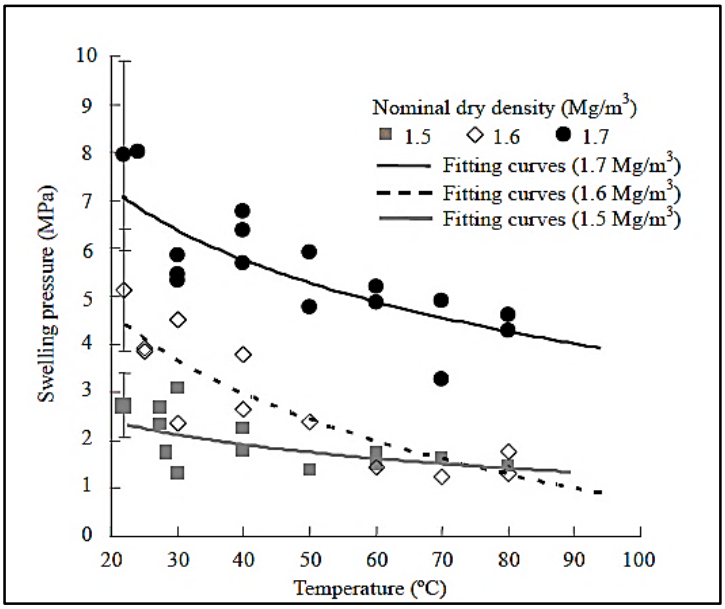

Figure 2.29. Swelling pressure as a function of temperature and dry density for saturated compacted FEBEX (Ca-bentonite) samples (Villar et al., 2010).

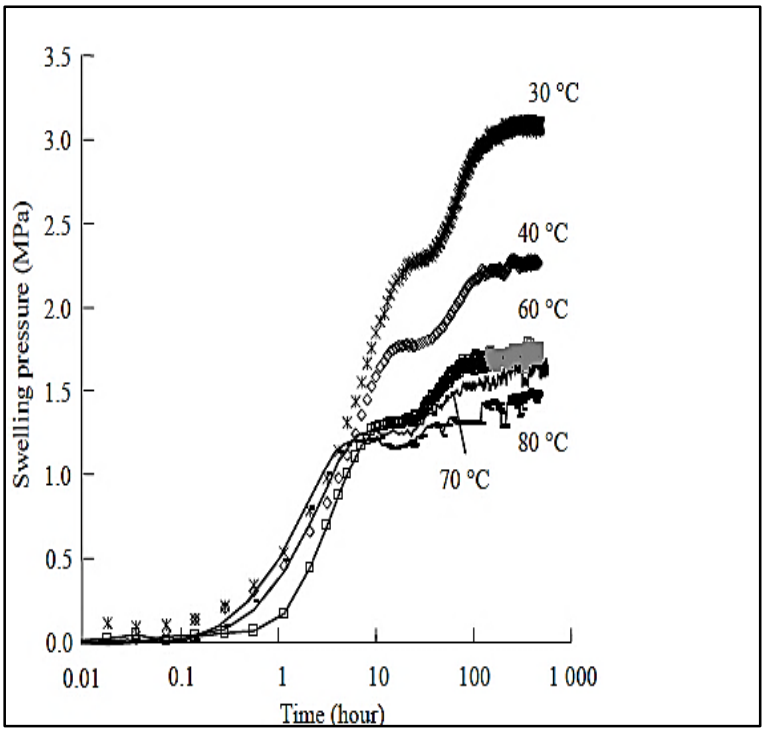

Figure 2.30. Variation of swelling pressure in infiltration tests performed at different temperatures for a compacted FEBEX bentonite sample (Villar et al., 2010).

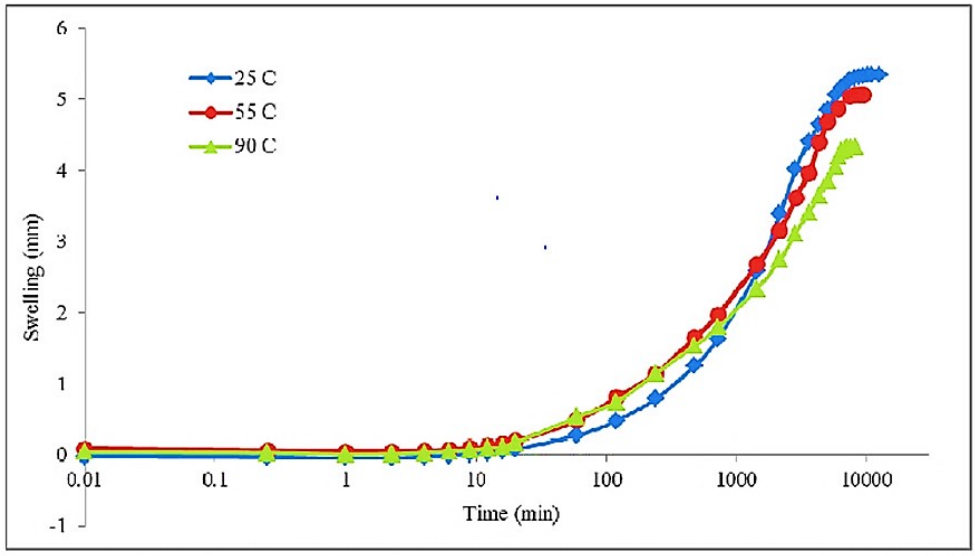

Figure 2.31. Free swelling of bentonite-sand mixture under constant vertical load of 15 kPa and temperatures of 25ºC, 55ºC and 90ºC (Shariatmadari and Saeidijam, 2011).

In contrast, the swelling pressure of Na-bentonite was found to increase with increasing temperature based on the experimental results of Pusch et al. (1990) and Ye et al. (2013). Ye et al. (2013) conducted swelling pressure and saturated infiltration tests with the temperature controlled on compacted GMZ01 bentonite with a dry density of 1.7 Mg/m^3, which contained 75.4 wt.% montmorillonite with major exchangeable cations, Na^+ 43.36%, Ca^{+2} 29.14%, Mg^{+2} 12.33%, and K^+ 2.51%, under different temperatures. The test results showed that the swelling pressure of Na-bentonite increases with increasing temperature, in which the samples tested at 40ºC and 20ºC record swelling pressures equal to 3.41 and 3.02 MPa, respectively, after reaching full saturation, as shown in Figure 2.32.

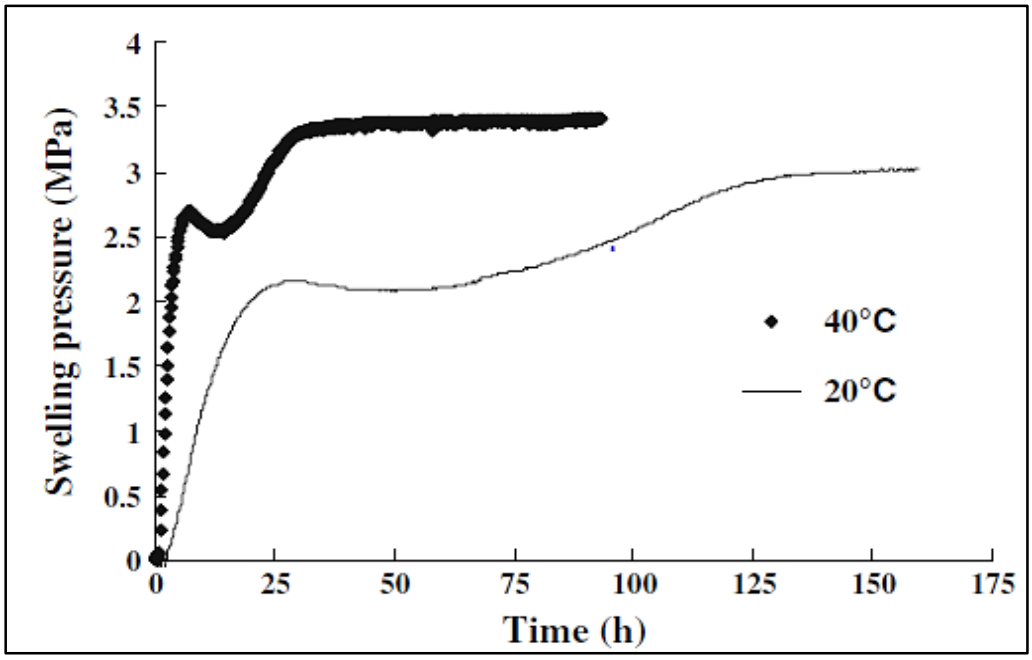

Figure 2.32. Swelling pressure of compacted GMZ01 (Na-bentonite) with dry density of 1.7 Mg/m^3 at different temperatures (Ye et al., 2013).

2.5.2 Hydraulic conductivity

Low hydraulic conductivity is considered to be one of the most important properties of buffers in order to eliminate groundwater contamination by preventing or delaying groundwater penetration into disposal repositories (Cho et al., 1999). However, the hydraulic conductivity of compacted bentonite is significantly affected by temperature changes. Villar and Lloret (2004), Villar et al. (2010), Cho et al. (1999) and Ye et al. (2013) investigated the impact of radioactive decay heat on the hydraulic conductivity of buffers. Their test results confirmed that hydraulic conductivity tends to increase with increasing temperature for both Na-bentonite and Ca-bentonite.

Ye et al. (2013) conducted infiltration experiments on compacted GMZ01 bentonite, with a dry density of 1.7 Mg/m^3, under different temperatures over time. The test results demonstrated that hydraulic conductivity increases with increasing temperature, as shown in Table 2.5. Once the test was started, the hydraulic conductivity sharply increased at a temperature of 40ºC, then was gradually reduced until it became stable

after 700 hours where it was recorded to be 2.75 x 10^{-13} m/s. It was observed that the increase in the hydraulic conductivity values with increase in temperature from 50ºC to 60ºC is nearly equal to the reduction in the hydraulic conductivity values when the temperature is reduced from 60ºC to 50ºC, as shown in Figure 2.33. Thus, the changes in hydraulic conductivity are independent of temperature change paths and any variation in the sample microstructure is reversed after removing the test conditions (Ye et al., 2013).

Table 2.5. Hydraulic conductivity of compacted GMZ bentonite independent of temperature change paths (data from experimental results in Ye et al. (2013)).

Temperature	**Hydraulic conductivity (m/s)**
40º C	2.75 x 10^{-13}
50º C	3.41 x 10^{-13}
60ºC	4.36 x 10^{-13}
50ºC	3.36 x 10^{-13}
20ºC	1.55 x 10^{-13}

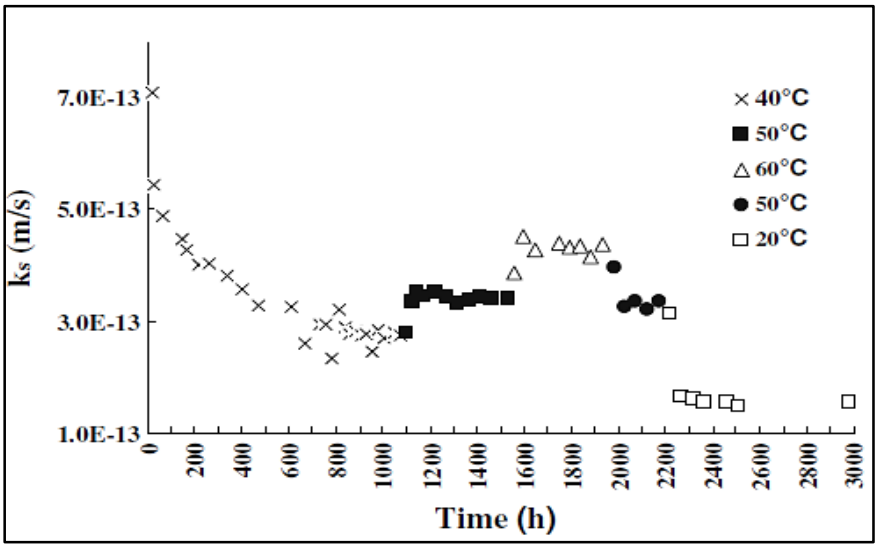

Figure 2.33. Hydraulic conductivity of compacted GMZ bentonite changes at different temperatures with time (Ye et al., 2013).

2.5.3 Possible mineralogical changes in bentonite

Elevated temperatures and high underground water salinity could affect the mineralogical stability of bentonite buffer based material when used as a component of an EBS and may cause: (i) smectite-to-illite conversion, and (ii) smectite to Fe-rich clay conversion (described in more detail below).

2.5.3.1 Smectite-to-illite conversion

In the literature, there are many discussions about the illization process. The conversion of montmorillonite to illite is controlled by temperature, the pH of the pore fluid, and concentration of potassium (Elert et al. 2008). Huang et al. (1993) concluded that smectite to illite conversion is mainly dependent on temperature, time and concentration of K^+ (Huang et al., 1993). Honty et al. (2004) indicated that temperature and water chemistry are the most important parameters that control illite formation. According to Wersin et al. (2007), smectite is naturally converted to illite at a very slow rate under heat conditions and in the presence of potassium. Finally, Quintessa (2011) concluded that temperature and time are the main parameters that allow a smectite-illite conversion.

Pore water chemistry and pH are the main factors that control the montmorillonite-illite conversion (Ureana et al., 2103; Eberl et al. 1993). The test results in Eberl et al. (1993) indicated that illization takes place in NaOH and KOH solutions under a temperature of 35ºC. Montmorillonite layers naturally convert to illite layers very slowly under high concentrations of potassium (Garrels, 1984), as shown below:

$$K^+_{0.33}(Al_{1.5}Fe^{3+}Mg^{2+}_{0.27})(Al_{0.06}Si_{3.94})O_{10}(OH)_2 + 0.47KAlSi_3O_8 \rightarrow$$

$$K^+_{0.80}(Al_{1.5}Fe^{3+}Mg^{2+}_{0.27})(Al_{0.53}Si_{3.47})O_{10}(OH)_2 + 1.88SiO_2$$

The availability of monovalent (Na, K) and divalent cations (Ca, Mg) in bentonite pore water replaces the initial Na-montmorillonite (exchange reaction) and/or converts the

swelling components into non-swelling components, such as illite, in the presence of silica sand and accessory minerals, such as calcite, gypsum, celestite, fluorite and quartz.

The illitization process could happen due to the:

I. changes in the composition of the interlayers where Na^+ is substituted with K^+ in the presence of strong solutions, and Al^{3+} is replaced with Si in the tetrahedral position without any changes in the octahedral layer (Garrels, 1984), or
II. dissolution and precipitation process, where smectite dissolves and induces Si which participates as a cement component of SiO_2 (Eberl et al., 1993; Pusch, 1998, 2002; Wersin et al., 2007; Kaufhold and Dohrman, 2011), as illustrated below:

$$\text{Na-smectite} + K^+ + Al^{3+} \rightarrow \text{Illite} + Si^{4+} \qquad \text{(Wersin et al., 2007)}$$

Laboratory experiments by Ureana et al. (2103) confirmed that the montmorillonite to illite conversion takes place within 15 to 30 days of curing with magnesium hydroxide, seawater, or olive mill wastewater with different concentrations. Furthermore, Karnland and Birgersson (2006) concluded that bentonite that contains at least 75% montmorillonite by mass, requires the availability of 5% K^+ by mass in order to have full illization of the buffer material.

2.5.3.2 Smectite to Fe-rich clay conversion

In DGRs for SF and HLW, copper, iron and steel are the main proposed materials for container materials (RWM, 2003; NWMO, 2007). The presence of these types of nuclear waste containers in contact with underground saline water under water with heat decay conditions for a long period of time may lead to container corrosion and the release of iron (Fe) as a corrosion product (NWMO, 2007; Nagra et al., 2008). Therefore, the interaction between bentonite and Fe in the presence of highly saline water and under thermal conditions for a long period of time could cause mineralogical changes in

bentonite (Kamei et al., 1999; Drief et al., 2001; Wilson et al., 2007; Mosser-Ruck et al., 2010; Osacký et al., 2010).

The interaction of bentonite and Fe has been studied for many years and the reaction pathways have been found to depend on the temperature, pH, liquid to clay ratio (L/C), Fe to clay ratio (Fe/C), and the nature of the initial bentonite (Lantenois et al. 2005; Mosser-Ruck et al., 2010), as shown in Figure 2.34. The expected reaction pathways for bentonite and the corrosion product of the nuclear waste could be:

I. conversion of montmorillonite to Fe-rich smectite in an ion exchange reaction, where Na^{+} is replaced with Fe^{2+} without changing the minerals in the bentonite (Kamei et al. 1999; Wilson et al., 2006a), and
II. montmorillonite converts to non-swelling Fe-rich 1:1 7 Å clay (berthierine, odinite) or 14 Å (chlorite) under very high temperature conditions (Drief et al. 2001; Guillaume et al., 2003; Lantenois et al., 2005; ; Wilson et al. 2006; Mosser-Ruck et al., 2010; Osacký et al., 2010).

Lantenois et al. (2005) investigated the interaction between smectite and Fe at a temperature of 80ºC for 45 days and under basic pH conditions (pH > 7). The test results demonstrated that smectite destabilized to form a phyllosilicate 1:1 layer structure clay (7 Å phase) through the reaction pathway given below:

Metal Fe + smectite $\longrightarrow$ 1:1 Fe-rich phyllosilicate (odinite) + Fe oxides

When smectite interacts with Fe at a high temperature of 300ºC, the reaction pathway is different and the subsequent crystallization products are Fe rich 14 Å chlorite phase and releases quartz, feldspars and zeolites (Guillaume et al., 2003).

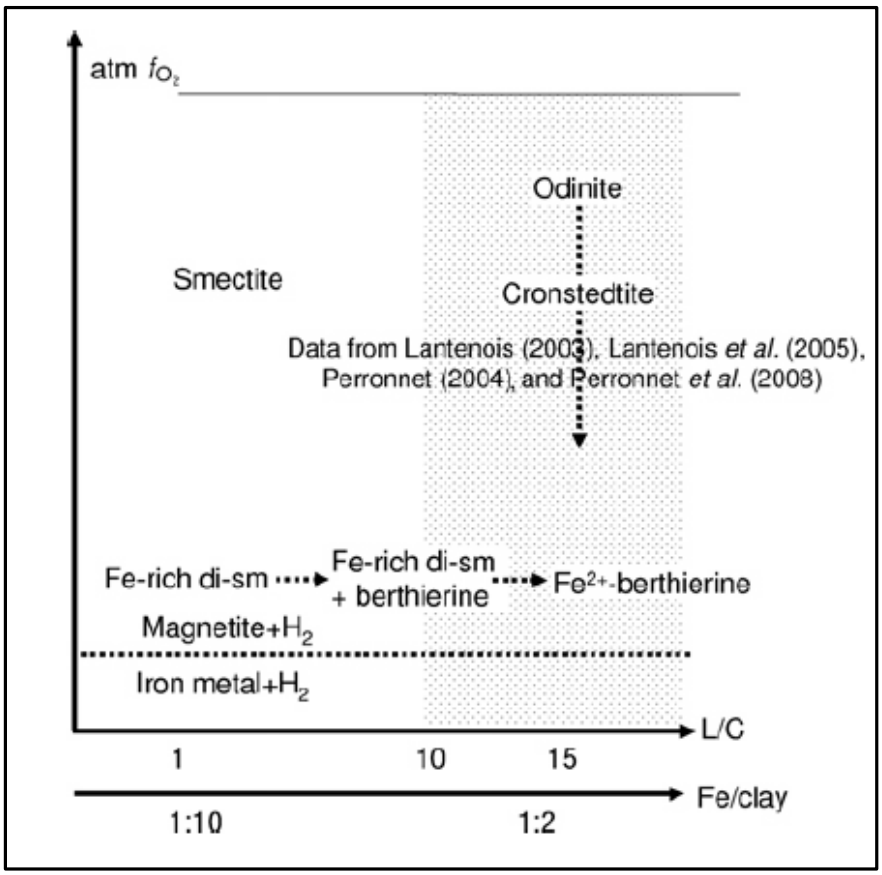

Figure 2.34. Smectite and Fe reaction pathway which depends on the redox state, availability of Fe, and liquid to clay ratio at low temperatures (source: Mosser-Ruck et al., 2010).

2.6 Conclusions

The following conclusions can be drawn from the literature review presented in this chapter.

- Bentonite has an excellent swelling potential and very low hydraulic conductivity, and chosen for usage as an engineered barrier material in DGRs in Canada and many other countries.
- The Canadian DGR has been proposed to be constructed in one of sixteen locations in Ontario or in one of three locations in Saskatchewan. The DGR will be constructed at a depth of 300 to 700 m, and it is anticipated that the temperature of the container surface and bentonite buffer will remain under 100ºC (RWM, 2003;

NWMO, 2012). The geochemical nature of the underground water within the sedimentary formations that underlie Ontario at a depth of more than 200 m is characterized by highly salinized water.

- Previous studies have shown that the swelling pressure of compacted bentonite increases with increases in the degree of saturation up to 7 MPa and may produce high pressure (mechanical stress) onto the canisters and the surrounding rocks (Pusch and Yong, 2006; Quintessa, 2011). Therefore, Canada and many other countries are considering mixing bentonite with sand to reduce the mechanical stress (RWM, 2003; Quintessa, 2011; Cho et al., 2011). The minimum acceptable mixing weight ratio is 30% bentonite to 70% ballast (Pusch and Yong, 2006; Quintessa, 2011).
- The water salinity of the reacting solutions significantly affects the swelling capacity and hydraulic conductivity of bentonite. Furthermore, the swelling pressure and hydraulic conductivity of bentonite not only differs from one solution to another, with regards to the ionic strength, but also varies with chemical concentration for the same solution (Batenipour, 2008; Karnland et al., 2007). The temperature significantly impacts the hydraulic conductivity of bentonite as well as the swelling potential. The mineralogical composition of the bentonite may change after reacting with a saline water solution or nuclear waste corrosion product under thermal conditions for a long period of time (Kamei et al., 1999; Drief et al., 2001; Wilson et al., 2007; Mosser-Ruck et al., 2010; Osacký et al., 2010).
- None of the previous studies have investigated the coupled effect of the underground water chemistry found in Ontario and the expected heat decay of a DGR on a bentonite-sand mixture (30/70, by weight, as the proposed mixture ratio for the buffer and backfill materials). In order to simulate the possible reaction conditions in a DGR located in Ontario, the triple effects of corrosion products from the nuclear waste container, underground water chemistry found in Ontario, and elevated temperature on the bentonite-sand mixture should be investigated and considered in the design of the EBS. No studies have been addressed in the literature to discuss these issues until now.

2.7 References

Alonso, J. (2003) bentonite barriers in integrated performance assessment - BENIPA Project, ENRESA, Spain. Scientific and Technical Report EUR

Athanassopoulos, C. (2011) Natural Sodium versus Activated Calcium Bentonite in Geosynthetic Clay Liners (GCLs) , Solid Waste & Recycling conference with Trade Show, May.

Baisden, P.A. and Choppin, G.R (2007) nuclear waste management and the nuclear fuel cycle. Radiochemistry and Nuclear Chemistry. Radiochemistry and nuclear chemistry – vol. 2

Batenipour, Hamid (2008) Effect of water salinity on the hydro-mechanical behavior of granular bentonite as light backfill material, GeoEdmonton'08/GéoEdmonton2008

Canadian Nuclear Safety Commission (CNSC) Nuclear Power Plants website http://www.nuclearsafety.gc.ca/eng/licenseesapplicants/powerplants/index.cfm

Carlson, L. (2004) Bentonite mineralogy, Part 1: Methods of investigation – a literature review, Part 2: Mineralogical research of selected bentonites, working report 2004–02, Posiva Oy, Olkiluoto, Finland

Cho, W., Kim, J., and Choi, J. (2011) Influence of Water Salinity on the Hydraulic Conductivity of Compacted Bentonite, J. of the Korean radioactive waste society. vol.9 (4), pp. 199-206, Dec.

Cho, W., Lee, J. and Kwon, S. (2012) An analysis of the factors affecting the hydraulic conductivity and swelling pressure of Kyungju ca-bentonite for use as a clay-based sealing material for a high-level waste repository, Nuclear Engineering and technology, vol.44 no.1 February

Cho, W.J. , Lee, J.O. and Kang, C.H. (2000) Hydraulic Conductivity of Bentonite-Sand Mixture for A Potential backfill Material for a High-level Radioactive Waste Repository, J. of the Korean nuclear society, vol. 32, pp. 495-503.

Cho, W.J., Lee, J.O., Chun, K.S. and Hahn, D.S.(1999) Basic Physicochemical Properties of Domestic Bentonite for Use as a Buffer Material in a High-level Radioactive Waste Repository," J. of the Korean Nuclear Society, vol. 31, pp. 39-50

Cho, W.J., Lee, J.O., Chun, S.K. (1999a) The temperature effects on hydraulic conductivity of compacted bentonite, Applied Clay Science 14 47–58

Cui, S., Zhang, H., and Zhang, M. (2012) Swelling characteristics of compacted GMZ bentonite–sand mixtures as a buffer/backfill material in China. Engineering Geology 141–142, 65–73

Delage, P., Cui, Y. J. and Tang, A. M (2010) Clays in radioactive waste disposal, Journal of Rock Mechanics and Geotechnical Engineering. 2 (2): 111–123

Dhawan, S. and Rao, M. (2010) effect of heating and pore water salinity on the swelling characteristics of bentonite buffer. Clays in natural & engineered barriers for radioactive waste confinement, 4TH International meeting – March 2010 – Nantes, France

Dollar, P.S. (1988) Geochemistry of Formation Waters, Southwestern Ontario, Canada and Southern Michigan, U.S.A. Implications for Origin and Evolution. M.Sc. Thesis. University of Waterloo, Canada.

Drief, A., Nieto, F., and Sanchez-Navas, A. (2001) Experimental clay-mineral formation from a subvolcanic rock by interaction with 1 m naoh solution at room temperature. Clays and Clay Minerals, VoL 49. No. I. 92-106. 2001.

Eberl, D.D., Velde, B. and McCormick, T. (1993) Synthesis of illite-smectite from smectite at earth surface temperatures and high pH. Clay Minerals 28, 49–60.

Elert, K., Sebastian, E., Valverde, I. and Rodriguez-Navarro, C. (2008) Alkaline treatment of clay minerals from the Alhambra Formation: Implications for the conservation of earthen architecture. Appl Clay Sci 39:122–32.

García-Gutiérrez, M., Cormenzana, J.L., Missana, T., Alonso, U. and Mingarro, M. (2011) Diffusion of strongly sorbing cations (60Co and 152Eu) in compacted FEBEX bentonite. Physics and Chemistry of the Earth, 2011, Vol.36 (17), pp.1708-1713 [Peer Reviewed Journal]

Garrels, R. (1984) Montmorillonite/Illite stability diagrams. Clays and Clay Minerals, Vol. 32, No. 3, 161-166.

Gens, A. and Alonso, E.E. (1992) A framework for the behavior of unsaturated expansive clays. Canadian Geotechnical Journal, 29: 1013-1032.

gesellschaft für anlagen-und reaktorsicherheit. November. GRS – 295, ISBN 978-3-939355-72-4.

Grim, R. (1968) Clay mineralogy. Book 2nd Edition, McGraw-Hill, 1968.

Grim, R. and Güven, N. (1978) Bentonite: Geology, Clay Mineralogy Properties and Users. Vol. 24 Developments in Sedimentology. Elsevier, 1978.

GRS (2011) Fe-bentonite experiments and modelling of the interactions of bentonites with iron.

Guillaume, D., Neaman, A., Cathelineau, M., R. Mosser-Ruck, Peiffert, C., Abdelmoula, M., Dubessy, J., VilliE, F., Baronnet, A. and Michau, N. (2003) Experimental synthesis of chlorite from smectite at 300ºc in the presence ofmetallic Fe. Clay Minerals 38,281 –302

Herbert, H., Kasbohm, J., Sprenger, H., Fernández, A.M. and Reichelt, C. (2008) Swelling pressures of MX-80 bentonite in solutions of different ionic strength, Physics and Chemistry of the Earth 33. S327–S342

Hicks, T.W., White, M.J. and Hooker, P.J. (2009) Role of bentonite in determination of thermal limits on Geological Disposal Facility design. Galsons Sciences Ltd., Report 0883-1 (v 2.0) for Nuclear Decommissioning Authority, Harwell.

Honty, M, Uhlik, P., Sucha, V, Caplovicova, M., Francu, J, Clauer, and Biron, N.(2004) smectite-to-illite alteration in salt-bearing bentonites (the East Slovak Basin) Clays and Clay Minerals, Vol. 52, No. 5, 533–551.

Huang, W.L, Longo, J.M. and Pevear, D.R. (1993) An experimentally derived kinetic model for smectite-to-illite conversion and its use as a geothermometer. Clays and Clay

IAEA (2007) Estimation of Global Inventories of Radioactive Waste and Other Radioactive Materials. Iaea-Tecdoc-1591. June.

IMA-NA (2009) The Industrial Minerals Association - North America

Jensen, M., Lam, T., Luhowy, D., McLay, J., Semec, B. and Frizzell, R. (2009) Ontario Power Generation's Proposed L&ILW Deep Geologic Repository: An Overview of Geoscientific Studies. Nuclear Waste Management Organization, GeoHalifax2009/GéoHalifax2009

Johannesson, L.E. and Börgesson, L. (2002) Friedland Clay as backfill material Results of laboratory tests and swelling/compression calculations. Äspö Hard Rock Laboratory, SKB International Progress Report, 2002-50.

Kamei, G., Oda, C., Mitsui, S., Shibata, M. and Shinozaki, T. (1999) Fe (II)-Na ion exchange at interlayers of smectite: adsorption-desorption experiments and a natural analogue. Eng. Geol. 54, 15–20.

Karnland, O., Olsson, S., Nilsson, U. and Sellin, P. (2007) Experimentally determined swelling pressures and geochemical interactions of compacted Wyoming bentonite with highly alkaline solutions, Physics and Chemistry of the Earth 32, 275–286.

Karnland,O., Olsson, S. and Nilsson, U. (2006) Mineralogy and sealing properties of various bentonites and smectite-rich clay materials. Clay Technology AB, Technical Report TR-06-30.

Kaufhold, S and Dohrman, R. (2011) Stability of bentonites in salt solutions III — Calcium hydroxide. Applied Clay Science 51 (2011) 300–307.

Kim, J.S., Kwon, S.K., Sanchez, M. and Cho, G.C. (2011) Geological Storage of High Level Nuclear Waste. KSCE Journal of Civil Engineering 15(4):721-737

King, F., LeNeveu, D.M. and Jobe, D.J. (1994) Modelling the effects of evolving redox conditions on the corrosion of copper containers, Mat. Res. Soc. Symp. Proc. Vol. 333. ©1994 Materials Research Society

Komine, H. (2004) Simplified evaluation on hydraulic conductivities of sand–bentonite mixture backfill. Applied Clay Science 26, 13– 19

Kursten, B., Smailos, E., Azkarate, I., Werme, L., Smart, N.R., Marx, G., Cuñado, M.A. and Santarini, G. (2004) Corrosion evaluation of metallic materials for long-lived hlw/spent fuel disposal containers: Review of 15-20 Years of Research. EURADWASTE '04 (6th EC conference on the management and disposal of radioactive waste) March – 1 April, Luxembourg

Laine, H. and Karttunen, P. (2010) Long-Term Stability of Bentonite- A Literature Review, Working Report 53, POSIVA

Lantenois, B., lanson, B., Muller, F., Bauer, A., Jullien, A. and Plancë, A. (2005) Experimental study of smectite interaction with metal Fe at low temperature: 1. Smectite destabilization. Clays and Clay Minerals, Vol. 53, No. 6, 597±612.

Liu, L., Neretnieks, I. and Moreno, L. (2011) Permeability and expansibility of natural bentonite MX-80 in distilled water. Physics and Chemistry of the Earth 36, 1783–1791

Lloret, A., Villar, M. V., Sanchez, M., Gens, A., Pintado, X. & Alonso, E. E. (2003) Mechanical behaviour of heavily compacted bentonite under high suction changes, Géotechnique, 2003, Vol.53(1), pp.27-40

Madsen, F. T. (1998) Clay mineralogical investigations related to nuclear waste disposal. Clay Minerals (1998) 33, 109-129.

Man, A. , Priyanto, D., Siemens, G. and Blatz, J.(2010) The effect of pore fluid chemistry on strength and stress strain behaviour of light and dense backfill materials, clays in natural & engineered barriers for radioactive waste confinement, 4th international meeting – March 2010 – nantes, France

Martin, F.A., Bataillon, C. and Schlegel, M.L. (2008) Corrosion of iron and low alloyed steel within a water saturated brick of clay under anaerobic deep geological disposal conditions: An integrated experiment. Journal of Nuclear Materials 379, 80–90.

Marty, N.C.M., Fritz, B., Clément, A. and Michau, N. (2010) Modelling the long term alteration of the engineered bentonite barrier in an underground radioactive waste repository. Applied Clay Science 47, 82–90.

Melamed, A. and Pitkanen, P. (1996) Chemical and mineralogical aspects of water-bentonite interaction in nuclear fuel disposal conditions, VTT Communities and Infrastructure.

Mesri, G., and Olson, R. E. (1970) Shear strength of montmorillonite, Ge´otechnique, Vol. 20, No. 3, pp. 261–270.

Meunier, A. (2005) Clays. Springer-Verlag Berlin Heidenberg Germany (book)

Mitchell, J. K., Soga, K. (1993) Fundamentals of Soil Behavior, Book 2nd Edition, John Wiley & Sons, Inc.

Moore, D.M. and Reynolds, R.C. (1989) X-ray diffraction and the identification and analysis of clay minerals. New York City: Oxford University Press; Oxford.

Mosser-Ruck, R., Cathelineau, M., Guillaume, D., Charpentier, D., Rousset, D., Barres, O. and Michau N. (2010) Effects of temperature, pH and iron/clay and liquid/clay ratios on experimental conversion of dioctahedral smectite to berthierine, chlorite, vermiculite, or saponite. Clays and Clay Minerals, Vol. 58, No. 2, 280–291.

Nagra, P. W., Birgersson, M., Olsson, S., Karnland, O., Snellman, M., Oy, S. and Oy, R. (2008) Impact of corrosion-derived iron on the bentonite buffer within the KBS-3H disposal concept. The Olkiluoto site as case study. R-08-34.

NWMO (2007) Overview of a Carbon Steel Container Corrosion Model for a Deep Geological Repository in Sedimentary Rock. Nuclear Waste Management Organization TR-2007-01

NWMO (2010) Moving forward together: process for selecting a site for Canada's deep geological repository for used nuclear fuel, Nuclear Waste Management Organization, MAY 2010.

NWMO (2011) OPG's deep geologic repository project for low and intermediate level waste. Environmental impact statement volume 1: main report, 00216-REP-07701-00001-R000. Nuclear Waste Management Organization, March 2011

NWMO (2011a) Regional hydrogeochemistry – Southern Ontario. Nuclear Waste Management Organization, NWMO DGR-TR-2011-12.

NWMO (2012) Newsletter, Nuclear Waste Management Organization, volume 10, issue 3 June.

Osacký, M., Šucha, V., Czímerová, A. and Madejová, J. (2010) Reaction of smectites with iron in a nitrogen atmosphere at 75 °C. Applied Clay Science 50, 237–244

Pastina, B. and Hellä, P. (2006) Expected evolution of a spent nuclear fuel repository at Olkiluoto. posiva report 2006-05. Posiva Oy, Olkiluoto, Finland

Pucsh, R. (2008) Geological Storage of Highly Radioactive Waste: Current Concepts and Plans for Radioactive Waste Disposal. Springer,

Pusch, R. (1982) Mineral-water interactions and their influence on the physical behaviour of highly compacted Na bentonite. Canadian Geotechnical Journal, 19: 381-387

Pusch, R. (2001) Experimental study of the effect of high porewater salinity on the physical properties of a natural smectite clay, Technical Report TR-01-07, KSB

Pusch, R., and Yong, R. N. (2006) Microstructure of Smectite Clays and Engineering Performance. Book, Taylor & Francis.

Pusch, R., Karlnland, O. and Hokmark, H. (1990) GMM-a general micro-structural model for qualitative and quantitative studies of smectite clays. SKB Technical Report, Stockholm, Sweden 90–93

Quintessa (2011) Bentonite; A Review of key properties, processes and issues for consideration in the UK context. QRS-1378ZG-1, Version 1.1, February

Rautioaho, E. and Korkiala-Tanttu, L. (2009) Bentomap: Survey of bentonite and tunnel backfill knowledge. VTT Technical Research Centre of Finland. 1459-7683. ISBN 978-951-38-7194-9.

Rebak, R. B. (2011) Environmental degradation of engineered barrier materials in nuclear waste repositories, Uhlig's Corrosion Handbook, Third Edition, Edited by R. Winston Revie. John Wiley & Sons, Inc.

RWM (2003) Engineered Barrier Systems and the Safety of Deep Geological Repositories, Radioactive Waste Management, ISBN 92-64-18498-8

Saito, Ed. and Murata, S. (2003) Environmental Rock Engineering (book) CRC Press; ISBN-10: 9058095568. Edition: 1st.

Samuels, S.G. (1950) The effect of Base Exchange on the engineering properties of soils. Build. Res. Stn. G.B., Note, C176.

Savage, D. (2005). The effects of high salinity groundwater on the performance of clay barriers. SKI Report 2005-54. Swedish Nuclear Power Inspectorate, Stockholm, Sweden.

Shariatmadari, N. and Saeidijam, S. (2012)The effect of thermal history on thermo-mechanical behavior of bentonite-sand mixture. International Journal of Civil Engineering, Vol. 10, No. 2, June.

Siemens, G. and Blatz, J.A. (2007) Development of a hydraulic conductivity apparatus for bentonite soils, Can. Geotech. J. 44: 997–1005.

Steefel, C., Rutqvist, J., Tsang, C.F., Liu, H.H., Sonnenthal, E., Houseworth, J. and Birkholzer, J. (2010) Reactive transport and coupled THM processes in engineering barrier systems (EBS). Lawrence Berkeley national laboratory (LBNL), 09-10-2010.

Ureana, C., Azañón, J.M. ,Corpas, F., Nieto, F., León, C. and Pérez, L. (2103) Magnesium hydroxide, seawater and olive mill wastewater to reduce swelling potential and plasticity of bentonite soil. Construction and Building Materials 45, 289–297

Ureana, C., Azañón, J.M., Corpas, F., Nieto, F., León, C. and Pérez, L. (2013) Magnesium hydroxide, seawater and olive mill wastewater to reduce swelling potential and plasticity of bentonite soil. Construction and Building Materials 45, 289–297.

Villagran, J.E. (2012) Development of a Monitoring Program for a Deep Geological Repository for Used Nuclear Fuel NWMO. NWMO TR-2012-18.

Villar, M. V., Gómez-Espina, R. and Lloret, A. (2010) Experimental investigation into temperature effect on hydro-mechanical behaviors of bentonite, Journal of Rock Mechanics and Geotechnical Engineering. 2 (1): 71–78

Villar, M.V. and Lloret, A. (2004) Influence of temperature on the hydro-mechanical behaviour of a compacted bentonite, Applied Clay Science 26 (2004) 337– 350

Villar, M.V. and Lloret, A. (2008) Influence of dry density and water content on the swelling of a compacted bentonite, Applied Clay Science 39 (2008) 38–49

Wang, Q.,Tang, A., Cui, Y., Delage, P. and Gatmiri, B. (2012) Experimental study on the swelling behaviour of bentonite/claystone mixture. Engineering Geology 124, 59–66

Wersin, P, Johnson, L.H and McKinely, I.G. (2007) Performance of the bentonite barrier at temperatures beyond 100ºC: A critical review. Physics and Chemistry of the Earth 32, 780–788.

Wilson, J., Cressey,G., Cressey, B., Cuadros , J., Ragnarsdottir, K., Savage, D. and Shibata, M. (2006) The effect of iron on montmorillonite stability.(II) Experimental investigation. Geochimica ET Cosmochimica Acta 70, 323–336

Wilson, J., Cuadros, J., Ragnarsdottir, K., Savage, D. and Shibata, M. (2006a) The effect of iron on montmorillonite stability. (I) Background and thermodynamic considerations. Geochimica ET Cosmochimica Acta 70, 306–322

WNA (2014) World Nuclear Association, Radioactive Waste Management. http://www.world-nuclear.org/info/Nuclear-Fuel-Cycle/Nuclear-Wastes/Radioactive-Waste-Management.

Ye, W. M., Wan, M., Chen, B., Chen, Y.G., Cui, Y. J. and Wang, J. (2013) Temperature effects on the swelling pressure and saturated hydraulic conductivity of the compacted GMZ01 bentonite, Environ Earth Sci, 68:281–288, DOI 10.1007/s12665-012-1738-4

Chapter 3- Technical Paper I: Impact of groundwater chemistry and temperature on the engineering, micro-and nano-structural properties of bentonite-sand barrier materials for nuclear waste repositories

Abstract

Compacted bentonite-sand materials are evaluated as the key materials for the construction of an engineered barrier system (EBS) for a deep geological repository (DGR) in Canada and also for other countries. The bentonite based barrier will be simultaneously exposed to a wide range of aggressive underground water chemistry (C) and thermal (T) conditions. Thus, the understanding of the coupled effects of these T and C conditions on the evolution of the engineering properties (swelling and hydraulic properties), as well as on the micro- and nano-structures of the bentonite-based barrier, is essential for the assessment of the durability and safety of the EBS in a DGR in Ontario. This study experimentally investigates the impact of deep underground water (C), impact temperatures (T), and coupled effect of C and T in Guelph and Trenton, Ontario, on the engineering properties, microstructure and nano-structure of a bentonite-sand barrier mixture (30 to 70% by weight). The results obtained show that the groundwater chemistry found in Ontario has a significant impact on the swelling characteristics and hydraulic conductivity of the studied bentonite-sand material. The swelling ability significantly decreases and the hydraulic conductivity increases more than three orders. The temperature has a limited effect. Future safety assessments and the final engineering design of an engineered barrier for a DGR in Ontario should take into consideration the

possibility of the long term deterioration of a bentonite-sand barrier by chemical attacks induced by the aggressive groundwater.

3.1 Introduction

Nowadays, there are numerous applications for nuclear technology, in medical, industrial, transportation and agricultural fields. Nuclear power produces about 11 percent of the electricity in the world, without releasing any greenhouse gas, according to a report by the World Nuclear Association (2013). Canada and more than 30 countries, such as Belgium, Finland, France, Sweden, and Japan, are using nuclear technology which results in producing millions of spent fuel (SF) bundles, and low and intermediate level (L & IL) radioactive waste every year. Deep geological repositories (DGRs) for nuclear waste have been recognized as a promising technology for the long term management of this type of radioactive waste. Therefore, several countries, including Canada, are planning to construct DGRs for nuclear waste.

A DGR is a permanent storage place for nuclear waste for thousands of years. The DGR would be located at a depth of 500 to 700 m under the ground surface and surrounded by multiple natural barriers of solid bed rock formations as well as engineered barrier systems (EBS) to protect the surrounding environment (RWM, 2003, NWMO; 2010). Compacted bentonite has been studied for more than three decades as an appropriate material that would be a component of the EBS in a DGR (Cho et al; 1999; Karnland; 2006, Quintessa; 2011). This is due to its contents of clay minerals of the smectite group which has excellent swelling ability and adsorption capacity, high cation exchange capacity (CEC), low permeability and thermal conductivity, high plasticity, and self-sealing properties (Pusch, 1982; Mitchell, 1993; Melamed and Petteri, 1996; Quintessa, 2011). These favorable engineering properties restrict the transport of contaminants into the biosphere, which is critical for safety with the use of a DGR. However, compacted bentonite has a very high swelling pressure which increases with increases in the degree of saturation. The development of excessive swelling pressure of compacted bentonite, when it comes into contact with underground water in a DGR, may lead to the mechanical damage of the canisters and surrounding rocks (Pusch and Yong,

2006). This would obviously jeopardize safety with the use of the DGR. For this reason, Canada and many other countries have considered the use of a mixture of bentonite with sand as the barrier material in order to reduce the mechanical stress (RWM, 2003; Quintessa, 2011; Cho et al., 2011).

The Nuclear Waste Management Organization (NWMO) is currently investigating sixteen locations in Ontario and three locations in Northern Saskatchewan to construct a DGR for burying nuclear wastes (NWMO, 2012). For example, the construction of a DGR for low and intermediate level radioactive waste (L&ILW) in the Municipality of Kincardine at a depth of 680 m is currently being investigated. However, the deep groundwater in the Kincardine region, like in many regions in Ontario, is characterized by water with high salinity (Jensen et al., 2009; NWMO, 2013). In addition, the presence of bentonite-sand in a DGR that is surrounded by highly salinized groundwater under confining stress and high temperature may deteriorate the favorable engineering (e.g. swelling and hydraulic properties) and physiochemical properties of the compacted bentonite-sand material. As a result, the performance and durability of the engineered system could change and affect the overall safety of the DGR (Villar and Lloret, 2004; Karnland et al., 2007; Herbert et al., 2008; Cho et al., 2011). No studies have addressed this issue until now.

The objective of this research is therefore to investigate the impact of the underground water salinity found in Ontario and heat generated by nuclear waste on the engineering (swelling and hydraulic properties), microstructural and nano-structural properties of bentonite-sand based materials.

3.2 Experimental Program

3.2.1 Materials

All of the experiments have been conducted by using a mixture of MX-80 bentonite-sand (30% and 70% by mass, respectively) mixed with one of three water solutions, which simulate the typical groundwater salinity or 2 chemistry conditions found in Ontario.

3.2.1.1 Bentonite

Commercial MX-80 bentonite from Wyoming, USA, is used to perform all of the experiments in this study. X-ray diffraction (XRD) was performed to characterize the mineralogical properties of the MX-80 bentonite powder materials by using a Scintag XDS 2000 diffractometer. The XRD patterns illustrated in Figure 3.1 demonstrate that the MX-80 bentonite contains 92% montmorillonite and variable quantities of feldspar, quartz, calcite and kaolinite. The CEC is 105 meq/100 g and Na^+ is the predominant exchangeable cation. The grain size distribution of the bentonite was determined by following ASTM standard (D422-63) to perform sieve analysis on particle sizes larger than 75 μm (retained on sieve No. 200) and the sedimentation process on particle sizes smaller than 75 μm. The test results demonstrated that the entire bentonite sample passes through the No. 100 sieve (150 μm) and 87.7% pass through the No. 200 sieve as shown in Figure 3.1. The bentonite used has a liquid limit of 530%, a plastic limit of 48.5% and an average specific gravity of 2.66. The chemical composition of the MX-80 is given in Table 3.1.

Table 3.1. Chemical composition of MX-80 bentonite

Element	Composition	Percentage (%)
Silicon Dioxide (total)	SiO_2	63.59
Aluminum Oxide	Al_2O_3	21.43
Iron Oxide	Fe_2O_3	3.78
Calcium Oxide	CaO	0.66
Magnesium Oxide	MgO	2.03
Sodium Oxide	Na_2O	2.70
Potassium Oxide	K_2O	0.31
Bound Water	H_2O	5.50

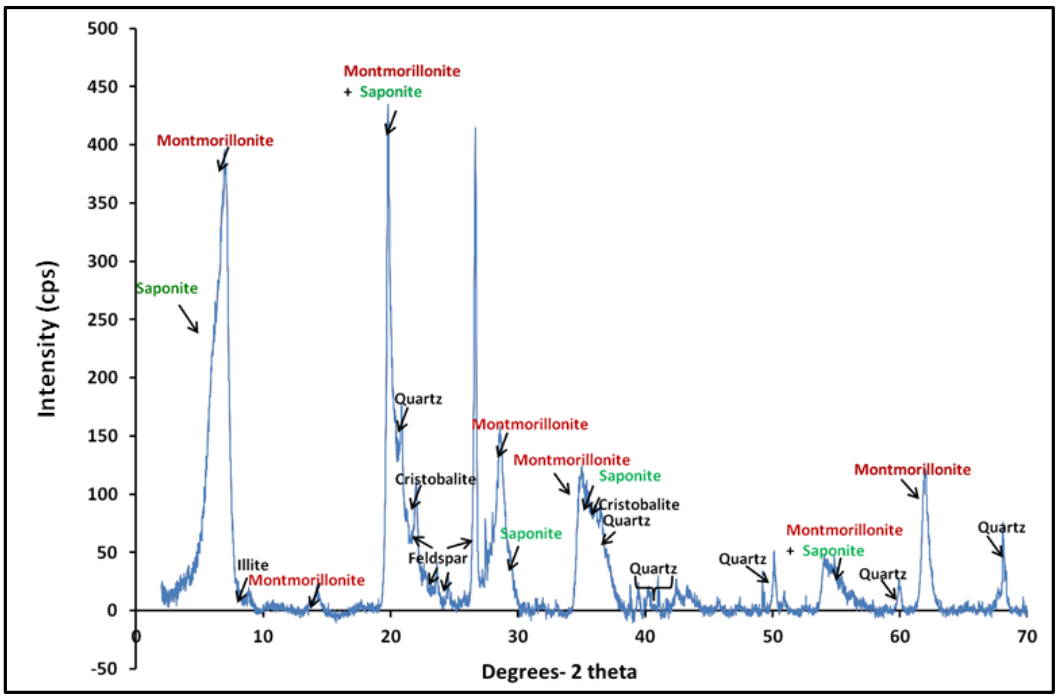

Figure 3.1. X-ray diffraction pattern of pure bentonite.

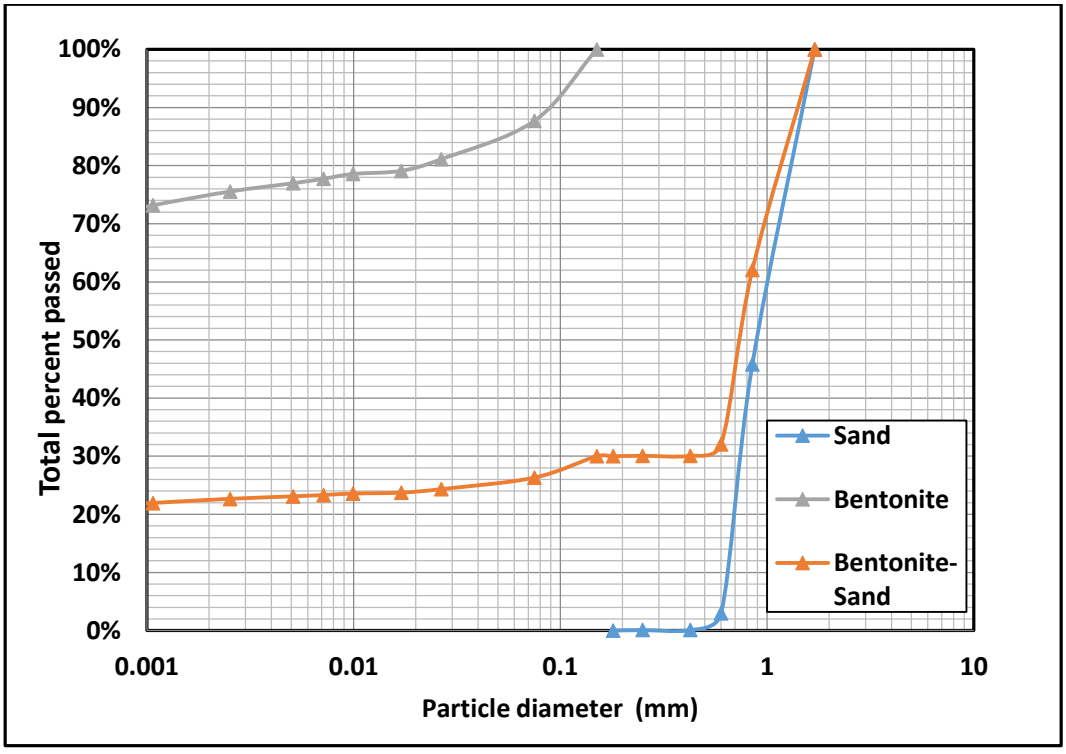

Figure 3.2. Sand, bentonite and bentonite- sand (30/70) grain size distribution

3.2.1.2 Sand

Quartz sand which contains 99.99% silica (SiO_2), with a fine to medium particle size and a specific gravity of 2.6, was used in the investigations. Sand sieve analysis was conducted by following an ASTM standard (D6913 – 04) and it was found that the grain size distribution ranges from 0.18 to 1.7 mm, as shown in Figure 3.2.

3.2.1.3 Water solutions

In this study, three different water solutions are used in all of the experiments; distilled water and two water solutions. The two water solutions were prepared in the laboratory to obtain the same chemical composition as that of the underground water located at more than a depth of 700 m in southwestern Ontario (Dollar 1988; NWMO 2011). The water types included:

- DW; distilled water
- a water solution (T) with a chemical composition similar to that of the underground water at a depth of 738 m in the region of Trenton (Ontario); and
- a water solution (G) with a chemical composition similar to that of the underground water at a depth of 726 m in the region of Guelph (Ontario), as shown in Table 3.2.

Table 3.2. Chemical composition of Water Solutions G and T (g/l) used in this study (sources: Dollar, 1988; NWMO 2011).

Element (g/l)	Distilled Water (DW)	Guelph Water (G)	Trenton Water (T)
$CaCl_2$	0	159.0	64.0
NaCl	0	100.0	102.0
$MgCl_2$	0	34.3	21.6
KCl	0	6.3	3.2
$.K_2SO_4$	0	0.4	1.2
TDS*	0	300.0	192.0
pH	7	5.7	6.5

*TDS: Total dissolved solids

3.2.2 Specimen preparation and mix proportions

An oven dried mixture of MX-80 bentonite-sand (30% and 70% by weight, respectively) was used in all of the experiments. Bentonite-sand mixture specimens were mixed with either DW, or Water Solution T or G, and all of the specimens were compacted to an initial dry density of 1.7 g/cm^3 and water content of 15%. The last step of the preparation for the specimens was the treatment for 15 days at three different temperatures of 23ºC, 40ºC and 80ºC, respectively (Figure 3.3).

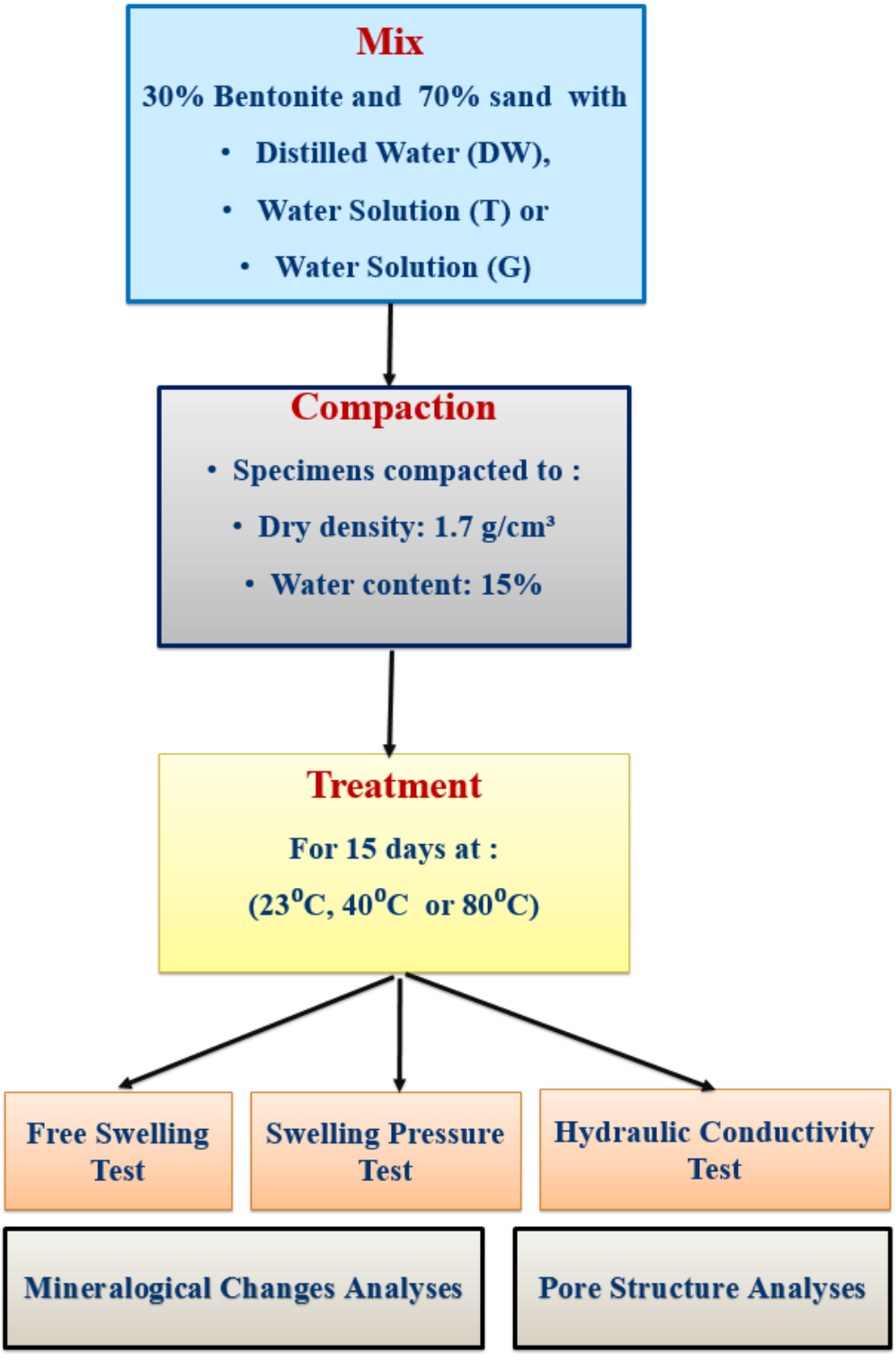

Figure 3.3. Experimental testing program

3.2.2.1 Compaction testing

Compaction tests were performed on the bentonite-sand mixture (30 and 70% by dry weight, respectively) at different water contents to determine the optimum water content and maximum dry density in accordance with ASTM D-698–12. The desired amount of bentonite and sand components, which all passed through sieve No. 10, were oven dried separately at 105ºC for 24 hours to remove all of the initial moisture gained during storage time. Eleven different specimens were prepared by mixing the bentonite-sand mixture with molding water contents that ranged from 6% to 26% in increments of 2% of DW. The specimens were kept in separately sealed plastic bags for 72 hours at room temperature (23ºC) to form homogeneous mixtures. The samples were then statically compacted in a standard proctor stainless steel cylinder mold with an inner diameter of 101.6 mm and height of 116.4 mm. Three layers of each sample were compacted in accordance with ASTM D-698-12. The water contents and the dry densities for all the samples were determined and the compaction curve was obtained, as shown in Figure 3.4. The test results demonstrated that the optimum water content for the mixture is about 15%, and the maximum dry density is about 1.682 g/cm^3. In this study, all of the samples are mixed with 15% water and compacted to a dry density of 1.7 g/cm^3 for simplicity and to avoid any experimental errors. The bentonite sand mixture had a saturated density of 1.955 g/cm^3.

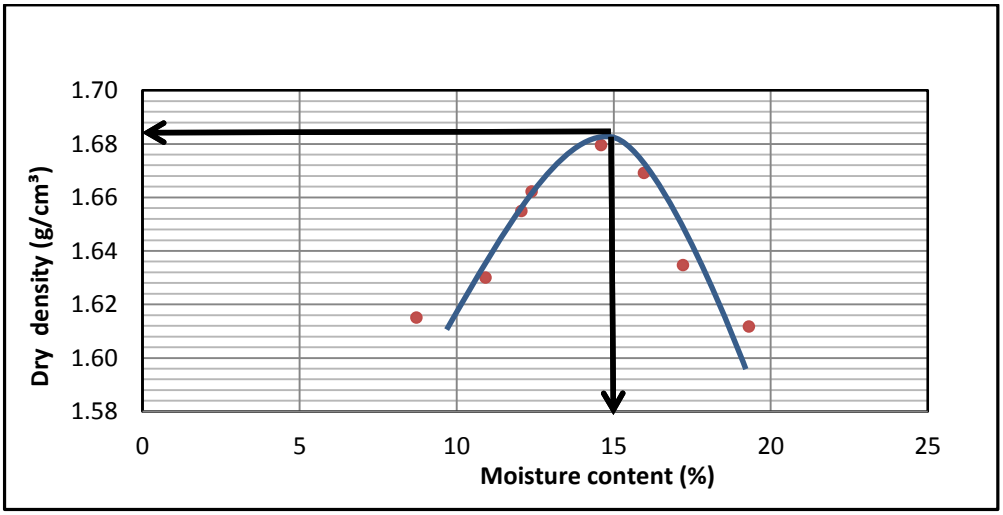

Figure 3.4. Bentonite-sand compaction curve.

3.2.2.2 Water content calculations

The water content was determined in the laboratory as follows.

- In the case of the bentonite-sand mixed with DW, the water content is equal to the ratio between the mass of water (Mw) and mass of dry soil (Md), as shown in Equation 1. The calculated water content for the specimens mixed with DW is 15%.

$$Wc = Mw/Md \quad \Rightarrow \quad Mw = Wc * Md \qquad \text{Equation (1)}$$

- In the case of the bentonite-sand mixed with saline water, the liquid content (Wl) is determined by the sum of the water mass (Mw) and mass of salt (Msalt) divided by the mass of the dry soil, as shown in Equation 2. The water content (Wc) is equal to the ratio between the solution mass (Msol) subtracted by the salt mass (Msalt) to the soil dry mass (Md), as shown in Equation 3. The bulk water content (W) is equal to the mass of water divided by the sum of the mass of the dry soil and salt, as illustrated in Equation 4, by following the calculation procedures for the volume-mass relationship shown previously (Priyanto and Baumgartner, 2008; Siddiqua et al., 2011).

$$Wl = (Mw + Msalt)/Md = (Msol)/Md \Rightarrow \quad Msol = Wl * Md \qquad \text{Equation (2)}$$

$$Wc = (Msol - Msalt)/Md \qquad \text{Equation (3)}$$

$$W = Mw/(Msalt + Md) \qquad \text{Equation (4)}$$

Solution concentration or salinity (Cm) can be defined as the mass fraction of the total mass of salt dissolved in the solution (TDS) and the mass of the solution or solution density (ρl)

$$Cm = TDS/(\rho l) \qquad \text{Equation (5)}$$

The relationship among the liquid, water, and bulk water contents is shown in Equation 6:

$WC = Wl\ (1- Cm)$ Equation (6)

$Msalt = Msol- Mw = Wl * Md - Wc * Md$ Equation (7)

therefore:

$Msalt = Md * (Wl - Wc)$ Equation (8)

from Equations 1, 4 and 7:

$W = Mw/(Msalt + Md) = (Wc * Md)/(Md\ (Wl - Wc) + Md)$

$= (Wc)/((Wl - Wc) + 1)$ Equation (9)

thus

$W = (Wc)/(1 + Wl - Wc)$ Equation (10)

Bulk water content can be determined from Equations 7 and 10:

$W = Wc/(1 - Wc + Wc/(1 - Cm))$ Equation (11)

Water content can be determined by rewriting Equation 11:

$Wc = (W\ (1 - Cm))/(1 - Cm\ (1 + W))$ Equation (12)

Liquid content can be determined from Equations 6 and 12:

$Wl = W/(1 - Cm\ (1 + W))$ Equation (13)

Therefore, the bentonite-sand mixture should be mixed with 18.1% of Water Solution T by mass or 20% of Water Solution G by mass in order to prepare compacted samples with a water content of 15% (see Section (A-1) water solutions for calculations details).

3.2.2.3 Specimen treatment and mix proportions

The desired amount of MX-80 bentonite and sand components were oven dried at 105ºC for 24 hours and then carefully mixed by using a spoon until a uniform bentonite-sand mixture was obtained. Three groups of samples were prepared:

- Group (1): the mixture was mixed with 15% of DW by weight ;
- Group (2): the mixture was mixed with 18.1% of Water Solution T by weight; and
- Group (3): the mixture was mixed with 20% of Water Solution G by weight.

All of the specimens were kept in separately sealed plastic bags for 3 days at the laboratory temperature (23ºC) for curing. The cured samples (Groups 1, 2 and 3) were compacted in accordance with ASTM D698-12 to a dry density of 1.7 g/cm^3 and a water content of 15% into two different cutting rings. For the swelling pressure and free swell tests, at least 18 specimens from each group were compacted into a rigid ring (63 mm in diameter and 13 mm in height). For the hydraulic conductivity test, 9 specimens from each group were compacted in an oedometer standard cutter ring with an inner diameter of 63 mm and height of 20 mm.

The last step for the preparation of the specimens was the treatment for 15 days at three different temperatures. Six specimens sized 63 mm x 13 mm and three specimens sized 63 mm x 20 mm from each group were treated at 23ºC, 40ºC and 80ºC, respectively, as illustrated in Table 3.3.

Table 3.3. Mixing solutions and treatment temperatures of the samples prepared.

	Group (1)			**Group (2)**			**Group (3)**		
Sample	DW23	DW40	DW80	T23	T40	T80	G23	G40	G80
Mixing and saturating solution	Distilled water			Water Solution T			Water Solution G		
Treatment temperature	23ºC	40ºC	80ºC	23ºC	40ºC	80ºC	23ºC	40ºC	80ºC

3.2.3 Testing of specimens

3.2.3.1 Swelling tests

One-dimensional free swell, swelling deformation, and swelling pressure tests were performed on the compacted specimens with an initial dry density of 1.7 g/cm^3 and water content of 15%, by following ASTM standard procedures. All of the tests were conducted at the laboratory temperature (23ºC). During the swelling test, all the samples were soaked in their initial mixing water solutions types.

3.2.3.1.1 One dimensional free swell test

For the one-dimensional free swell test, the sample was allowed to swell in the vertical direction and restricted in the lateral direction. The one dimension free swell of the bentonite-sand samples is graphically presented in Figure 3.5. The MX-80 bentonite contains about 92% montmorillonite, which is the swelling component, and 8% accessory minerals, which are non-swelling materials. Once the sample was supplied with water, the montmorillonite swelled and the sample volume only increased in the vertical direction (Komine, 2010).

The one-dimensional free swell test was conducted on compacted and treated specimens of 63 mm in diameter and 13 mm in height, by following ASTM standard D-4546-08. The specimens were inserted into 250 ml beakers with a 63 mm diameter (the same diameter as the specimen diameter) to prevent lateral swelling. The specimens were then saturated with 150 ml of the appropriate water solution. Groups (1), (2) and (3) specimens were saturated with DW, and Water Solutions T and G, respectively. The vertical free swell strain for each specimen was measured with time by using dial gauges until the specimens reached full saturation and stopped swelling between 7 to 39 days.

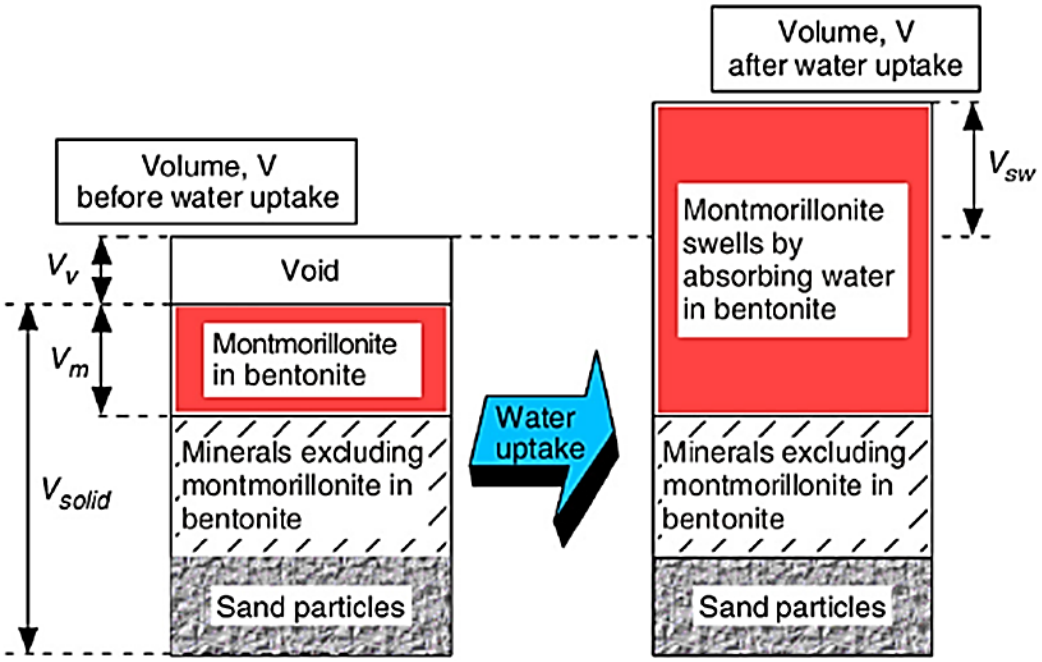

Figure 3.5. One-dimensional free swell mechanism (Komine, 2010)

3.2.3.1.2 Swelling pressure

The swelling pressure can be defined as the maximum pressure applied to a specimen to maintain a constant volume while preventing vertical deformation, and measured with time (Basma et al., 1995; Cui et al., 2012; Wang et al., 2012). The compacted and treated samples were inserted into a consolidometer ring (63 mm in diameter x 13 mm in height) between two filter papers and then placed between porous stones under a vertical seating load of 8.25 kPa. The samples were floated from the top by using their initial mixing water solutions. Group (1), (2) and (3) specimens were floated with DW, and Water Solutions T and G, respectively, until reaching full saturation from about 7 to 36 days. The specimens were allowed to swell up to 0.01 mm and then small pressure increments were added to bring the sample back to its initial volume. The same procedure was repeated until the specimens stopped swelling at their fully saturated state. The swelling strain was measured with time by using a dial gauge. The specimen swelling capacity was obtained by recording the pressure needed to keep the sample volume constant with time.

3.2.3.2 Hydraulic conductivity tests

An oedometer cell with an adjustable falling head apparatus was used to measure the hydraulic conductivity of the compacted bentonite-sand based material by following ASTM standard D-5084 – 10. The compacted and treated specimens were soaked in the same mixing water solution (DW, T or G) bath under confining stress to prevent vertical and lateral swelling. The degrees of saturation of the specimen were measured from time to time. Once the specimens were completely saturated after about 48 hours, the specimens (63 mm in diameter x 20 mm in height) were loaded in the oedometer cell inside the stainless steel cylindrical chamber. The specimens were placed between two filter papers and then between two porous stones under a vertical stress of 50 kPa. The vertical stress was calculated to simulate the actual confining stress impact on the bentonite-sand based materials in DGRs (Komine, 2010). The experimental hydraulic conductivity (K) was determined by measuring the initial fluid head (h1= 85.5 cm) at the beginning of the test (t1) and allowing the fluid (the same mixing and saturating water solution) to flow through the specimens from the bottom to the top. The change in the fluid head was measured with time and the final head difference (h2) was recorded at time (t= t2) at the end of the testing. The coefficient of permeability was calculated by using Equation 13 as follows:

$$\mathrm{K} = \frac{\mathrm{aL}}{\mathrm{At}} \ln \frac{h1}{h2} \qquad \text{Equation (13)}$$

where: K = coefficient of permeability, m/s

a = cross-sectional area of the reservoir that contained the influent liquid, m², and

A = cross-sectional area of specimen, m²,

L = length of specimen, m,

t1 = time at start of permeation trial, date: hr: min: sec,

t2 = time at end of permeation trial, date: hr: min: sec,

t = interval of time over which the flow had occurred, sec, t= t2 – t1

h1 = hydraulic head at the beginning of the testing, m

h2 = hydraulic head at the end of the testing, m

3.2.3.2.1 Investigation of impact of groundwater chemistry on bentonite- sand based material permeability with time: Case of G23

In order to understand the impact of the ground water chemistry on the permeability of the compacted bentonite-sand materials with time, the hydraulic conductivity falling head test was conducted over 14 cycles on the same sample (G23). At the beginning of the testing, the fluid container was filled with Water Solution G up to a certain hydraulic head (h1). The test started at time t1, which corresponded to h1, and Water Solution G was passed through the soil specimen from the bottom to the top. When the hydraulic head decreased to a certain height, h2, the test was stopped and the hydraulic conductivity value was determined (k1). The same test procedure was repeated for 14 cycles, and each time, the testing started and ended at the same values for h1 and h2, respectively. The hydraulic conductivity values are calculated for each cycle, as shown in Table A-2.

3.2.3.2.2 Investigation of changes in bentonite- sand permeability with time: case of DW23

For the sample mixed with DW and treated at room temperature (DW23), the hydraulic conductivity falling head test was continued for 28 days to investigate the changes in the bentonite-sand permeability with time. The hydraulic conductivity falling head test was started at time t1, and corresponded to a fluid head, h1. The changes in the hydraulic head (h2) were recorded with time and the hydraulic conductivity values were calculated for each corresponding time interval, as shown in Table A-3.

3.2.3.3 X-Ray diffraction

XRD analysis was conducted on the pure bentonite and treated bentonite-sand samples to determine the mineralogical changes due to the interactions with the highly saline water solutions and heat. The results obtained will help to explain the variations in the swelling capacity and the hydraulic conductivity of the bentonite-sand based material induced by aggressive conditions (high salinity and/or temperature). X-ray powder

diffraction analyses were performed by using a Philips X'Pert diffractometer with a Cu source and High Score Plus analysis software. The XRD patterns were measured at room temperature with an instrument power of 45 kV, 40 mA and an automatic divergent slit and 0.2 mm receiving slit. The scans were between 2-60 degrees 2Theta with a step size of 0.02 deg 2theta and 0.6 s continuous scan time per step.

3.2.3.4 Thermal analysis

Thermogravimetric (TGA) coupled with a derivative thermogravimetric (DTG) analyses were performed on several samples by using a thermal analyzer (TGA Q5000 V3.15 Build 263, University of Ottawa) under a nitrogen atmosphere with a flow rate of 25.0 ml/min. The samples were heated at temperatures that ranged from room temperature to 1000°C at a typical heating ramp of 10°C/ min. The TGA and DTG tests were conducted on powder samples of 17 to 20 mg in weight.

3.2.3.5 X-Ray Microanalysis

Electron dispersion spectroscopy (EDS) analyses was conducted by using (INCA-x-act, Oxford Instruments, Abingdon-Oxfordshire, UK) device. EDS analyses were performed on pure bentonite and treated bentonite–sand samples to investigate the changes in the microstructure and chemical compositions of pure bentonite and treated bentonite sand materials. A gold coating was used to overcome the charging effect, which was done through a sputtering process by using a Denton Vacuum Desk IV cold sputter system. The sputtering was done for 1 min in order to obtain a gold layer with a thickness between 10 and 20 nm on the top of the samples.

3.2.3.6 Surface area and pore size distribution

The surface area and pore size distribution analyses were performed on the powdered bentonite-sand samples. All of the ground samples were characterized by using nitrogen adsorption at 77 K to measure their structural properties with a Micrometrics ASAP 2020

adsorption analyzer. Before the adsorption measurements, all of the samples were degassed under vacuum (1×10-5 Torr) at 120°C for 3 hours to remove the adsorbed water. The surface area was calculated by using the Brunauer, Emmett and Teller (BET) method for single and multi-points from a nitrogen adsorption-desorption isotherm in a relative pressure range from 0.06 to 0.2. The total volume was considered as the volume of the liquid nitrogen adsorbed at P/P0 = 0.985, and the mean pore diameter was obtained by applying the Barrett, Joyner and Halenda (BJH) method.

3.3 Results and discussions

3.3.1 Swelling characteristics

3.3.1.1 Effect of temperature

The results of the impact of temperature on the swelling strain and pressure of the tested materials are shown in Figures 3.6 and 3.7, respectively. In Figure 3.6, it is shown in the one dimension free swell test results that the sample mixed with DW and kept at room temperature (DW23) records a maximum swelling strain of 198% within 32 days (Figure 3.6). The samples treated at 40ºC (DW40) gives a swelling strain of 192% within 26 days, while the sample treated at 80ºC (DW80) records a swelling strain of 194.5% within 30 days, as shown in Figure 3.6.

The swelling pressure test results show that DW23 records a pressure of 228 kPa, which is in good agreement with the test results of Pusch (1998, 2001) and Quintessa (2011) on 30/70 MX-80 bentonite/ballast mixtures. Moreover, the swelling pressure in this study is slightly higher than that of the test results in Mata and Ledesma (2003) on a 30/70 MX-80 bentonite/crushed rock mixture (196 kPa). This difference is due to the higher content of the swelling component in the bentonite used in this study (92%) compared to that of the bentonite used in the aforementioned study (75%). DW40 and DW80 record swelling pressures of 191 kPa and 201 kPa, respectively, as shown in Figure 3.7. These results are in good agreement with those in an experimental study by Pusch (2000) on bentonite powder steam treated at 90ºC and 110ºC, which showed no significant changes in the swelling pressure with increases in the temperature.

These test results demonstrate that the swelling strain decreases by 3%, and the swelling pressure decreases by 16% with increases to the treatment temperature from 23ºC to 40ºC. The sample treated at 80ºC shows less than a 2% decrease in the swelling strain and 12% decrease in the swelling pressure compared to the samples treated at 23ºC.

From the results presented in Figure 3.6 and discussed above, it can be concluded that the temperature does not have a significant impact on the swelling capacity of the studied bentonite-sand based barrier material.

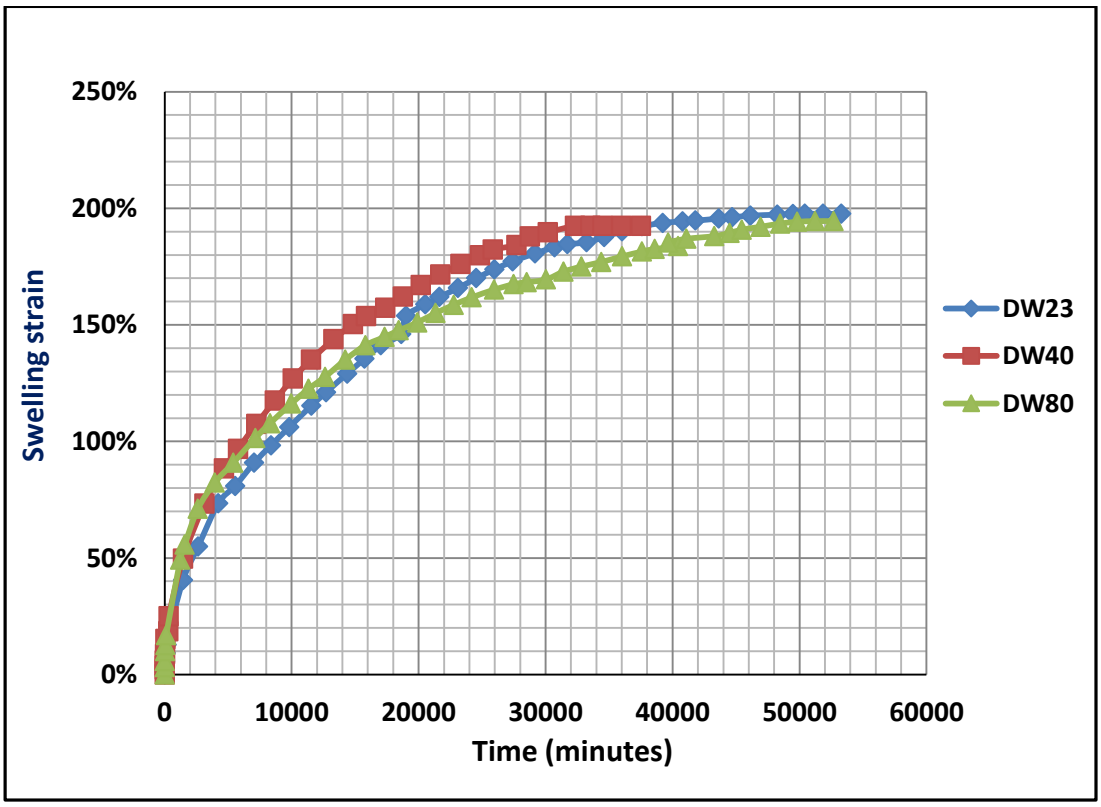

Figure 3.6. Effect of treatment temperature on the swelling strain of the studied compacted bentonite-sand

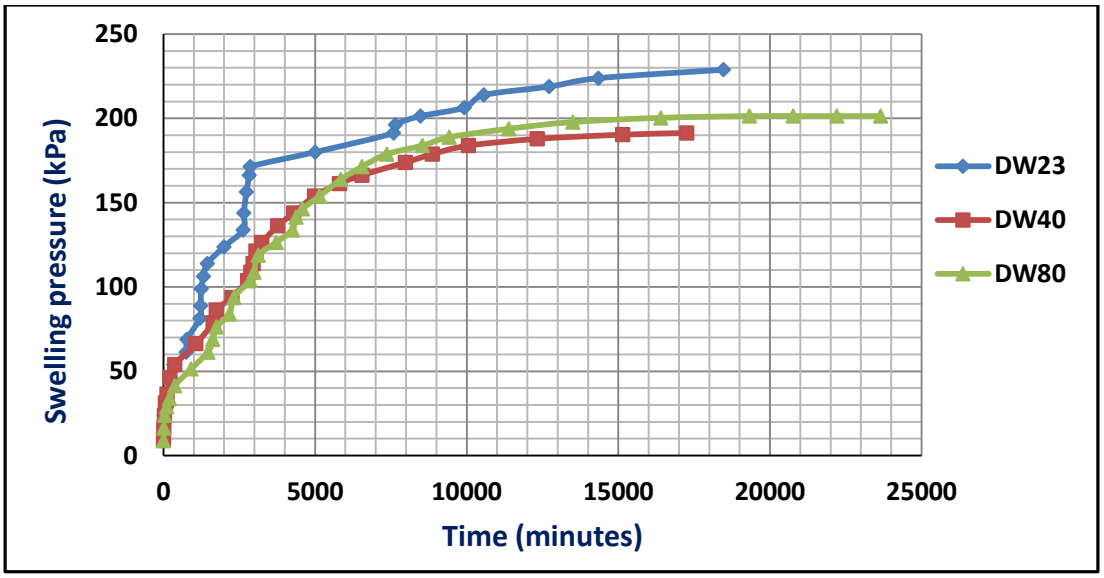

Figure 3.7. Impact of the treatment temperature on the swelling pressure of the compacted bentonite-sand.

3.3.1.2 Effects of groundwater chemistry (salinity)

Figures 3.8 and 3.9 depict the results of the effect of the chemical composition or salinity of the groundwater on the swelling strain and pressure of the studied materials, respectively. From these figures, it can be observed that the groundwater salinity has a significant impact on the swelling strain and pressure, i.e. on the swelling properties of the studied engineered barrier materials. The results of the swelling tests demonstrate that the sample mixed and saturated with DW records a swelling strain of 198%, while the samples mixed and saturated with Water Solutions T and G record a swelling strain of only 8% and 4.7%, respectively, as illustrated in Figure 3.8. The swelling pressure drops from a pressure of 228 kPa for the sample mixed and treated with DW to 16.35 kPa and 13.35 kPa for the samples mixed and treated with Water Solutions T and G, respectively, as shown in Figure 3.9. The porewater chemistry reduces the swelling pressure by more than 90% and the swelling strain by 95%. These results are in good agreement with those obtained by Pusch (1998, 2001) and Bradbury and Baeyens (2002), Dhawan and Rao (2012). Furthermore, Pusch (1998, 2001) showed through testing that the swelling pressure of 30/70 MX- 80 bentonite/ballast mixtures drops to almost zero when the material is saturated with Ca-dominant solutions with more than 3.5% salinity.

This observed severe degradation of the swelling capacity or properties of the bentonite-sand swelling exposed to highly saline water results from the mineralogical and chemical changes that occur in the barrier material because of the chemical attacks from the salinity. The microstructural and nano-structural tests (e.g. XRD, DES) results confirmed that the availability of monovalent (Na, K) and divalent cations (Ca, Mg) in the bentonite porewater cause cation exchange reactions, and montmorillonite-illite conversion in the presence of silica sand and accessory minerals (will be discussed later). Ca replaced the trace amounts of the initial Na of the Na-montmorillonite and produced Ca-montmorillonite with less swelling ability, whereas K and Al replaced the Na and Si and converted most of the montmorillonite to illite, which is characterized by a much lower swelling ability. The results of the microstructural and nano-structural tests will be discussed below in more detail.

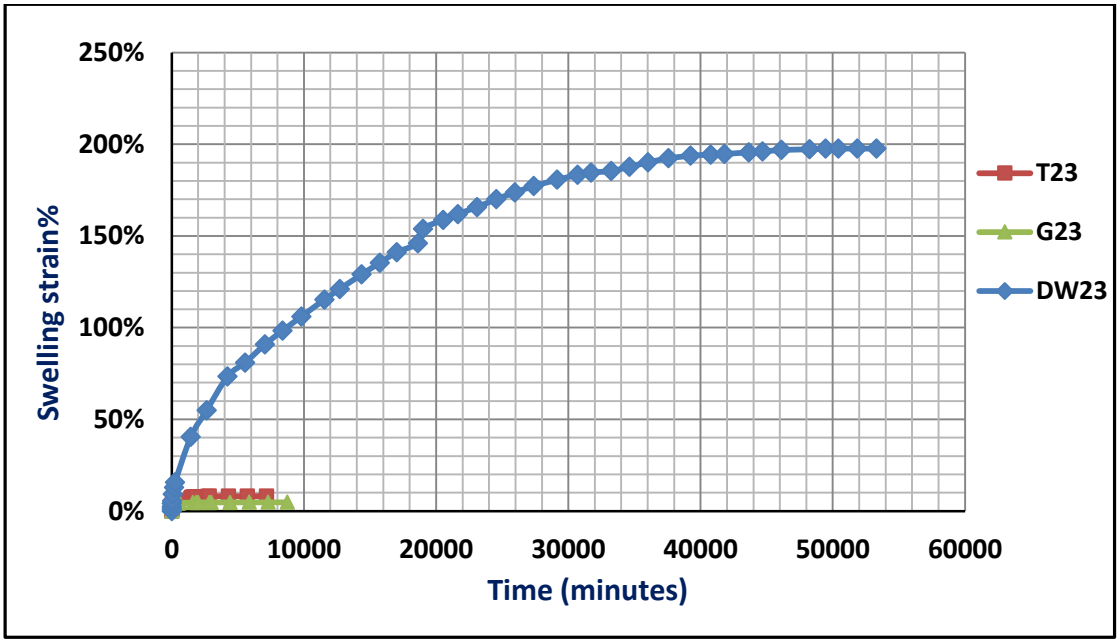

Figure 3.8. Groundwater chemistry impacts on the swelling strain of bentonite- sand based barrier material.

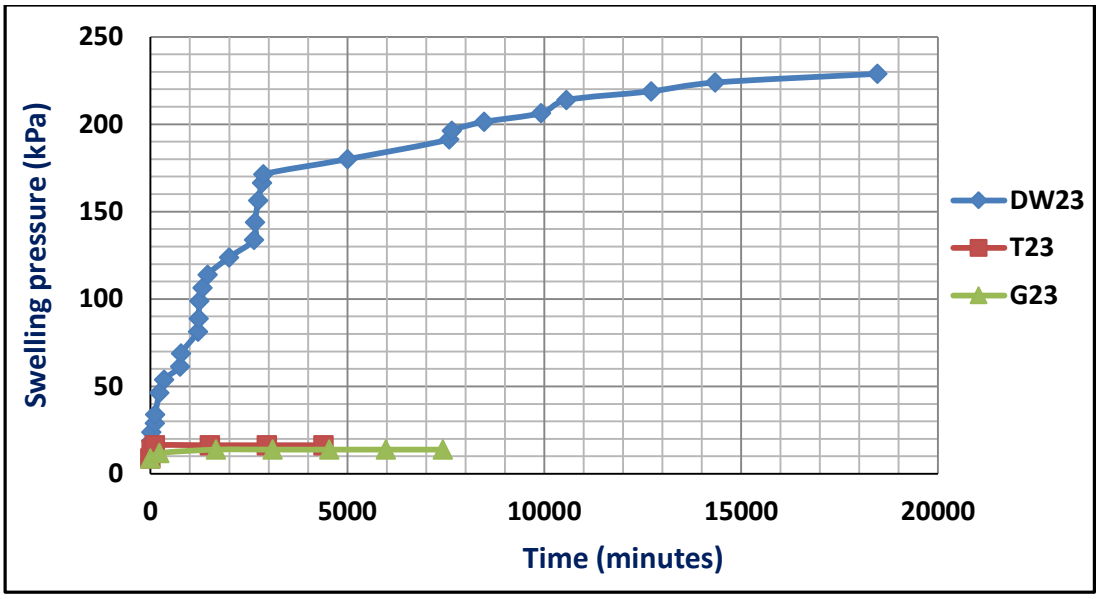

Figure 3.9. Groundwater chemistry impacts on the swelling pressure of bentonite- sand based barrier material.

3.3.1.3 Coupled effects of temperature and groundwater-chemistry

The results of the coupled effects of the temperature and groundwater chemistry on the swelling strain and pressure of the bentonite-sand material are depicted in Figures 3.10 and 3.11, respectively. The test results show that the coupled effects of temperature and groundwater chemistry influence the swelling capacity of the bentonite-sand barrier material (Figure 3.10). The swelling capacity of the bentonite-sand mixture is reduced by 95% for the samples mixed with Water Solutions T and G and treated at different temperatures. It can be observed that the samples mixed with Water Solution T or G and treated at 40ºC show swelling strains that are higher than those of the samples treated at 23ºC and 80ºC.

When the total dissolved solids (TDS) increased from 192 g/L in Water Solution T to 300 g/L in Water Solution G, the swelling strain decreased from almost 8.2% to 4.6% for samples treated at 23ºC and from 10.4 to 8.8% for samples treated at 40ºC. On the contrary, the swelling strain is increased from 5.1% to 6.4% for samples treated with Water Solutions T and G at 80ºC, respectively, as show in Figure 3.10.

The swelling pressure decreased with increasing TDS. The sample mixed with Water Solution T recorded a higher swelling pressure than that mixed with Water Solution G; that is, pressures of 16.35 kPa and 13.65 kPa, respectively. Furthermore, the swelling pressure for samples mixed with Water Solutions T and G treated at 23ºC recorded swelling pressures higher than those treated at 40ºC and 80ºC, as shown in Figure 3.11. This will be discussed in more detail in the next section.

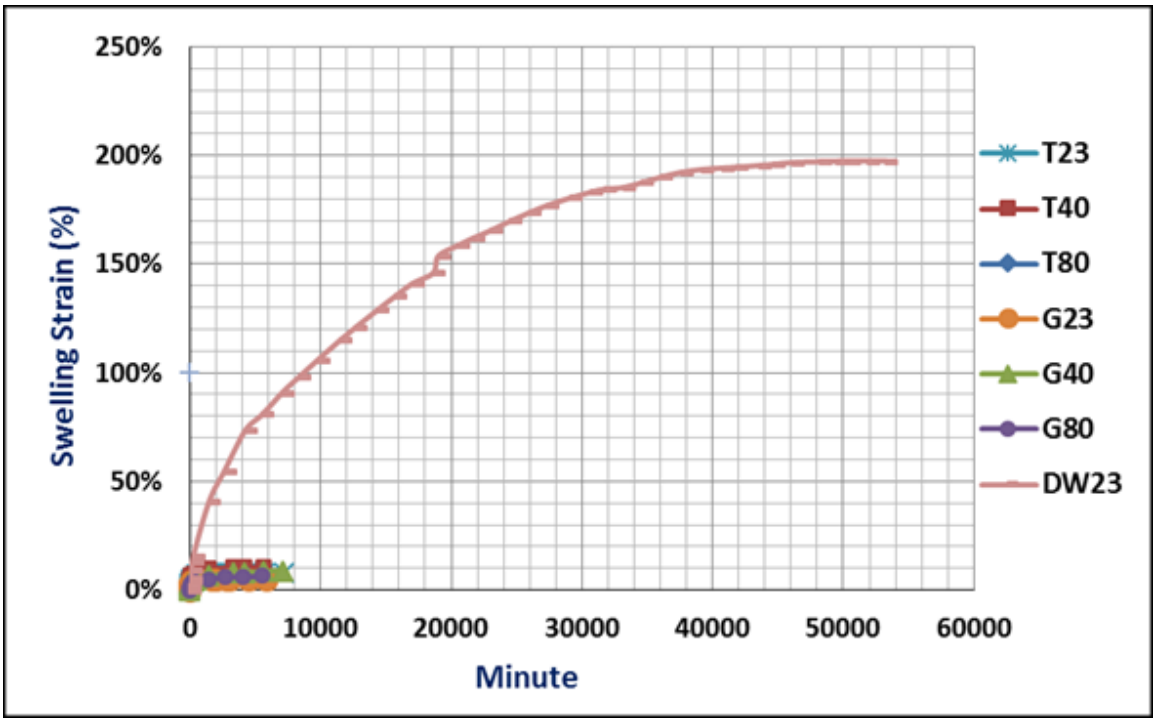

Figure 3.10. Effects of temperature and groundwater chemistry on swelling strain bentonite-sand based barrier.

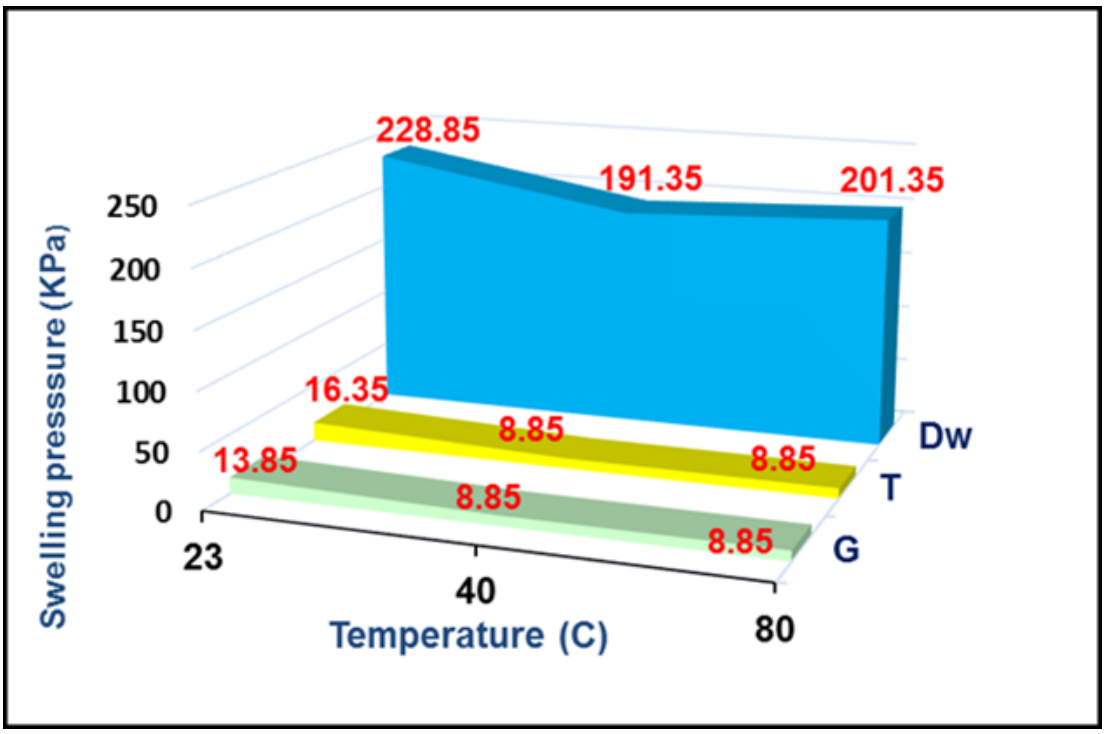

Figure 3.11. Coupled effects of temperature and groundwater chemistry on swelling pressure of bentonite-sand based barrier.

3.3.2 Hydraulic conductivity

3.3.2.1 Impact of groundwater chemistry and temperature on hydraulic conductivity of compacted bentonite-sand materials

The results of the combined effects of groundwater chemistry and temperature on the hydraulic conductivity of the bentonite-sand materials are shown in Figure 3.12. From this figure, it can be noticed that the hydraulic conductivity of the bentonite-sand samples treated at room temperature and percolated with DW is low (6.84×10^{-11} m/s). This result is in excellent agreement with the test results of Pusch (1998, 2002) and Quintessa (2011) for a 30/70 MX- 80 bentonite-ballast mixture.

The impact of treatment temperature on the samples mixed with DW is not significant as the changes in hydraulic conductivity induced by the temperature increase are lower than one order of magnitude, as shown in Table 3.4 and Figure 3.12. Villar and Lloret (2004)

also observed a small impact from temperature on the hydraulic conductivity of saturated compacted FEBEX clay. On the other hand, the test results clearly show that the hydraulic conductivity is strongly dependent on the salt concentration in the mixed and saturated water solutions. The hydraulic conductivity increases with increasing TDS. The samples mixed with Water Solutions T and G show a higher hydraulic conductivity than those mixed with DW and treated at the same temperature, as shown in Figure 3.12. These results compare quite well with the test results of Pusch (2001) for a 10% to 20% salt content.

Moreover, the obtained experimental results clearly indicate that the coupled effect of temperature and groundwater chemistry significantly increases the hydraulic conductivity of the specimens. The hydraulic conductivity of G80 (1.27×10^{-8} m/s) is increased by about one order of magnitude compared to that of T80 (4.70×10^{-9} m/s), and by three orders of magnitude compared to that of DW80 (5.07×10^{-11} m/s), as shown in Figure 3.12. The hydraulic conductivity of G23 is increased by one order of magnitude compared to that of DW23, while this increase is two and three orders of magnitude for G40 and G80, respectively.

This increase in hydraulic conductivity can be explained by the occurrence of the cation exchange reactions and the conversion of montmorillonite to illite in the bentonite-sand materials. This conversion is experimentally demonstrated by the XRD and surface area analyses presented below (will be discussed later). The particle size of illite is larger than that of montmorillonite and more than 200 times more permeable than montmorillonite (Terzaghi et al. 1996). Moreover, the montmorillonite-illite conversion is increased with increases in the curing temperature. Therefore, G80 has a higher percentage of illite and records a higher permeability as shown by the TGA and DTG analysis results (see Section 3.3.4)

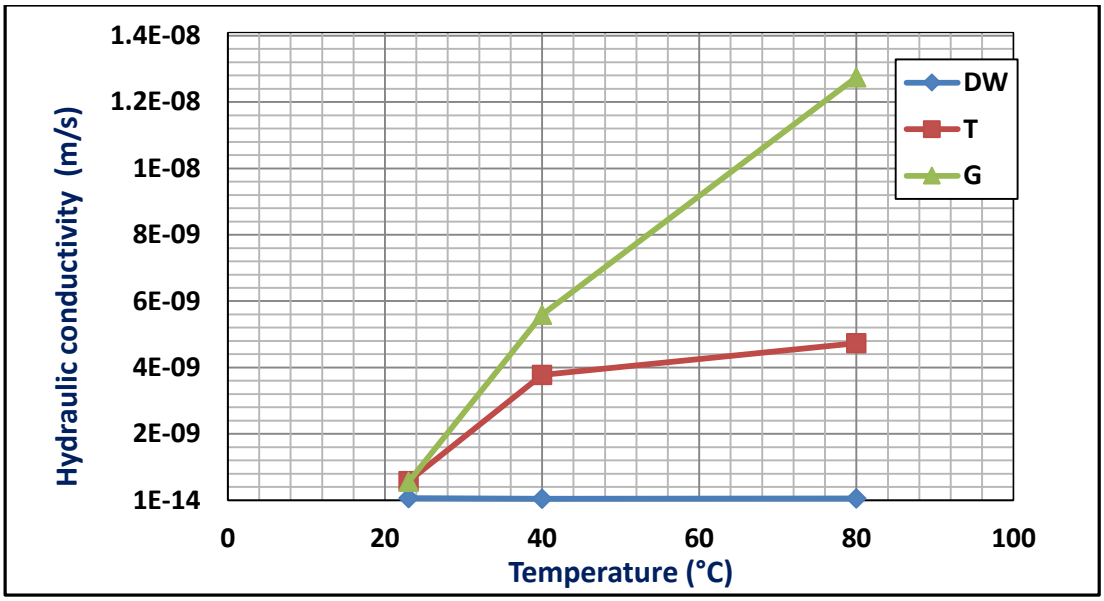

Figure 3.12. Impact of water salinity and treatment temperature on the hydraulic conductivity of compacted bentonite-sand materials.

Table 3.4. Changes in hydraulic conductivity of compacted bentonite-sand materials induced by temperature and groundwater chemistry

Temperature	Distilled Water (DW)	Trenton Water (T)	Guelph Water (G)
23ºC	6.84E-11	5.70E-10	5.59E-10
40ºC	4.36E-11	3.80E-09	5.59E-09
80ºC	5.07E-11	4.70E-09	1.27E-08

*Hydraulic conductivity (m/s)

3.3.3 Mineralogical evolution

The results of the XRD, EDS and TGA/DTG tests and analyses that are presented below reveal that the mineralogical composition (particularly the montmorillonite content) of the samples mixed with mildly acidic (pH < 6) water solutions, that is, Water Solutions G or T, treated at temperatures of 23ºC, 40ºC and 80ºC for 15 days, has changed. The montmorillonite-to-illite conversion, and Na-montmorillonite conversion to Ca-

montmorillonite in specimens G23, G40 and G80 have been identified and characterized by using XRD, SEM, and thermo- and differential gravimetric (TGA and DTG) analyses. Furthermore, the smectite-illite conversion is increased with increases in the treatment temperature, where the XRD pattern of G80 shows more illitization than those of G40 and G23. Consequently, the montmorillonite content is decreased in G23, G40 and G80, which results in a significant decrease of the swelling capacity and a high increase of the hydraulic conductivity by more than 3 orders of magnitude.

The conversion of montmorillonite (smectite) to illite and Na-montmorillonite to Ca-montmorillonite can be explained by the availability of monovalent (Na, K) and divalent cations (Ca, Mg) in the bentonite porewater due to the chemical composition of Water Solutions T and G (see Table 3.2) and by the presence of silica sand and other accessory minerals, such as; cristobalite, albite (plagioclase feldspar) and quartz. The conversion of montmorillonite can be caused by:

(i) the cation exchange reactions that occur where the Ca^{++} and Mg^{++} cations replace the Na^{+} cations, and the initial Na-montmorillonite converts to Mg and Ca-montmorillonite with less swelling capability, and

(ii) the smectite-to-illite conversion; in which montmorillonite is converted to illite due to:

- changes in the interlayer compositions where Na^{+} is substituted with K^{+} in the presence of strong solutions and Al^{3+} replaces Si in the tetrahedral position without any changes in the octahedral layer (Garrels, 1984) or
- a dissolution and precipitation process; in which smectite dissolution and cementation are due to SiO_2 precipitation (Eberl et al., 1993 Pusch; 1998, 2002; Wersin et al., 2007; Kaufhold and Dohrman, 2011) Montmorillonite layers naturally and very slowly convert to illite layers under high concentrations of potassium (Garrels, 1984).

The test results are in good agreement with the results of Ureana et al. (2103) and Eberl et al. (1993). Eberl et al. (1993) found that montmorillonite illization takes place in Wyoming bentonite samples, and the expandability is reduced from 97% to 84% within

42 days for specimens treated with a 3.0 M NaOH solution at a temperature of 35ºC. However, for the samples treated with a 3.0 M KOH solution at a temperature of 60ºC, the expandability is reduced to 33% within 28 days. Ureana et al. (2103) showed in laboratory experiments that the montmorillonite cation exchange reaction and montmorillonite to illite conversion occur within 15 to 30 days of curing with magnesium hydroxide, seawater or olive mill wastewater with different concentrations. It was found that the presence of montmorillonite is reduced, so that the swelling pressure of the specimens is reduced by 59% - 81%.

3.3.3.1 X-ray diffraction

The XRD patterns of DW23, G23, G40 and G80 are shown in Figure 3.13. The XRD spectrums confirm the smectite -to- illite conversion and cation exchange processes. Indeed, the XRD spectrum of DW23 shows that the first peak for Na-montmorillonite is at (2ɵ) 8.92º and the basal spacing is d (001) = 9.902 Å, while G23, G40 and G80 show their first peaks at (2ɵ) 6.288º, 6.200º and 6.632º with lower reflection intensities and d (001) = 14.044, 14.24 and 13.1357 Å, respectively. This observed shift to the left of the first peaks and increase of the interlamellar spacing are due to the ion diffusion and cation exchange processes. The peak shifting and lower reflection intensity indicate a reduction in the swelling component (Moore and Reynolds, 1989). Na^{+} was substituted by Ca^{2+} which resulted in the change of montmorillonite from a sodium-rich to a calcium- rich form with lower swelling capacity. In addition, K^{+} replaced Na^{+} and Al^{3+} replaced Si^{4+} and montmorillonite converted to a low-swelling component, illite (Figure 3.13), in the presence of the mildly acidic water solutions, that is, Water Solutions T and G, (Table 3.2), silica sand, and accessory minerals such as cristobalite, albite (plagioclase feldspar) and quartz. Therefore, the swelling potential of the samples exposed to the aforementioned solutions sharply decreases and their hydraulic conductivity significantly increases. This is especially the case for G80, in which the swelling strain is reduced by 97% and the hydraulic conductivity is increased by more than 3 orders of magnitude since most of the Na-montmorillonite has been converted to Ca-montmorillonite and illite (Figure 3.13).

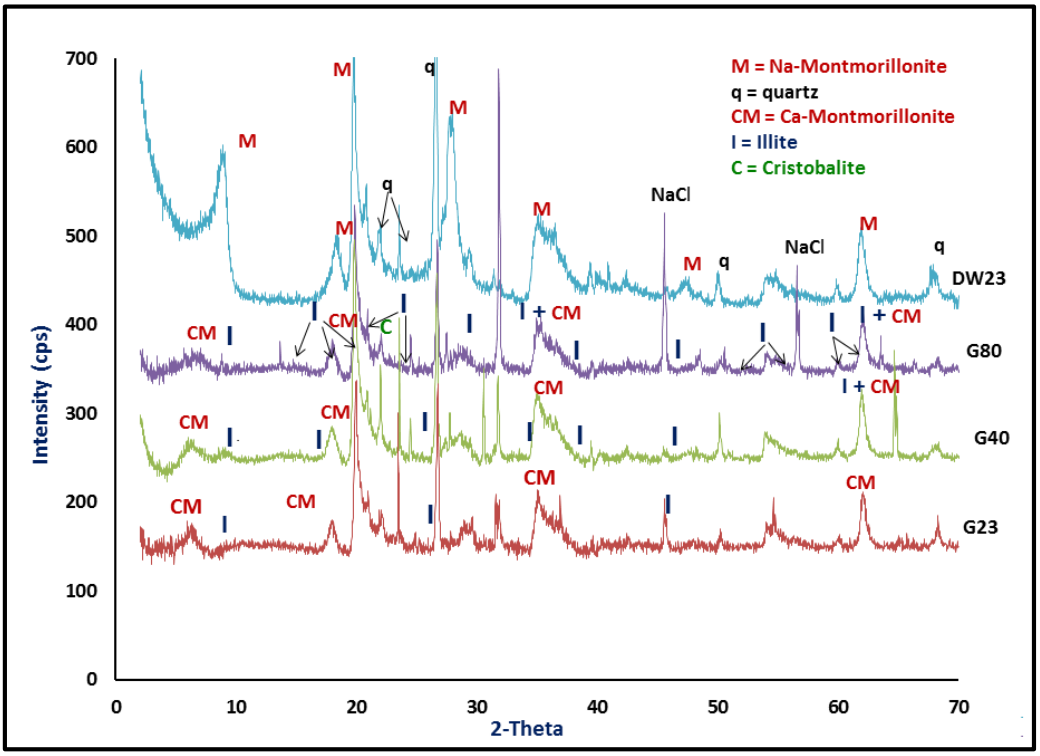

Figure 3.13. XRD patterns of DW23, G23, G40 and G80

3.3.3.2 X-Ray Microanalysis

The electron dispersion spectroscopy (EDS) test results, as illustrated in Figure 3.14, demonstrate that the presence of Al^{3+}, Ca^{2+} and K^{+} is increased, while that of Na^{+} and Mg^{2+} is reduced in G23, G40 and G80. These changes in the chemical composition of the bentonite-sand mixture occur due to the smectite-illite conversion and cation exchange processes. These results are in good agreement with the XRD results and explain the significant changes in the hydraulic conductivity and swelling pressure of the bentonite-sand mixture exposed to aggressive groundwater. It is well known that Ca-montmorillonite has a swelling capacity several times less than that of Na-montmorillonite (Grim and Güven, 1978). Moreover, illite has a low swelling capacity and is more than 200 times more permeable than montmorillonite (Terzaghi et al. 1996).

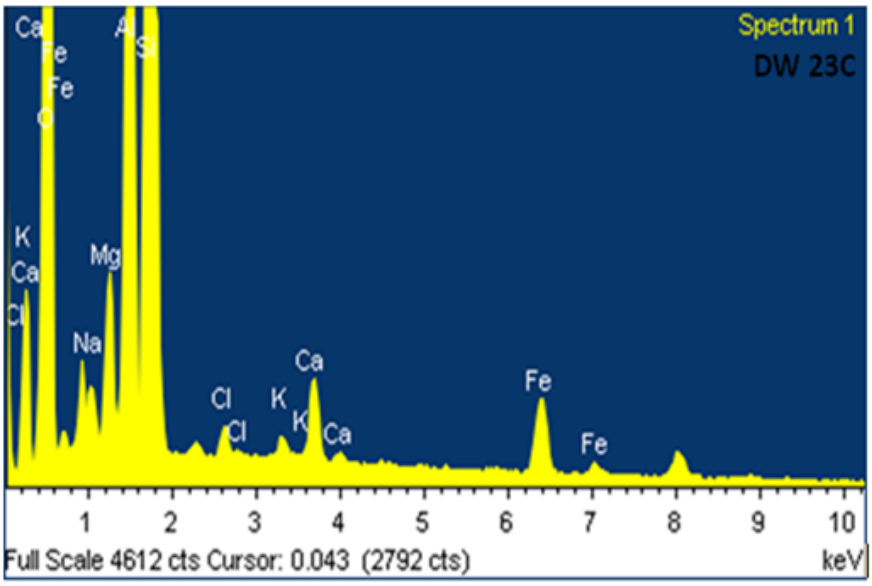

a) Sample mixed with DW and treated at 23℃ (DW23)

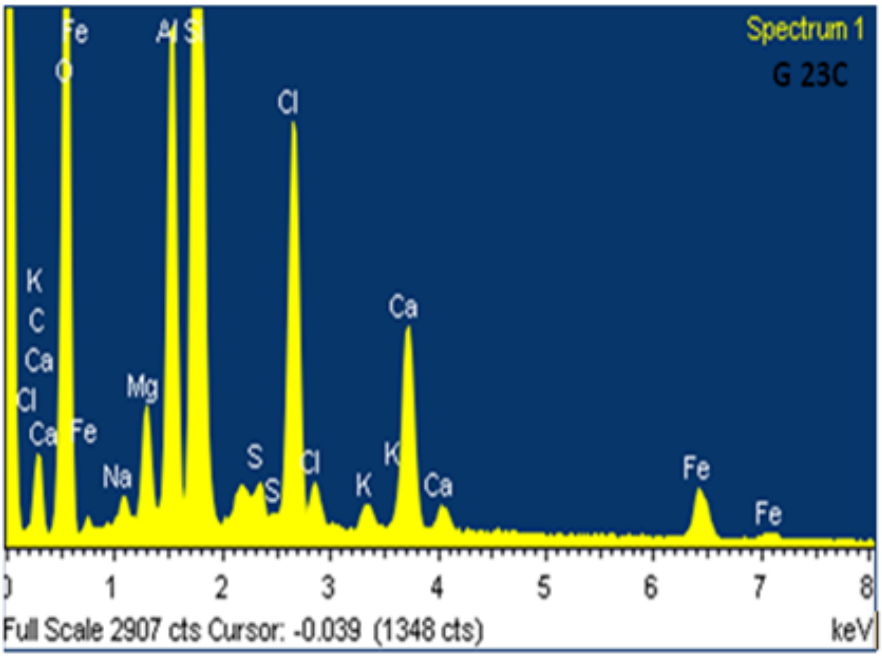

b) Sample mixed with Water Solution G and treated at 23℃ (G23)

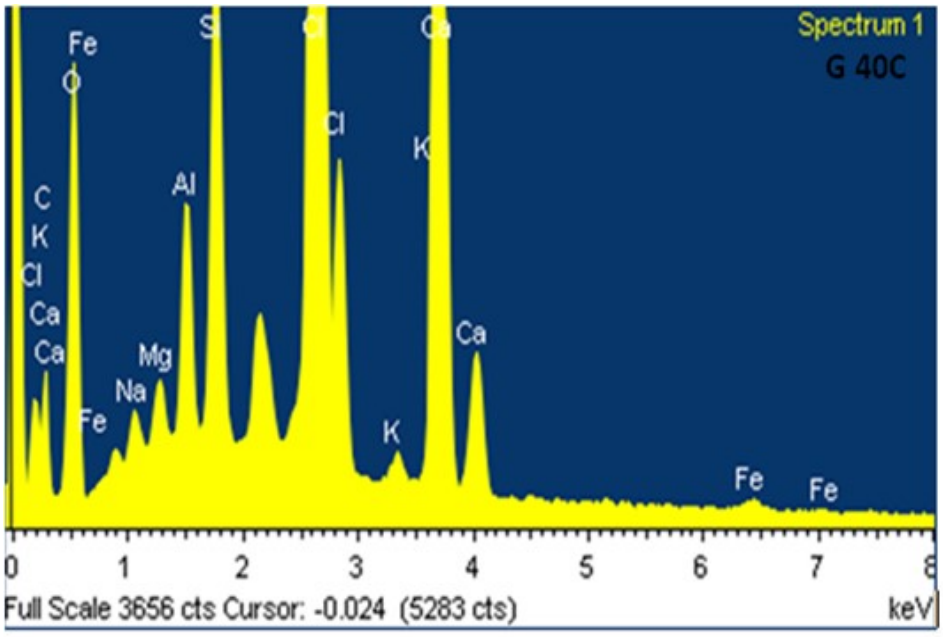

c) Sample mixed with Water Solution G and treated at 40ºC (G40)

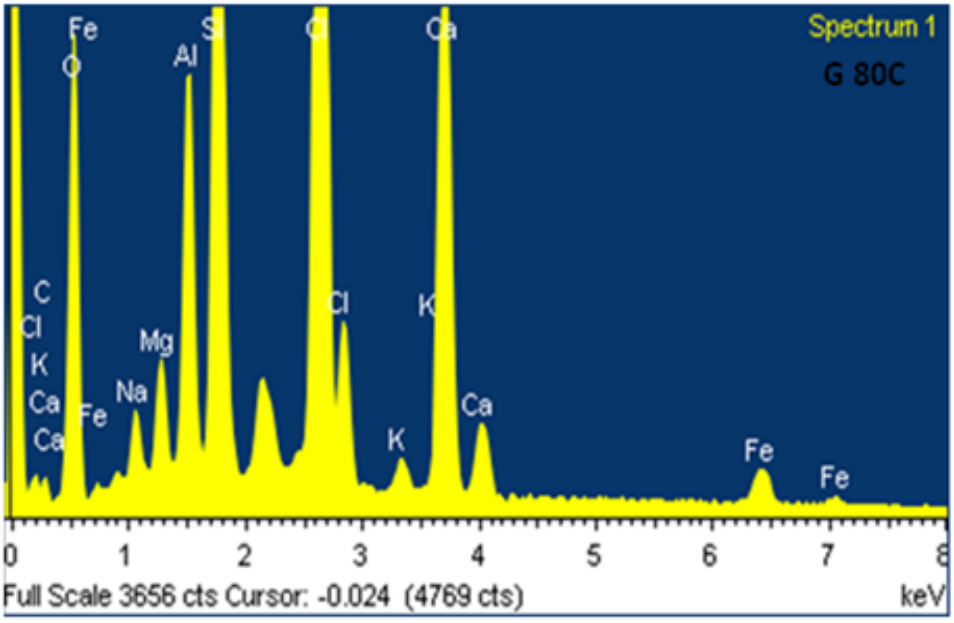

d) Sample mixed with Water Solution G and treated at 80ºC (G80)

Figure 3.14. EDS patterns of: a) DW23, b) G23, c) G40 and d) G80.

3.3.3.3 TGA and DTG analysis

The results of TGA coupled with DTG analyses for all the tested samples are presented in Figure 3.15. These test results also confirm the smectite-illite conversion and cation exchange processes that occur in the barrier material. The results presented in Figure 3.15 agree well with the fact that the replacement of Na cations with Ca^{2+}, K^{+} and Mg^{2+} increases the strength of the interlayer water adsorption bonds and the structure stability (Ureana et al., 2103) as discussed below. In addition, illite has very strong Al-OH bonds (Drits et al., 1998). Thus, G23, G40 and G80 show more thermal stability.

The TGA and DTG curves for DW23 show that an initial mass loss peak of 2.64 wt. % occurred at a very low temperature of 49.8ºC due to the removal of the surface water. The second water loss of 1.96 wt. % at temperatures of 200ºC to 600ºC corresponds to the water desorption from the interlayers, as illustrated in Figure 3.15.b. The last endothermic peak occurred at a temperature of 693.8ºC and mass loss of about 3.2 wt. % due to the dehydroxylation of the O-H structure and collapse of the smectite crystal structure (Drits et al 1998; Boudriche et al., 2012; Ouellet-Plamondon et al., 2014). It can be clearly observed that the water desorption from the interlayers and dehydroxylation processes of the O-H structure or the pure bentonite and DW23 occur at almost the same endothermic peaks, as shown in Figures 3.15.a and 3.15.b.

G23 and G40 show mass losses of 18.2% and 14.44% respectively, which correspond to the removal of adsorbed surface water molecules at a temperature range of 30°C to 126°C. As well, the interlayer or chemisorbed water is gradually removed at a temperature range of 160°C to 600°C, thus producing mass losses of 3.85% and 3.58%, respectively. It was also found that the clay structure collapsed and dehydroxylation occurred at the endothermic peaks of 819.6°C and 877.5°C, respectively, due to the very strong Al-OH bonds (Drits et al., 1998) as shown in Figures 3.15.c and 3.15.d.

G80 showed the maximum thermal stability and degradation resistance due to increasing smectite-illite conversion (treated at a higher temperature of 80ºC) which requires more thermal energy to break down (Drits et al., 1998). The G80 sample showed an initial peak mass loss of 11.34 wt. % at a temperature of 96.3ºC due to the removal of the surface water, followed by a 3.78 wt. % mass loss caused by the removal of the

interlayer water molecules at a temperature range of 200ºC to 600ºC. The dehydroxylation of the Al-OH bond structure occurred at a higher temperature at an endothermic peak of 923.9º, thus causing a 16.23% mass loss due to the presence of strong Al-OH bonds, see Figure 3.15.e.

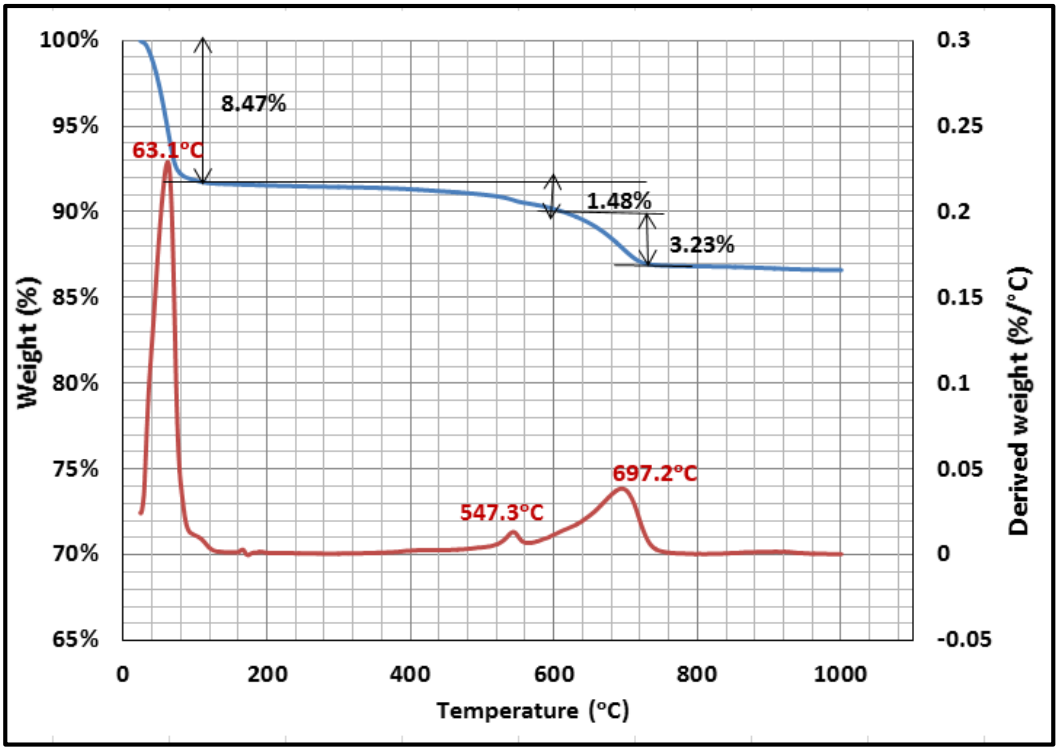

a) Pure bentonite

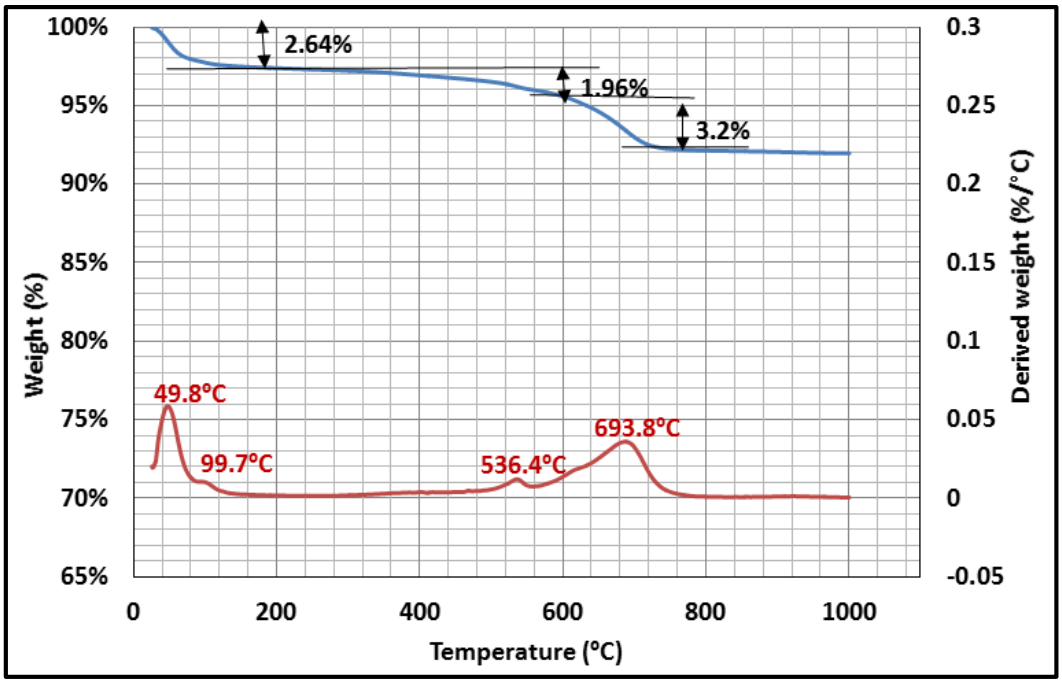
100%
95%
90%
85%
80%
75%
70%
65%
Weight (%)
0.3
0.25
0.2
0.15
0.1
0.05
0
-0.05
Derived weight (%/°C)
2.64%
1.96%
3.2%
49.8°C
99.7°C
536.4°C
693.8°C
0
200
400
600
800
1000
Temperature (°C)

b) DW23

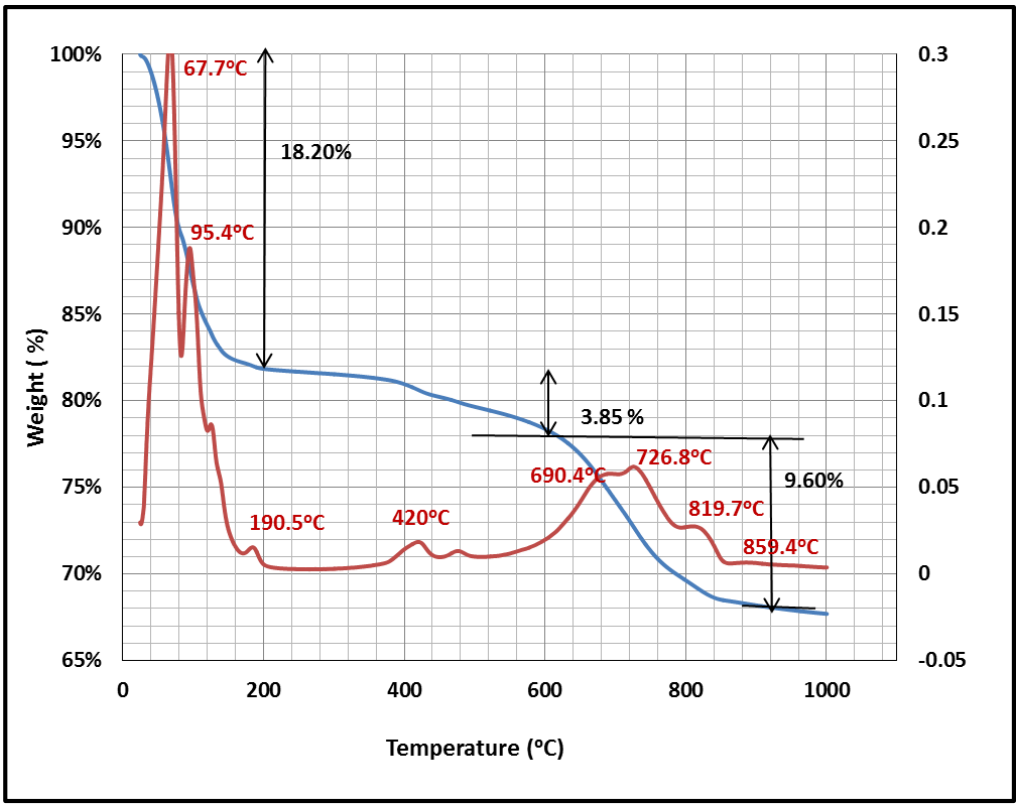
100%
95%
90%
85%
80%
75%
70%
65%
Weight (%)
0.3
0.25
0.2
0.15
0.1
0.05
0
-0.05
67.7°C
18.20%
95.4°C
3.85 %
726.8°C
690.4°C
9.60%
819.7°C
190.5°C
420°C
859.4°C
0
200
400
600
800
1000
Temperature (°C)

c) G23

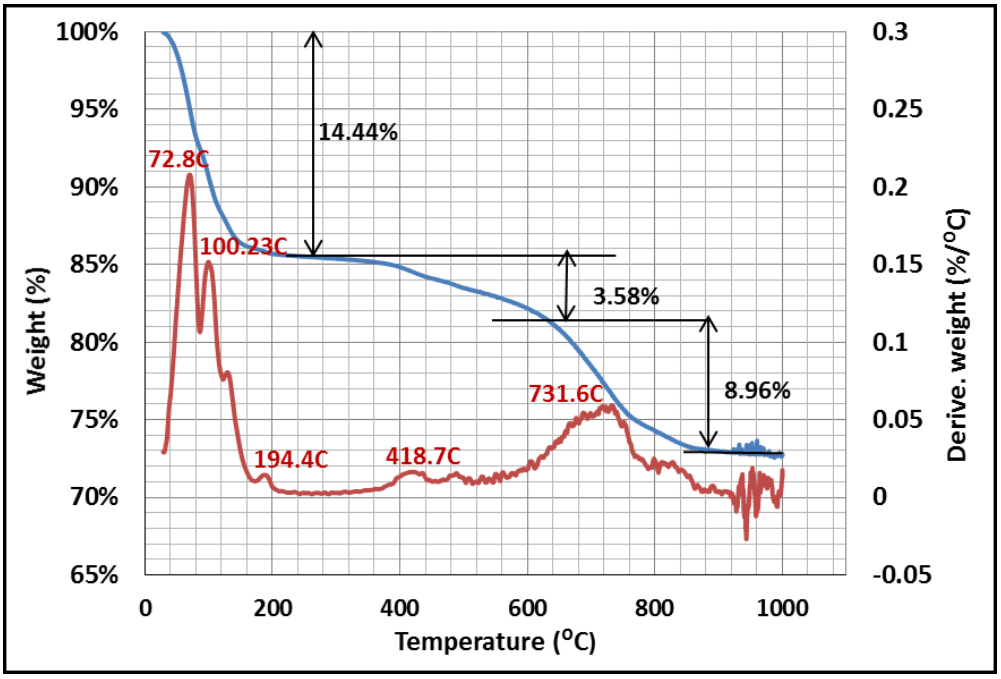

d) G40

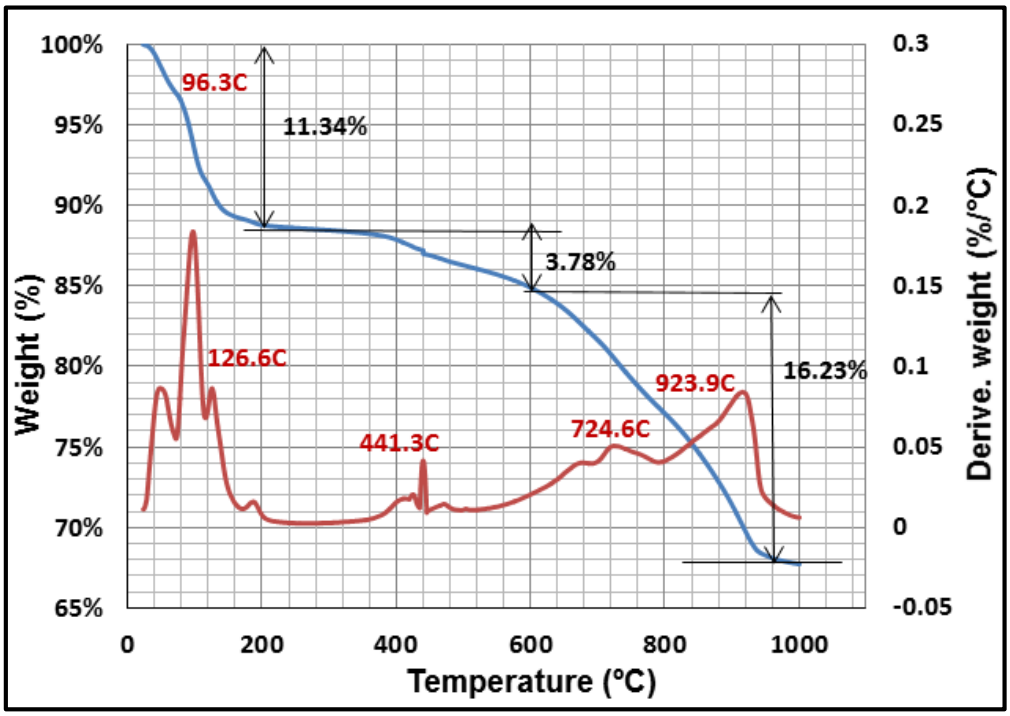

e) G80

Figure 3.15. TGA and DTG analyses for: a) pure bentonite, b) DW23, c) G23, d) G40, and e) G80.

3.3.4 Pore structure evolution (Surface area and pore size distribution)

The results of the surface area and pore size distribution analyses are presented in Figures 3.16 and 3.17. These figures depict that G23, G40 and G80 show a dramatic reduction in the surface area, pore size diameter, and volume of micro- and meso-pores compared to that of the samples of pure bentonite and DW23, which are also shown in Table 3.5. The isotherm curves for these samples fall into type IV isotherms in accordance with the International Union of Pure and Applied Chemistry (IUPAC) classification categories (Sing, 1982). This type of isotherm is characterized by weak nitrogen adsorbent—adsorbate interaction and exhibited by nonporous solids. The observed hysteresis loop indicates the presence of micro-pores (< 2 nm in diameter) and mesopores (2-50 nm in diameter) (Sing, 1982).

The DW23 adsorption–desorption curve shows that the total volume of nitrogen of 51.8 cm^3 was gradually adsorbed with increases in the relative pressure up to P/P0 = 0.985 until capillary condensation was reached, when nitrogen gas condenses to a liquid. Once the relative pressure started to decrease, the adsorbed nitrogen gradually evaporated from the pores in the hysteresis loop up to P/P0 = 0.5058 and then was sharply reduced until P/P0 = 0.4476 (Figure 3.16.a).

The N_2 adsorption–desorption isotherm curves for G23, G40 and G80 show that a very small amount of nitrogen (14.3 cm^3, 7.566 cm^3 and 9.525 cm^3 respectively) had been gradually adsorbed with increases in the relative pressure up to P/P0 = 0.985. Afterwards, the volume of N_2 slowly decreased with decreasing relative pressure in a hysteresis loop (Figures 3.16.b, c and d). Figure 3.17 shows the Barrett, Joyner and Halenda (BJH) adsorption pore distribution for DW23, G23, G40 and G80. The incremental pore volume and cumulative pore area have decreased by more than 75% for G23 compared to those of DW23. On the other hand, the incremental pore volume and cumulative pore area only slightly change with increases in the treatment temperature for G23, G40 and G80. The BET surface area and BJH incremental pore volume and cumulative pore area test results reflect the comprehensive impact of water chemistry on the engineering properties of bentonite-sand based materials.

These results indicate that the pore volume and the BJH and BET surface areas dramatically decrease with increases in the cation size. Na^{+} and Si^{4+} are replaced with larger cations in the octahedral and tetrahedral layers, such as Ca^{2+}, K^{+} and Al^{3+}, due to the smectite-illite conversion and cation exchange processes. The conversion of the Na-montmorillonite to the Ca-montmorillonite rich form and dissolution-precipitation processes produced coarse illite with a larger particle size and induced contraction in the lamellae stacks. Thus, the hydraulic conductivity is increased and the swelling capacity is decreased (Terzaghi et al.1996; Velde and Renac, 1996; Wang et al., 2004; Pusch and Yong, 2006; Dogan et al., 2007). As a result, most of the layers are damaged and block the interlayer space, thus sharply reducing N_2 accessibility and the surface area (Kaufhold, 2010).

On the contrary, Rutherford et al. (1997) and Kaufhold et al. (2010) concluded that the BET surface area and micropore volume increase with increases in the exchange cation size due to an increase in the interlayer space between the tetrahedral sheets in the quasi crystalline overlap regions.

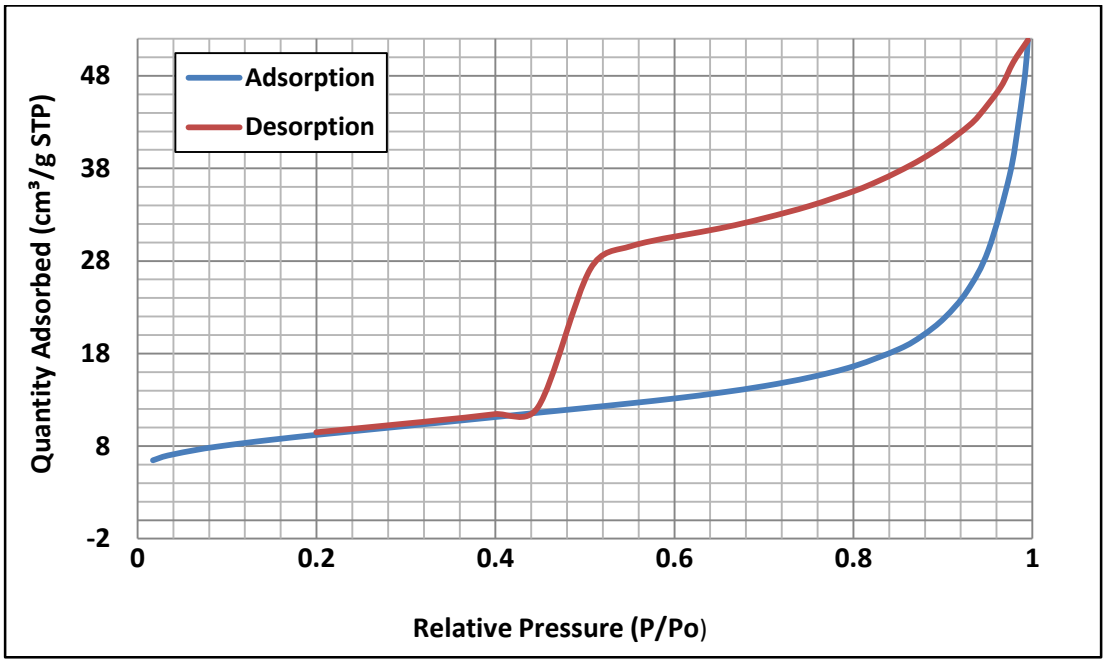

a) DW23

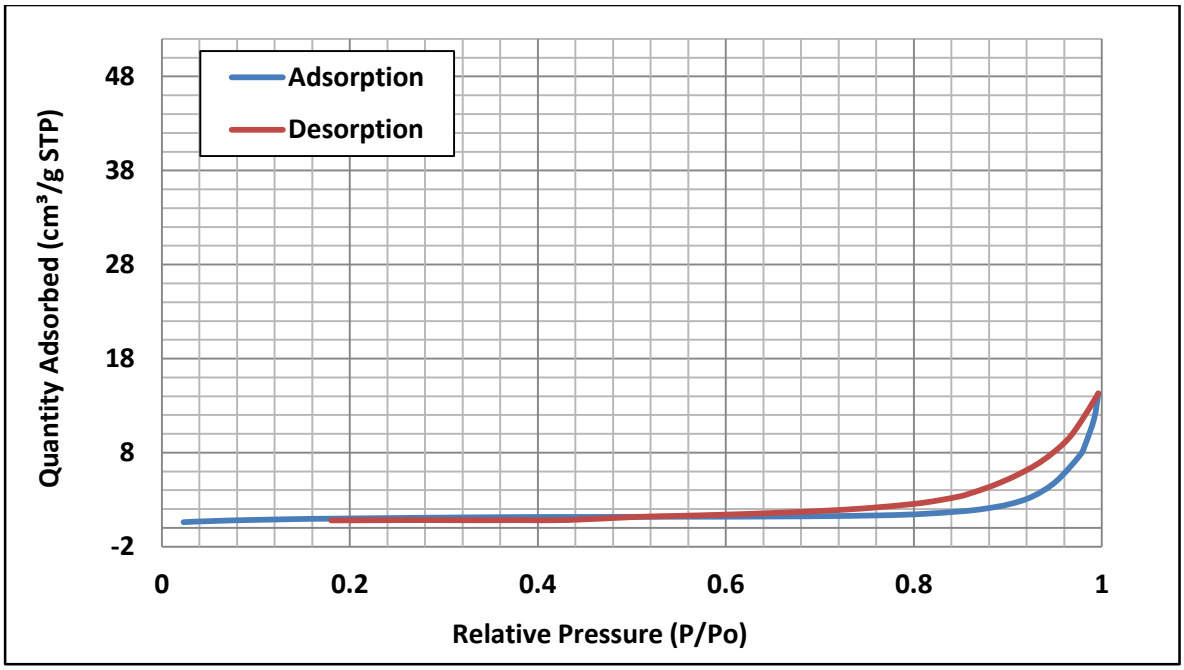
Adsorption
Desorption
Quantity Adsorbed (cm³/g STP)
48
38
28
18
8
-2
0
0.2
0.4
0.6
0.8
1
Relative Pressure (P/Po)

b) G23

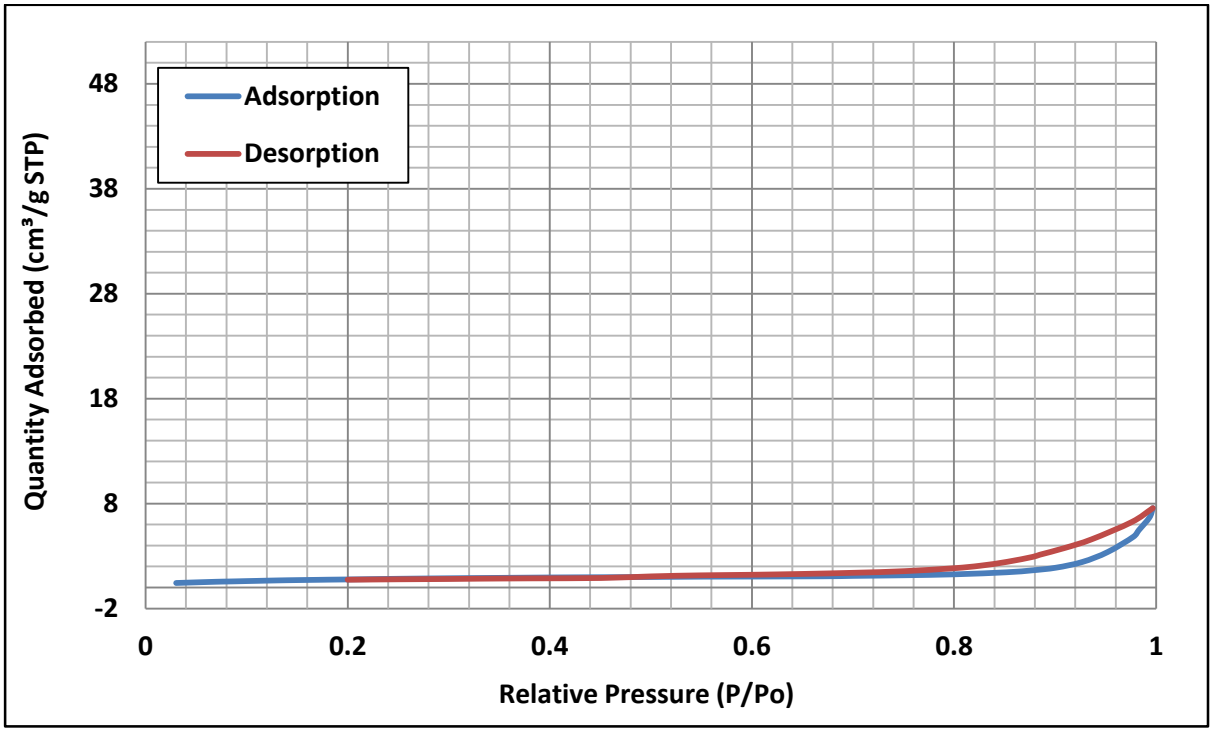
Adsorption
Desorption
Quantity Adsorbed (cm³/g STP)
48
38
28
18
8
-2
0
0.2
0.4
0.6
0.8
1
Relative Pressure (P/Po)

c) G40

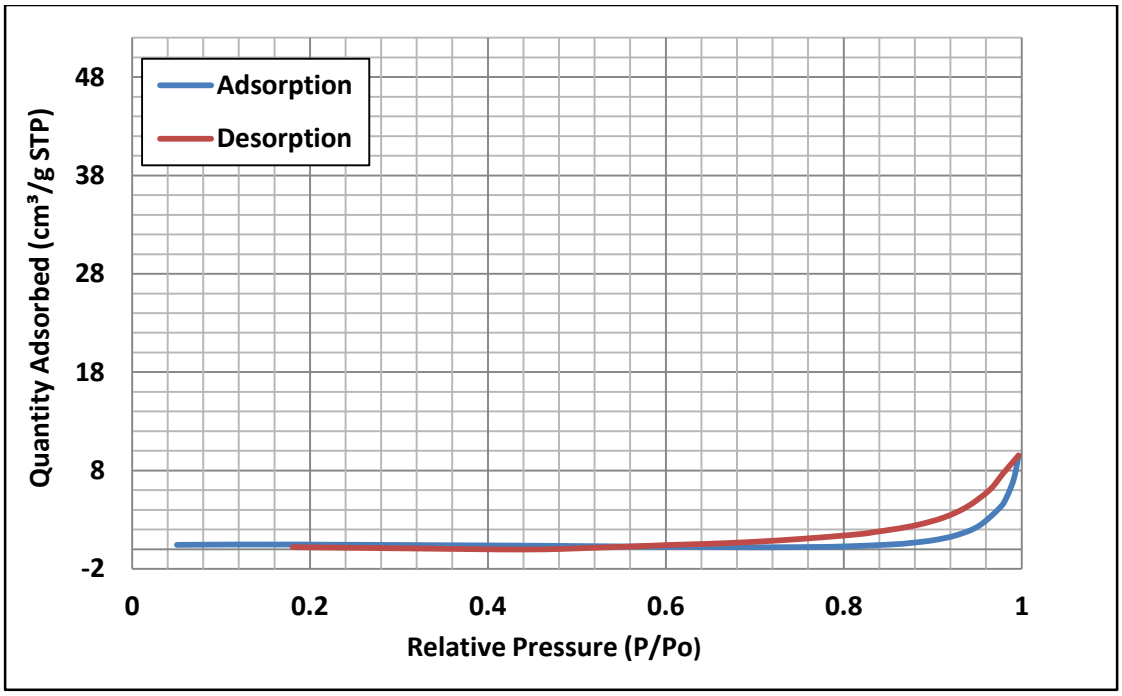

d) G80

Figure 3.16. Adsorption–desorption isotherms for: a) DW23, b) G23, c) G40, and d) G80.

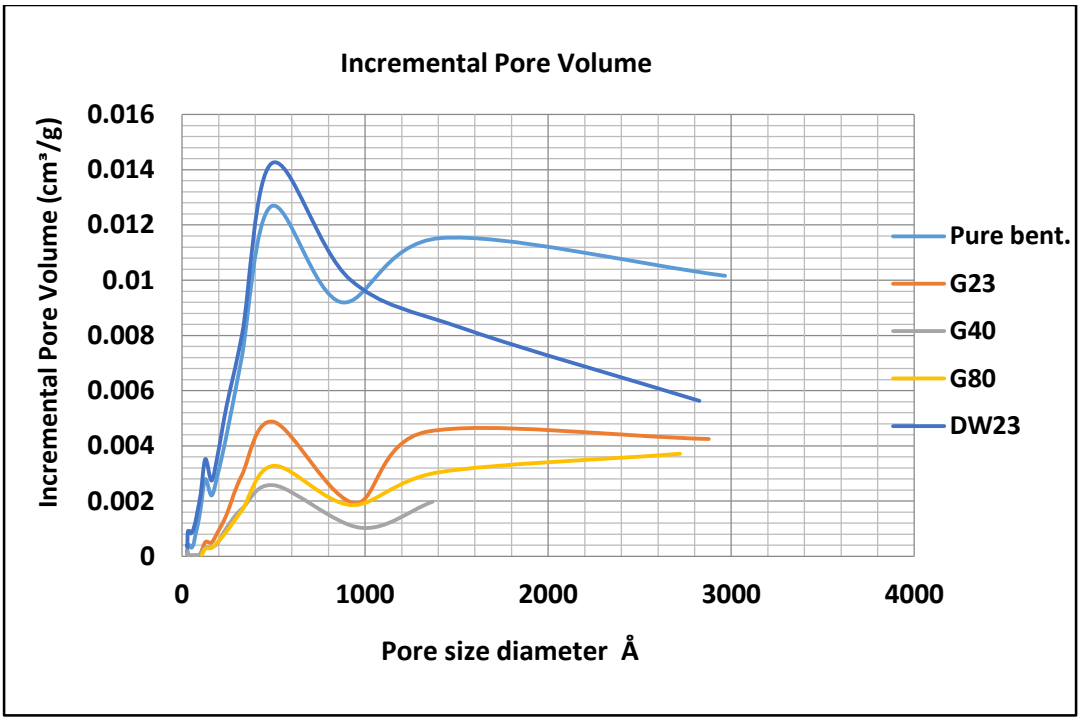

a) Incremental pore volume

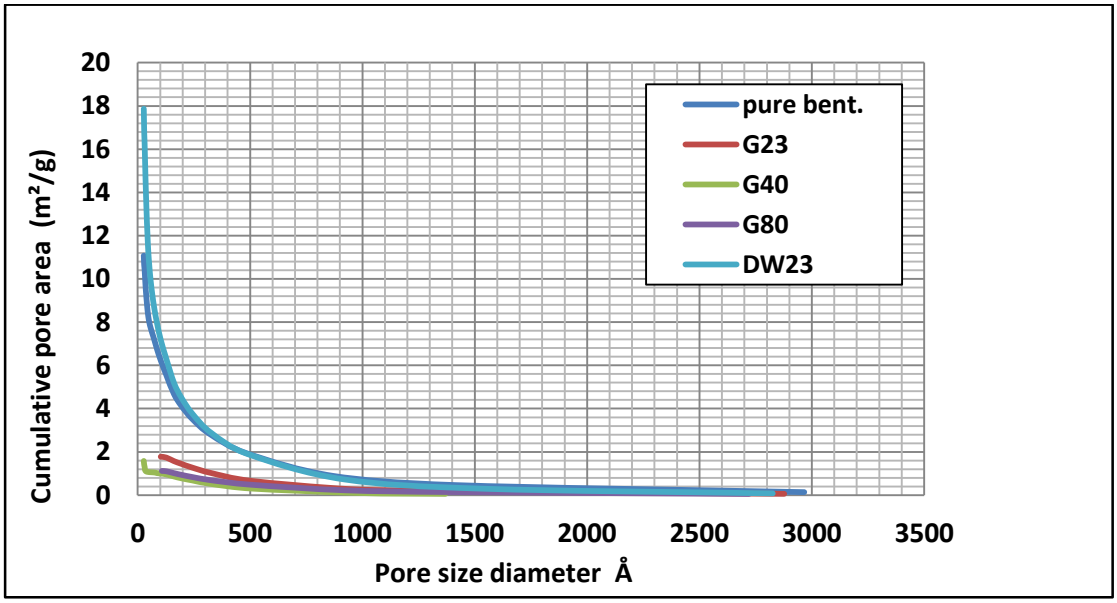

b) Cumulative pore area distribution

Figure 3.17. Comparison between BJH adsorption pore distributions for all samples.

Table 3.5. Comparison between surface area and volume of micro-pore and meso-pore of tested samples.

	Pure bent.	DW23	G23	G40	G80
BET Surface area (cm^2/g)	2.28E+05	3.27E+05	3.69E+04	2.96E+04	1.56E+04
Meso-pore volume (cm^3/g)	0.041593	0.054546	0.011863	0.007057	0.00588
Micro-pure volume (cm^3/g)	0.003362	0.003087	0.000062	0.000423	0.00064

3.4 Conclusions

The following conclusions can be drawn:

The test results demonstrate that the porewater chemistry or the groundwater chemistry found in Ontario has a significant impact on the swelling capacity and hydraulic conductivity of bentonite-sand barrier material. The swelling ability of the barrier material is significantly reduced and its hydraulic conductivity is increased more than three orders when exposed to saline groundwater.

The XRD, EDS, TGA and DTG analyses demonstrate that the bentonite mineralogical compositions have changed. Most of the Na-montmorillonite has converted to Mg, Ca-montmorillonite and illite when treated with highly saline water solutions, that is, Water Solution T or G in this study, in the presence of silica sand and accessory minerals. The swelling component or the montmorillonite has become Ca-montmorillonite which has a lower swelling capacity as well as non-swelling component, or illite. As a result, the thermal stability and degradation resistance of the sample are increased which confirms the occurrence of a montmorillonite –illite conversion.

The BJH and BET surface area and pore size distribution analyses show a dramatic decrease in the surface area, pore size diameter, and volume of the micro-pores and mesopores.

Furthermore, groundwater chemistry has the most significant impact on G80 due to higher smectite-illite conversion with increased treatment temperature, as indicated by the XRD analysis. Consequently, the swelling ability is dramatically reduced where the swelling strain reduced from 198% to 4.6% and the hydraulic conductivity is increased by three orders of magnitude from 6.84E-11 to 1.27E-08 m/s.

The groundwater and heat generated by nuclear waste also have a great impact on the swelling capacity and hydraulic conductivity of bentonite-sand based barriers and may affect the performance of EBS. These issues should be taken into consideration in the design of DGRs in saline groundwater environments such as those found in Ontario (Canada).

The results of this research provide valuable information that will contribute to a better understanding of the impacts of the groundwater chemistry found in Ontario and the heat generated by nuclear waste on the long term performance of a DGR in Ontario.

3.4 References

Basma, A.A., Al-Homoud, A.S.and Husein, A. (1995) Laboratory assessment of swelling pressure of expansive soils. Applied Clay Science 9 (5), 355–368.

Bohn,L., Myer, R. A. and O'Connor, G. (1985) Soil chemistry (book), 2nd Edition.

Boudriche, L, Calvetc, R, Hamdib, B and Balardd, H. (2012) Surface properties evolution of attapulgite by IGC analysis as a function of thermal treatment. Colloids and Surfaces A: Physicochem. Eng. Aspects 399, 1– 10

Bradbury, M.H. and Baeyens, B. (2002) Porewater chemistry in compacted re-saturated MX-80 bentonite: physicochemical characterisation and geochemical modelling. PSI Bericht 02–10, Villigen PSI and NTB 01– 08, Nagra, Wettingen, Switzerland

Cui, S.L., Zhang, H.U. and Zhang, M. (2012) Swelling characteristics of compacted GMZ bentonite–sand mixtures as a buffer/backfill material in China. Engineering Geology 141–142, 65–73

Dhawan, S., Rao, M. (2012) Effect of heating and pore water salinity on the swelling characteristics of bentonite buffer. Clays in natural & engineered barriers for radioactive waste confinement 4th international meeting – March 2010 – Nantes, France

Dogan, M., Dogan, A. U., Yesilyurt, F., Alaygut, D., Buckner, D. and Wurster, D. (2007) baseline studies of the clay minerals society special clays: Specific surface area by the brunauer emmett teller (BET) method. Clays and Clay Minerals, Vol. 55, No. 5, 534–541, 2007

Dollar, P.S. (1988) Geochemistry of Formation Waters, Southwestern Ontario, Canada and Southern Michigan, U.S.A. Implications for Origin and Evolution. M.Sc. Thesis. University of Waterloo, Canada.

Drits, V., Lindgreen, H., Salyn, A., Ylagan,R. and McCarty, D. (1998) Semiquantitative determination of trans-vacant and cis-vacant 2:1 layers in illites and illite-smectites by thermal analysis and X-ray diffraction. American Mineralogist, Volume 83, pages 1188–1198.

Eberl, D.D., Velde, B. and McCormick, T. (1993) Synthesis of illite-smectite from smectite at earth surface temperatures and high pH. Clay Minerals 28, 49–60.

Elert, K., Sebastian, E., Valverde, I. and Rodriguez-Navarro, C. (2008) Alkaline treatment of clay minerals from the Alhambra Formation: Implications for the conservation of earthen architecture. Appl Clay Sci; 39:122–32.

Garrels, R. (1984) Montmorillonite/Illite stability diagrams. Clays and Clay Minerals, Vol. 32, No. 3, 161-166.

Herbert, H.J., Kasbohm, J., Sprenger, H., Fernández, A.M. and Reichelt, C. (2008) Swelling pressures of MX-80 bentonite in solutions of different ionic strength, Physics and Chemistry of the Earth 33, S327–S342

Honty, M, Uhlik, P., Sucha, V, Caplovicova, M., Francu, J, Clauer, and Biron, N. (2004) smectite-to-illite alteration in salt-bearing bentonites (the East Slovak Basin) Clays and Clay Minerals, Vol. 52, No. 5, 533–551.

Huang, W.L, Longo, J.M. and Pevear, D.R. (1993) An experimentally derived kinetic model for smectite-to-illite conversion and its use as a geothermometer. Clays and Clay Minerals, Vol. 41, No. 2, 162-177, 1993

Jensen, M, Lam, T., Luhowy, D., McLay, J., Semec, B. and Frizzell, R. (2009) Ontario Power Generation's Proposed L&ILW Deep Geologic Repository: An Overview of Geoscientific Studies. Nuclear Waste Management Organization, GeoHalifax2009/GéoHalifax2009

Karnland, O. and Birgersson, M. (2006) Montmorillonite stability with respect to KBS-3 conditions. SKB Technical Report TR-06-11. Swedish Nuclear Fuel and Waste Management Company, Stockholm, Sweden.

Kaufhold, S and Dohrman, R. (2011) Stability of bentonites in salt solutions III — Calcium hydroxide. Applied Clay Science 51, 300–307

Kaufhold, S., Dohrmann, R., Klinkenberg, M. and Siegesmund, S. (2010) N2-BET specific surface area of bentonites. Journal of Colloid and Interface Science 349, 275–282

Kim, J.S., Kwon, S.K., Sanchez, M. and Cho, G.C. (2011) Geological storage of high level nuclear waste. KSCE Journal of Civil Engineering, 15(4):721-737

Komine, H. (2004b) Simplified evaluation on hydraulic conductivities of sand-bentonite mixture backfill, Elsevier, Applied Clay Science Vol. 26, Amsterdam, The Netherlands, pp. 13–19.

Komine, H. (2010) Predicting hydraulic conductivity of sand–bentonite mixture backfill before and after swelling deformation for underground disposal of radioactive wastes. Engineering Geology 114, 123–134

Lloret, A., Villar, M. V., Sanchez, M., Gens, A., Pintado, X. and Alonso, E. E. (2003) Mechanical behaviour of heavily compacted bentonite under high suction changes. Géotechnique 53, No. 1, 27-40

Mata, C., and Ledesma, A. (2003) Hydro-chemical behaviour of bentonite based mixtures in engineered barriers. In Proceedings of International Workshop on Large Scale Field Tests in Granite: Advances in Understanding and Research Needs, Sitges, Spain, 12–14 November 2003. Universitat Polite`cnicia de Catalunya- ENRESA. Sitges, Spain. Paper No. 22. Minerals 41, 162–177.

Mojovic , Z., Jovic-Jovicic, N., Milutinovic-Nikolic, A. Bankovic, P., Abu Rabi-Stankovic , A. and Jovanovic, D. (2011) Phenol determination on HDTMA-bentonite-based electrodes. Journal of Hazardous Materials 194, 178–184

Moore, D.M. and Reynolds, R.C. (1989) X-ray diffraction and the identification and analysis of clay minerals. New York City: Oxford University Press; Oxford.

NWMO (2011) OPG's Deep Geological Repository for Low and Intermediate Level. Waste, Regional Hydrogeochemistry – Southern Ontario. NWMO DGR-TR-2011-12.

NWMO (2012) Nuclear Waste Management Organization, Newsletter volume 10, issue 3 June.

NWMO (2013) Website http://www.nwmo.ca/dgrprojectschedule

Ouellet-Plamondona, C, Stasiakb, J. and Al-Tabbaa, A. (2014) The effect of cationic, non-ionic and amphiphilic surfactants on the intercalation of bentonite. Colloids and Surfaces A: Physicochem. Eng. Aspects 444, 330– 337

Priyanto, D. and Baumgartenr, P. (2008) Volume-mass relationships of soil with fresh water and saline water solutions. Nuclear Waste Management Organisation, Appendix D: Technical report TR-2008-04\

Pusch, R. (1998) Backfilling with mixtures of bentonite/ballast materials or natural smectitic clay. SKB Technical Report.TR-98-16 Swedish Nuclear Fuel and Waste Management Company, Stockholm, Sweden.

Pusch, R. (2001) Experimental study of the effect of high porewater salinity on the physical properties of a natural smectitic clay, SKB, Swedish Nuclear Fuel and Waste Management Co., Technical Report TR-01-07, KSB

Pusch, R. (2002) The Buffer and Backfill Handbook. Part 1. SKB Technical Report TR-02-20. Swedish Nuclear Fuel and Waste Management Company, Stockholm, Sweden

Pusch, R., and Yong, R. N. (2006) Microstructure of Smectite Clays and Engineering Performance. Book, Taylor & Francis

Quintessa (2011) Bentonite a Review of key properties, processes and issues for consideration in the UK context. QRS-1378ZG-1, Version 1.1, February.

Rutherford, D. W., Chiou, C. Y. and Eberl D.D. (1997) Effects of exchanged cation on the micropority of montmorillonite. Clays and Clay Minerals vol. 45, 534–543F

RWM (2003) Engineered barrier systems and the safety of deep geological repositories. Radioactive Waste Management, ISBN 92-64-18498-8

Sedmale, G., Cimmers, A., Sedmalis, U. (2009) Characteristics of illite clay and compositions for porous building ceramics production. Chemine Technologija ISSN 1392-1231. Nr.2 (51) 18.

Shirazi, S.M., Wiwat, S., Kazama, H., Kuwano, J., Shaaban, M.G. (2011) Salinity effect on swelling characteristics of compacted bentonite swelling. Environment Protection Engineering, Vol. 37.

Siddiqua, S., Blatz, J. and Siemens, G. (2011) Evaluation of the impact of pore fluid chemistry on the hydromechanical behaviour of clay-based sealing materials. Canadian Geotechnical Journal, 2011, 48(2): 199-213, 10.1139/T10-064

Sing, K. S. W. (1982) Reporting physisorption data for gas/solid systems with special reference to the determination of surface area and porosity. Pure & Appl.Chem, Vol.54, No.11, pp.22OI—22l8.

Terzaghi, K., Peck, R.B. and Mesri, G. (1996) Soil Mechanics in Engineering Practice, Third Edition, 71-84

Ureana, C., Azañón, J.M., Corpas, F., Nieto, F., León, C. and Pérez, L. (2013) Magnesium hydroxide, seawater and olive mill wastewater to reduce swelling potential and plasticity of bentonite soil. Construction and Building Materials 45, 289–297.

Velde, R. and Renacation, C. (1996) Smectite to illite conversion and k-ar ages. Clay Minerals 31, 25-32.

Villar, M.V. and Lloret, A. (2004) Influence of temperature on the hydro-mechanical behaviour of a compacted bentonite, Applied Clay Science 26, 237– 350

Wang, C.C., Juang, L.C., Lee, C.K., Hsu, T.C., Lee, J.F. and Chao, H.P. (2004) Effects of exchanged surfactant cations on the pore structure and adsorption characteristics of montmorillonite. Journal of Colloid and Interface Science, Vol. 280, 1 December 2004, Pages 27–35

Wang, Q., Tan, A., Cu, Y.i, Delage, P. and Gatmiri, B. (2012) Experimental study on the swelling behaviour of bentonite/claystone mixture. Engineering Geology 124, 59–66.

Wersin, P, Johnson, L.H. and McKinely, I.G. (2007) Performance of the bentonite barrier at temperatures beyond 100ºC: A critical review. Physics and Chemistry of the Earth 32, 780–788.

Chapter 4- Technical Paper II: Effect of Corrosion Products on the Swelling, Microstructural and Nano-structural Characteristics of Bentonite-Sand Barrier in Deep Geological Repositories for Nuclear Wastes

Abstract

The purpose of this paper is to evaluate the performance of engineering barrier systems (EBS) in deep geological repositories (DGRs) for high level nuclear waste (HLW) under critical conditions, such the underground water chemistry, the presence of heat and corrosion products of steel containers. The triple combined impact of the deep underground water solution found in Ontario, iron powder as corrosion product, and heat on the engineering behavior of an MX-80 bentonite-sand mixture as well as the nanostructure are studied in a series of experiments with samples treated at temperatures of 23ºC, 40ºC and 80ºC. The experiments have been analyzed by using x-ray diffraction (XRD), X-Ray microanalysis (DES), surface area and pore size distribution analyses (BET, BJH) and differential gravimetric (TGA and DTG) analyses.

The test results confirm that exposing a bentonite-sand mixture to these three conditions lead to mineralogical changes in smectite. For samples treated at 23ºC, Na-smectite changes from its rich form to Ca-smectite with less swelling capacity, while for samples treated at a higher temperature (80ºC), the smectite clay 2:1 structure becomes a non-swelling Fe-rich phyllosilicate 1:1 clay structure (odinite).

4.1 Introduction

The Nuclear Waste Management Organization (NWMO) has proposed construction of DGRs to store safely HLW for a long period of time at a depth between 300 and 700 m beneath the surface. Sixteen locations in Ontario and three in Northern Saskatchewan have been investigated in order to choose the best location for this DGR (NWMO, 2012). According to Canadian design concepts, the initial temperature of the overpack material in the repository will vary between 80^{o}C and 100^{o}C (RWM, 2003; Pastina and Hellä 2006; Steefel et al., 2010).

The interaction of smectite and corrosion products has been investigated over many years in order to assess the durability of EBS in DGRs for HLW and the overall safety of these DGRs (Kamei et al., 1999; Lantenois et al., 2005; Wilson et al. 2006; Mosser-Ruck et al., 2010; Drief et al. 2001; Osacký et al., 2010). The natural analogue of the alteration between smectite and corrosion products depends on the temperature, pH, liquid to clay ratio (L/C), Fe to clay ratio (Fe / C), and the nature of the initial bentonite (Lantenois et al. 2005; Mosser-Ruck et al., 2010; Perronnet et al., 2007).

In previous studies, smectite converted to Fe-rich smectite in an ion exchange reaction without changing the bentonite mineral, where Na^{+} is naturally replaced with Fe^{2+} in reduced conditions at a pH of about 5 (Kamei et al. 1999; Wilson et al. 2006a). Drief et al. (2001), Lantenois et al. (2005), Wilson et al. (2006), Mosser-Ruck et al. (2010) and Osacký et al. (2010) investigated the alteration of original clay minerals with a ratio of 2:1 and the crystallization of newly formed 1:1 Fe-rich clay (7 Å phase), such as berthierine and odinite. Under high thermal conditions, at a temperature of 300^{o}C, montmorillonite destabilizes the 1:1 Fe-rich 14 Å chlorite phase (Guillaume et al., 2003).

Bentonite-sand barrier systems will be exposed to the critical conditions of underground water and heat and corrosion products at the same time, which may affect the bentonite-sand mixture engineering and nano-structural properties. However, none of the previous studies have investigated the triple combined effects of these conditions on a bentonite-sand mixture 30% and 70% by mass, respectively. However, it is acknowledged that a

30% Na-bentonite to 70% ballast mixture is the minimum acceptable mixing weight ratio (Pusch and Yong, 2006; Quintessa, 2011).

In this study, the experimental conditions have been chosen to simulate combined extreme conditions, such as temperature decay, the underground water found in Ontario, and corrosion product conditions in a DGR. A series of experiments have been conducted on a bentonite-sand mixture 30% to 70% by mass to investigate the triple combined effect on the mixture swelling capacity and mineralogical changes.

4.2 Experimental Program

The experimental program commenced with the preparation of all the materials used in the experiments, such as the water solutions, sand, bentonite and corrosion product. The preparation and mixing of specimens to investigate the impact of groundwater chemistry, heat and corrosion products required specific procedures. The procedures include mixing, treatment, filtration, drying, and grounding and compaction processes, respectively, as shown in Figure 4.1. After that, one-dimensional free swell and swelling pressure tests were conducted on the treated and compacted specimens.

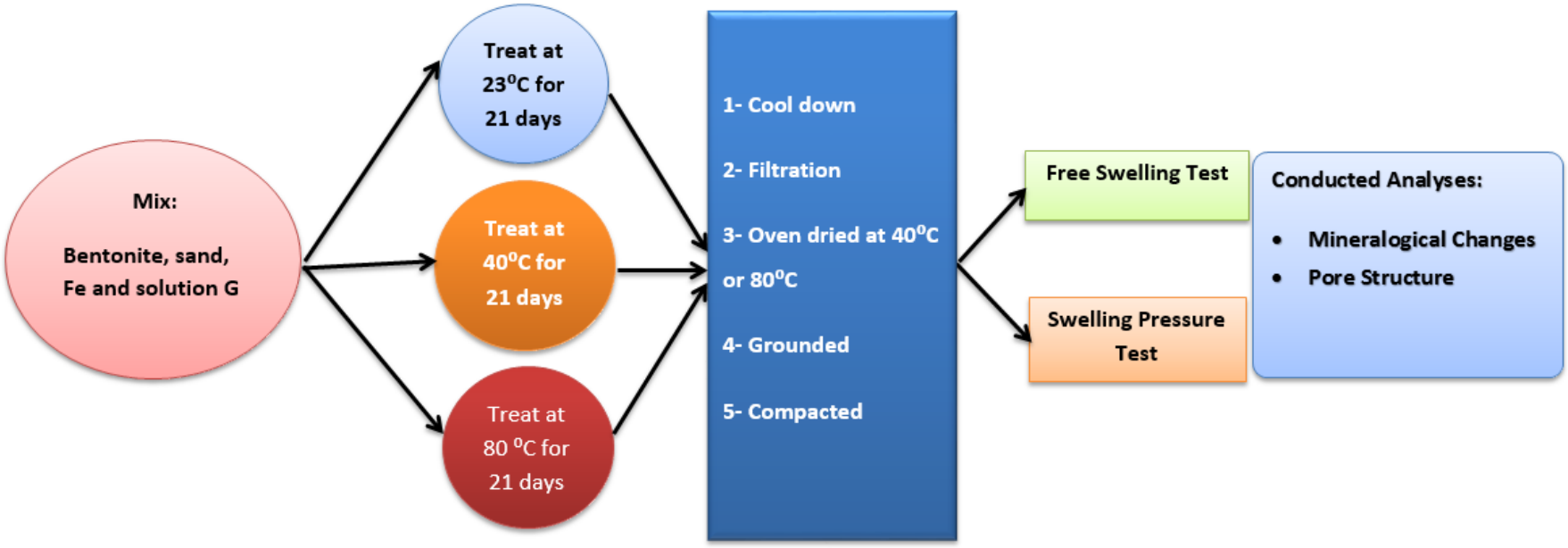

Figure 4.1. Sample preparation and test program

4.2.1 Materials used

4.2.1.1 Bentonite

All of the experiments were conducted on commercial MX-80 bentonite powder from Wyoming, USA. According to the X-ray diffraction (XRD) pattern shown in Figure 4.2, the MX-80 bentonite sample contains 92% montmorillonite and variable quantities of feldspar, quartz, calcite and kaolinite. The cation exchange capacity (CEC) was 105 meq/100 g, and Na^+ was the predominant cation.

Sieve analyses were conducted on bentonite particle sizes larger than 75 μm (retained on sieve No. 200), and the sedimentation process was performed on particle sizes smaller than 75 μm in accordance with ASTM standard D422 − 63. The test results showed that all of the bentonite samples pass through the No. 100 sieve, and 87.7% of the samples pass through the No. 200 sieve, as shown in Figure 4.3. The liquid limit of the bentonite is 530%, and the plastic limit is 48.5%. The bentonite has an average specific gravity of 2.66. The chemical composition of the MX-80 bentonite is listed in Table 4.1.

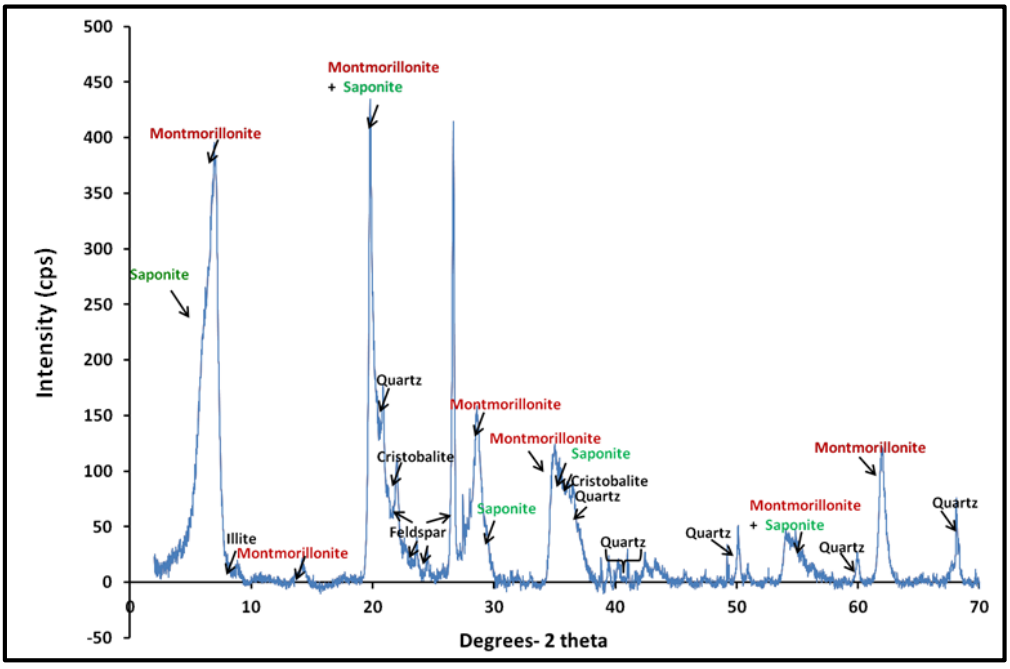

Figure 4.2. X-ray diffraction of MX-80-bentonite used

Table 4.1. Chemical composition of MX-80 bentonite

Element	Composition	Percentage (%)
Silicon Dioxide (total)	SiO_2	63.6
Aluminum Oxide	Al_2O_3	21.4
Iron Oxide	Fe^2O_3	3.8
Calcium Oxide	CaO	0.7
Magnesium Oxide	MgO	2.0
Sodium Oxide	Na_2O	2.7
Potassium Oxide	K_2O	0.3
Bond Water	H_2O	5.5

4.2.1.2 Sand

Fine to medium quartz sand that contained 99.99% silica (SiO_2) with a specific gravity of 2.6 is used in all of the experiments for this study. The sand grain size distribution analysis was conducted by following ASTM D-6913–04 standards. The particle size ranges from 0.18 to 1.7 mm, as illustrated in Figure 4.3.

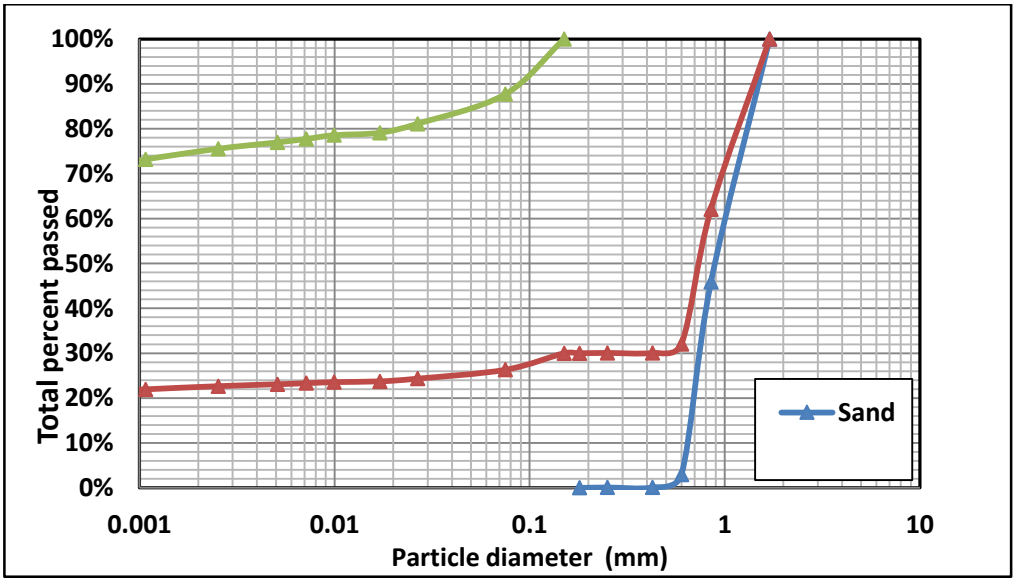

Figure 4.3. Grain size distribution of sand, bentonite and bentonite- sand mix (30/70)

4.2.1.3 Water

In this study, distilled water (DW) as well as a water solution (G) with a chemical composition similar to that of the groundwater located at a depth of 726 m in Guelph (Ontario) are used to mix and saturate all of the samples. The chemical composition of Water Solution G is given in Table 4.2.

Table 4.2. Chemical compositions of Water Solution G (g/l) (sources: Dollar, 1988; NWMO, 2011a).

Element (g/l)	Distilled Water (DW)	Guelph Water (G)
$CaCl_2$	0	159.0
NaCl	0	100.0
$MgCl_2$	0	34.3
KCl	0	6.3
$.K_2SO_4$	0	0.4
TDS*	0	300.0
pH	7	5.7

*TDS: Total dissolved solids

4.2.1.4 Corrosion products

A finely grounded metallic iron powder with a grain size of 6-10 μm was used to produce the corrosion materials in order to simulate the corrosion conditions of a nuclear waste canister in a DGR.

4.2.2 Specimens preparation and mix proportions

In the experiments, a bentonite-sand mixture was reacted with native Fe then mixed with either DW or Water Solution G. The preparation of the specimens required special care

in order to induce corrosion materials. The main steps for the preparation of the specimens and mix proportions are described below.

- **Mixing**: Desired amounts of bentonite and sand were dried for 24 hours at 105 ± 5ºC to remove all moisture. A mixture of bentonite-sand (30 wt.% and 70 wt.%, respectively) was prepared. Native Fe, with a grain size of 6-10 μm, was then added by dry weight to the bentonite-sand mixture at a ratio of 1:10 (Fe to bentonite ratio was 1:3). Then, the Fe-bentonite-sand mixture was mixed with the water solutions (DW or G) in a liquid to solid mass ratio of 5:1 (liquid to clay ratio was 18.22:1).
- **Treatment**: Three mixtures, GC23, GC40 and GC80, were prepared and then treated at 23°C, 40°C and 80°C, respectively, in Nalgene polypropylene containers with thermal and chemical resistance for three weeks, as shown in Figure 4.4. The mixtures were shaken four times daily for 5 minutes each time. The liquid to solid ratio was maintained constant during the treatment process.
- **Filtration process**: After 21 days, the treated solutions were stored at room temperature to cool down and then the mineral suspensions were separated by using a filter cloth with a mesh of 0.45 μm (Kamei et al., 1999; Guillaume et al., 2003; Lantenios et al. 2005).
- **Drying and grounding process:** The specimen treated at 80ºC (GC80) was dried in an oven at a temperature of 80ºC, while the samples treated at 23ºC (GC23) and 40ºC (GC40) were oven dried at 40ºC. All of the dried mixtures were then gently grounded and passed through sieve No. 100, as illustrated in Figure 4.5.
- **Compaction process**: The grounded mixture powders were then mixed with the designated filtered water solutions, as illustrated in Table 4.3. The treated specimens were subsequently compacted by using standard cutter rings with an inner diameter of 63 mm and height of 13 mm, by following an ASTM standard (D-4546-08) to a dry density of 1.7 g/cm³ and optimum water content of 15%.

Table 4.3. Preparation of samples

Sample	DW23	GC23	GC40	GC80
Mixing and saturating solution	Distilled water	Water solution G		
Native Fe	None	Fe powder		
Treatment temperature	23°C	23°C	40°C	80°C

a) Mixtures GC23, GC40 and GC80 before treatment

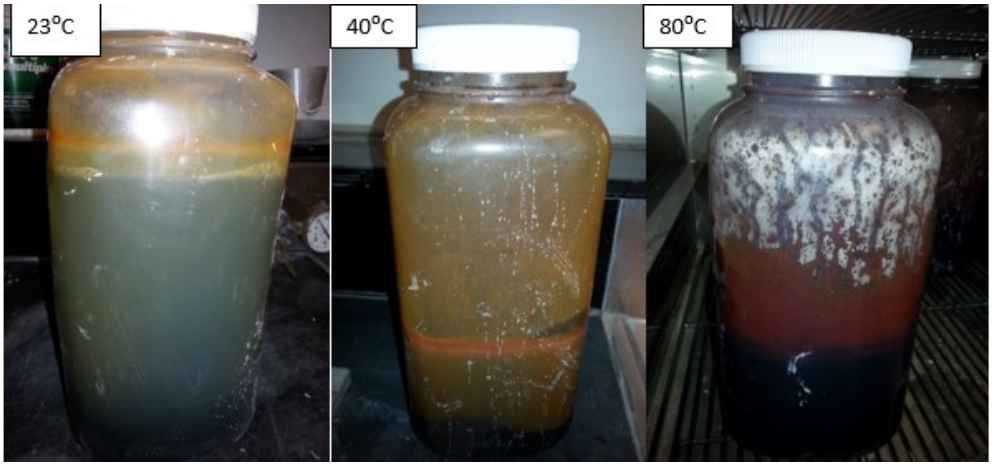

b) Mixtures GC23, GC40 and GC80 after 5 days of treatment

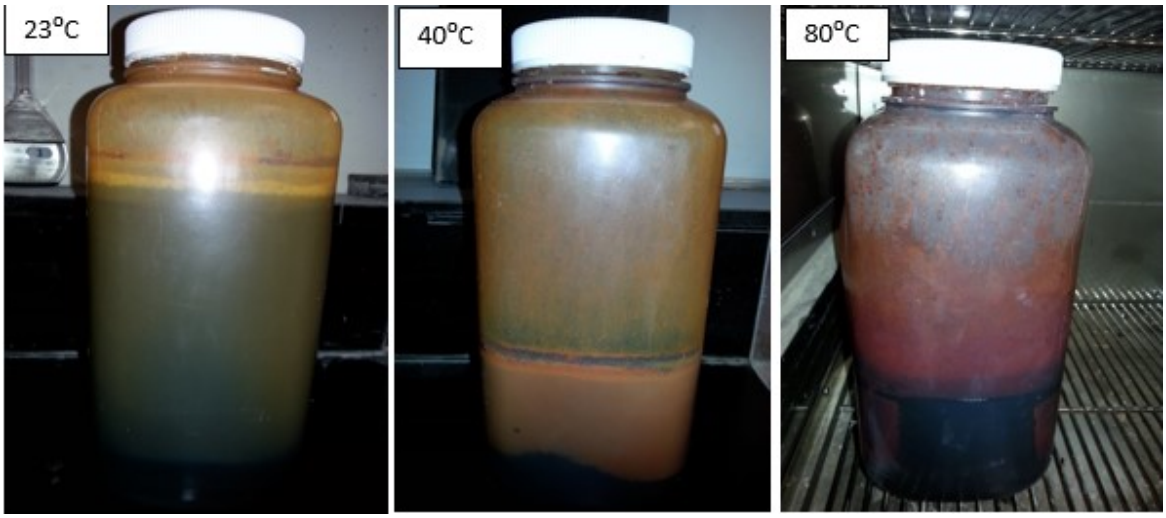

c) Mixtures GC23, GC40 and GC80 after 15 days of treatment

d) Mixtures GC23, GC40 and GC80 after 21 days of treatment

Figure 4.4. Treatment process for Mixtures GC23, GC40 and GC80 at different temperatures (23°C, 40°C, and 80°C).

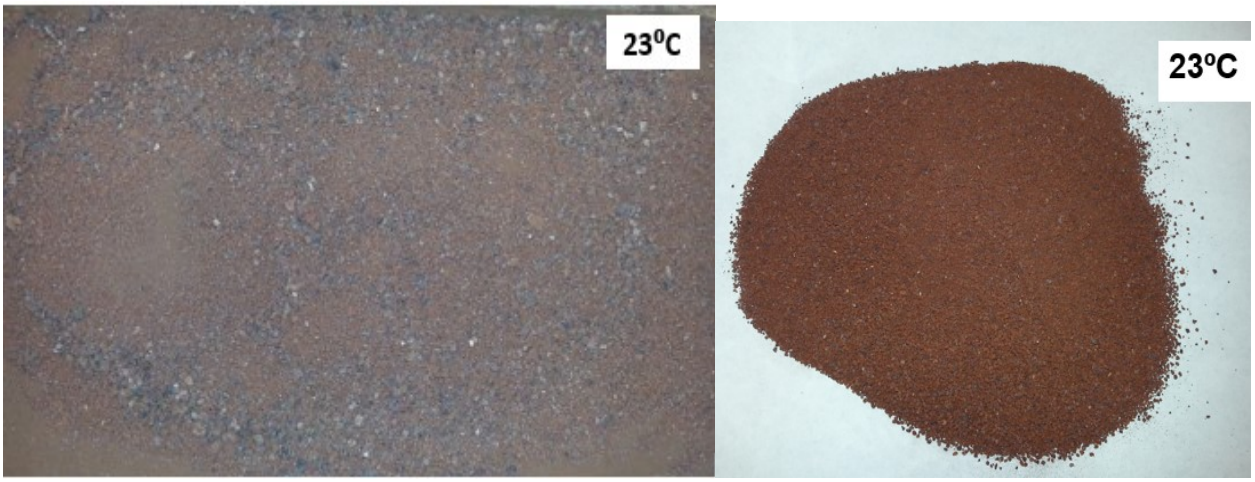

a) Mixture GC23

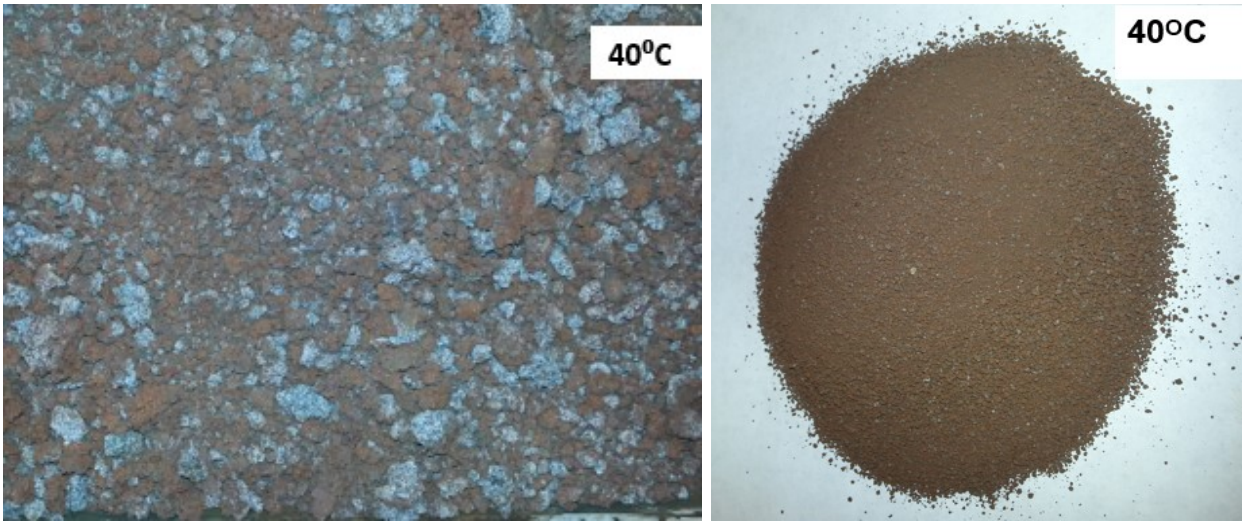

b) Mixture GC40

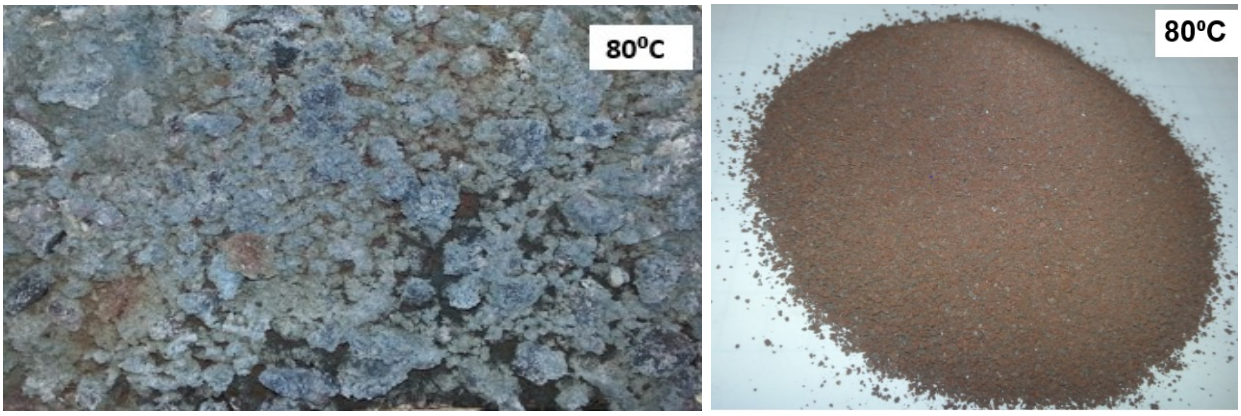

c) Mixtures GC80

Figure 4.5. Dried (left) and grounded (right) GC23, GC40 and GC80 mixtures

4.3 Testing of specimens

4.3.1 Swelling tests

4.3.1.1 Free swell test

A one-dimensional free swell test was conducted by following an ASTM standard (D-4546-08) to measure the vertical swelling of the bentonite-sand samples under restricted lateral deformation. The specimens were inserted into 250 ml beakers with a 63 mm diameter, which is the same as the diameter of the specimens, to prevent lateral swelling. Dial gauges were used to measure the vertical free swell strain over time for all of the samples until the samples stopped swelling.

4.3.1.2 Swelling pressure

The treated samples (63 mm in diameter and 13 mm in height) were loaded into consolidometer cells. Lateral deformation was restricted in all of the experiments, and the samples were allowed to only swell in the vertical direction. The samples were placed between two porous stones under a vertical load of 3.25 kPa. The samples were saturated with the desired water solution from the top. After the experiments were set up, solution molecules interacted with the clay surfaces and penetrated into the innercrystalline structure, thus causing innercrystalline swelling. Once the sample swelled to 0.01 mm, which was measured by the dial gauges, small increments of pressure were added to bring the sample back to its initial volume.

The same procedure was repeated until the sample stopped swelling at its fully saturated state. Specimens were floated with DW or Water Solution G at the laboratory temperature until reaching full saturation. The test stopped between 8 and 35 days. The swelling pressure of the specimens was obtained by recording the pressure needed to keep the sample volume constant with time (Basma et al., 1995; Wang et al., 2012).

4.3.2 Elements and pH analysis

Water samples (100 ml) were taken from Water Solution G and the mixture solutions, GC23 and GC80, to measure different element concentrations as well as the solutions' pH. A conventional chromatographic coupler (inductively coupled mass spectrometry, ICPMS) was used to provide superior sensitivity and specificity of the element concentrations. The pH values for Water Solution G, GC23 and GC80 were measured by using a digital meter (symPHony, SB8OPD) in the laboratory.

4.3.3 X-Ray diffraction

XRD was used to assess the qualitative distribution of the minerals in several of the samples. A Philips X'Pert diffractometer (45 kV, 40 mA), with a Cu source and High Score Plus analysis software was used. The scans were taken from 2-60°2θ with a step size of 0.02° 2θ and 0.6 s continuous scan time per step.

4.3.4 Thermal analysis

Thermogravimetric analysis (TGA) coupled with derivative thermogravimetric (DTG) analysis was conducted on 15 to 23 mg of each sample. A thermal analyzer (TGA Q5000 V3.15 Build 263, University of Ottawa) under a nitrogen atmosphere with a flow rate of 25.0 ml/min was employed. All tests were conducted under a heating temperature range of 23°C to 1000°C with a typical heating ramp of 10 °C/ min.

4.3.5 X-Ray Microanalysis System

Scanning electron microscopy (SEM) with an EVO-MA10 scanning electron microscope (Zeiss, Germany) was carried out by using 20-keV electron energy, and electron dispersion spectroscopy (EDS) with an INCA-x-act (Oxford Instruments, Abingdon-Oxfordshire, UK) at the University of Ottawa to analyze all of the samples. A gold coating was used to overcome the charging effect; this was done by a sputtering

process with a Denton Vacuum Desk IV cold sputter system. The sputtering was done for 1 min in order to obtain a gold layer on top of the samples with a thickness that ranged between 10 and 20 nm.

4.3.6 Surface Area and Pore Size Distribution

A Micrometrics ASAP 2020 adsorption analyzer was used to characterize all of the samples through nitrogen adsorption at 77 K in order to measure their structural properties. The samples were degassed under vacuum (1×10^{-5} Torr) at 120°C for 3 hours before adsorption measurements were taken in order to remove the adsorbed water. The surface area was calculated by using the Brunauer, Emmett and Teller (BET) method for single and multi-points from the nitrogen adsorption-desorption isotherms in a relative pressure range from 0.06 to 0.2. The total volume was considered as the volume of the liquid nitrogen adsorbed at P/P0 = 0.985. The mean pore diameter was obtained by applying the Barrett, Joyner and Halenda (BJH) method.

4.4 Results and discussions

4.4.1 Swelling tests

Figure 4.6 depicts the results of the swelling tests. The free swell test results demonstrate that DW23 has a high swelling strain (198%), while GC23 and GC40 show very low swelling strains of 45.4 and 26.5%, respectively. On the contrary, GC80 has only a 2% swelling strain, as shown in Figure 4.6.a. The test results of the swelling pressure (Figure 4.6b) showed a similar trend as the free swell results. DW23 had a high swelling pressure of 229 kPa, whereas GC23 and GC40 have swelling pressures of 23.25 kPa and 13.25 kPa, repectively. GC80 showed almost no swelling pressure (Figure 4.6b).

These test results, presented in Figure 4.6 and above, indicate that the swelling capacity of the bentonite-sand mixture sharply decreases for the samples mixed with Fe and then mixed with Water Solution G. Furthermore, the triple effects of Water Solution G, the

presence of Fe, and treatment temperature significantly impact the swelling capacity of the mixtures. This can be explained by the fact that this triple effect results in mineralogical and chemical changes of the treated bentonite-sand material. This argument is supported with the results of the XRD, EDS, TGA and BET analyses, which will be discussed in the following sections in more detail.

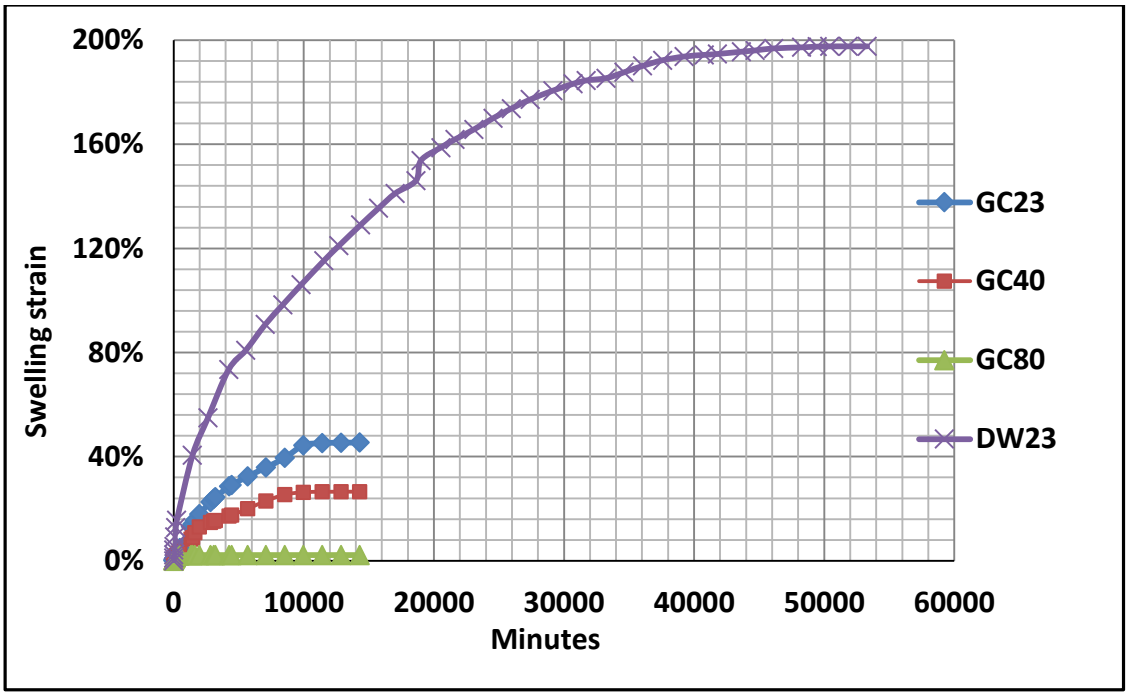

a) Free swell test

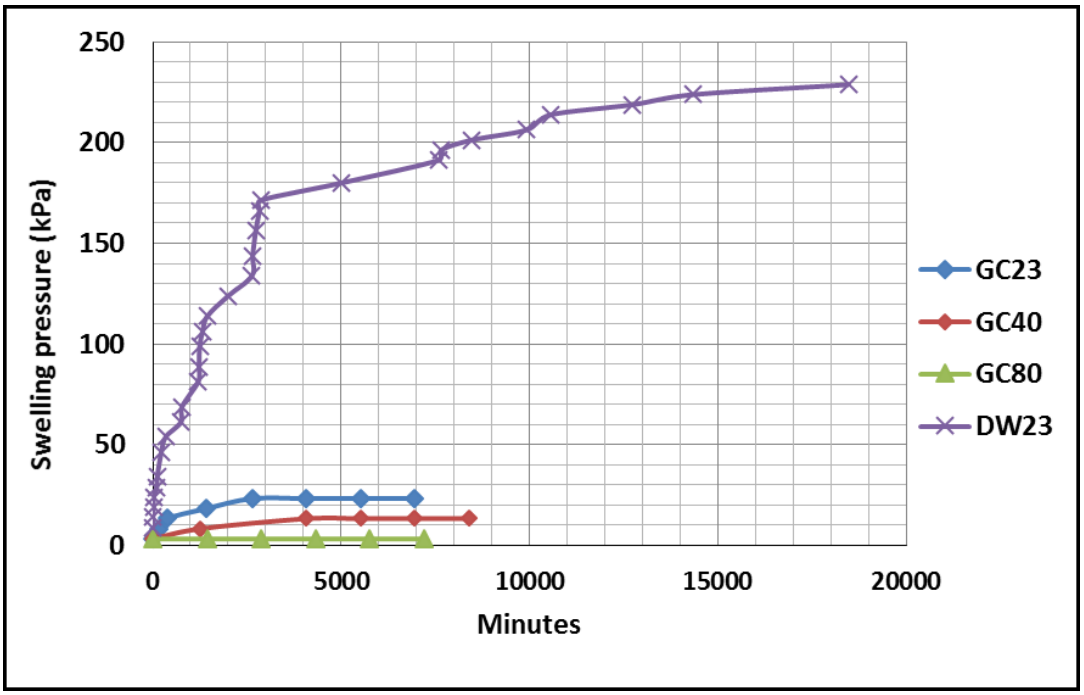

b) Swelling pressure test

Figure 4.6. Swelling capacity of all the treated samples: a) free swell test and b) swelling pressure test.

4.4.2 Mineralogical evolution

The XRD, EDS, TGA and TGA test results confirmed that there are mineralogical and chemical transformations of the bentonite based materials after reacting with native Fe powder and Water Solution G with a mildly acidic pH condition. The ability of cations in the solution to access the smectite interlayers is a key parameter to the smectite destabilization process. The treatment temperature played a significant role in this reaction. While the samples treated at 23ºC had a brown color, which indicated a low F-activity and higher swelling capacity, samples treated at 40°C had a mixed brown and gray color and showed less expansion. On the other hand, samples treated at 80°C converted to non-swelling components with a dark gray color, which reflected high Fe-activity (GRS, 2011) (Figure 4.5).

Montmorillonite converted from a sodium-rich form to a calcium- rich form with a lower swelling capacity (Melamed and Pitkanen, 1996; Ureana et al. 2013). Therefore, GC23 has a swelling strain of only 45% and swelling pressure of 23 kPa. In addition, Fe oxidized to Fe_2O_3 red hematite with a brown reddish color, as shown in Figure 4.5.a. Other reactions also took place and new minerals formed, including quartz, feldspar (anorthite), halite and bischofite.

With regards to the sample treated at 80°C (GC80), the XRD, TGA and DTG analyses confirmed that some of the montmorillonite layers lost one side of the tetrahedral sheets and converted to a Fe-rich (1:1) layer of odinite (7 Å phase) (Drief et al. 2001; Lantenois et al., 2005; Wilson et al. 2006; Mosser-Ruck et al., 2010; Osacký et al., 2010). This transformation occurred due to the dissolution of the smectite layers and precipitation of odinite combined with the rearrangement of the interlayer structure. Fe^{2+}, Ca^{2+} and Mg^{2+} replaced Na^{+}, Al^{3+} in the octahedral structure, and Al^{3+} was exchanged with Si^{4+} in the tetrahedral layers (Bailey, 1988; Kamei et al., 1999; Lantenois et al., 2005; Wilson et al., 2006; Mosser-Ruck et al., 2010; Drief et al., 2001).

The XRD pattern showed peak shifting and a d-spacing of 15.2379 Å, which reflect the presence of Fe-smectite in the sample. It also showed that Na is replaced or partially replaced with Fe; however, the smectite does not undergo any changes (Kamei et al.,

1999; Wilson et al., 2006), but causes a reduction in the swelling component (Moore and Reynolds, 1989). Furthermore, Na, Al, Ca and Mg crystallized into the coarse crystals of halite, anorthite and hydrated calcium magnesium chloride, as described in the equations below:

1) GC23 treated at 23ºC for 21 days:

Na-smectite + Fe + Water Solution G ⟶

Ca-smectite + Fe_2O3 (Hematite) + NaCl (Halite) + $MgCl_2.6H_2O$ (Bischofite) + $CaAl_2Si_2O_8$ (Anorthite) + Quartz

2) GC80 treated at 80ºC for 21 days:

Na-smectite + Fe + Water Solution G ⟶

Odinite + Fe-smectite + NaCl (Halite) + $CaAl_2Si_2O_8$ (Anorthite) + Ca Mg2Cl6 (H_2O) 12

4.4.2.1 Elements and pH analysis

The elemental and pH analyses of the different water solutions after the treatment process are shown in Table 4.4. The analysis results for the water solution with GC80 show that the concentration of the elements, Fe, Mg and K, is significantly decreased as well that 23 mg/L of the elemental Al has been released into the solution, whereas Fe and Mg have replaced Al in the octahedral layers of the montmorillonite. The solution pH is slightly increased.

In the water solution of GC23, the concentration of Mg and K is decreased while Na is increased due to the replacement of Na with Ca. Although Table 4.4 shows that the Ca concentration in GC23 has increased, this could be due to an error during the analysis. Otherwise, the results of the chemical analysis of the concentration of the elements are in good agreement with the results of the XRD, TGA, and EDS analyses.

Table 4.4. Chemical composition of water solutions after reaction.

Element (mg/l)	G	GC23	GC80
pH	5.68	5.67	5.94
Total Aluminum (Al)	ND	34	23
Total Calcium (Ca)	57000	58000	46000
Total Iron (Fe)	ND	440	1100
Total Magnesium (Mg)	8700	8300	5500
Total Potassium (K)	3300	3200	2600
Total Sodium (Na)	39000	41000	1400

G: Water Solution G, GC23: Water Solution G with iron powder and treated at 23ºC
GC80: Water Solution G with iron powder and treated at 80ºC, ND: not found.

4.4.2.2 X-ray diffraction

The XRD patterns of DW23, GC23 and GC80 are presented in Figure 4.7. The XRD pattern of DW23 shows the first peak for Na-montmorillonite at (2ɵ) 8.92º and a basal spacing of d (001) = 9.902 Å. In the case of GC23, the first peak shifts to the left to (2ɵ) 5.9715º and there is a d-spacing of 14.8008 Å due to increase in the interlamellar spacing. This is because the Ca^{2+} has a larger atom size which replaced the Na^{+}, thus causing the montmorillonite to change from sodium-rich to calcium-rich (Ureana et al. 2013). The peaks identified in the XRD pattern correspond to hematite, quartz, feldspar, halite and bischofite.

For GC80, the first peak shifts to the left at (2ɵ) 5.7952º and has a d-spacing of 15.2379 Å. This shifting of the peaks and lower reflection intensity could be explained by the occurrence of ion exchange reactions in which Na is replaced with Fe (Kamei et al., 1999; Wilson et al., 2006). In addition, the XRD patterns show a large peak of 7 Å for the newly formed green clay, odinite. The XRD patterns also reflect the presence of other minerals, such as halite, anorthite and hydrated calcium magnesium chloride, see Figure 4.7.

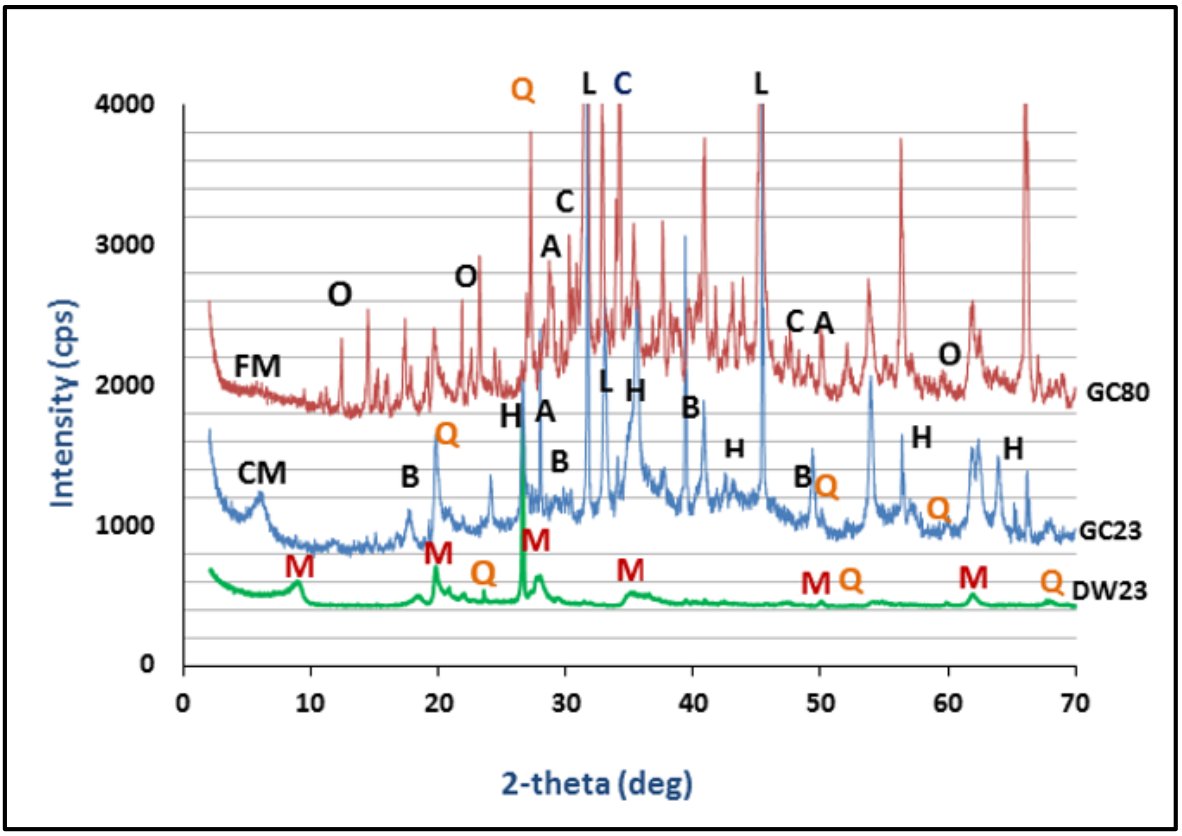

Figure 4.7. Comparison between XRD patterns of DW23, GC23 and GC80; H: hematite, L: halite, Q: quartz, B: bischofite, A: anorthite, C: hydrated calcium magnesium chloride, O: odinite , M: Na-montmorillonite, CM: Ca-montmorillonite and FM: Fe-montmorillonite.

4.4.2.3 Thermal analysis (TGA, DTG)

The TGA and DTG test results for DW23, GC23 and GC80 are illustrated in Figure 4.8. The latter shows that the triple effect of Water Solution G, presence of Fe and heat affects the thermal resistance or behaviour of bentonite-sand based materials, which indicates mineralogical changes in the barrier material.

There is a loss of 2.64% and 1.96% of DW23 by weight, at the first peak between 30°C and 120°C (this is due to loss of surface water or physisorbed water) and at the second peak between 200°C and 540°C (due to the loss of the interlayer water molecules), respectively. The third peak occurs between 540°C and 720°C which corresponds to a mass loss of 3.2% by weight, which was due to the dehydroxylation of the semectite and

collapse of the clay structure (Drits et al., 1998; Boudriche et al., 2012; Ouellet-Plamondon et al., 2014).

GC23 showed a significant weight loss at the beginning of the testing. The sample lost 15% water by mass, due to the evaporation of the surface water at temperatures between 40°C and 120°C. In addition, the interlayer of the chemisorbed water was gradually removed in the temperature range of 160°C -600°C and caused a weight loss of 5.5% of the total sample mass. Furthermore, an exothermic peak occurred at a high temperature (921.7°C) where the sample lost 13.5% water by mass, due to the dehydroxylation (breaking of the OH bonds) of the Ca-montmorillonite and melting of the hematite, halite and bischofite components (Neuman, 1977; Drits et al., 1998; Antao and Hassan, 2002; Földvári, 2011; Boudriche et al., 2012; Ouellet-Plamondon et al., 2014).

The TGA and DTG test results for GC80 showed high degradation in resistance and weight loss of Fe-rich clay, halite, anorthite, and hydrated calcium magnesium chloride of up to 1000°C. The sample lost 10.6% of the water by mass at a temperature range of 40-120°C , and 5.4% at a temperature range of 140-560°C due to the slow departure of the interlayer of water and oxidation of the internal Fe^{2+} to Fe^{3+} (Mackenzie and Berezowski, 1984; Földvári, 2011). The third mass loss of water of 3% occured at 662.9°C due to the dehydroxylation of the OH groups of smectite and odinite (Mackenzie and Berezowski, 1984; Hattab et al., 2013). The fourth mass loss of water of 28% took place at temperatures between 720°C and 1000°C due to the dissolution of the halite, anorthite, and calcium magnesium chloride components (Neuman, 1977; Antao and Hassan, 2002; Olevsky and Bordia, 2010; Földvári, 2011).

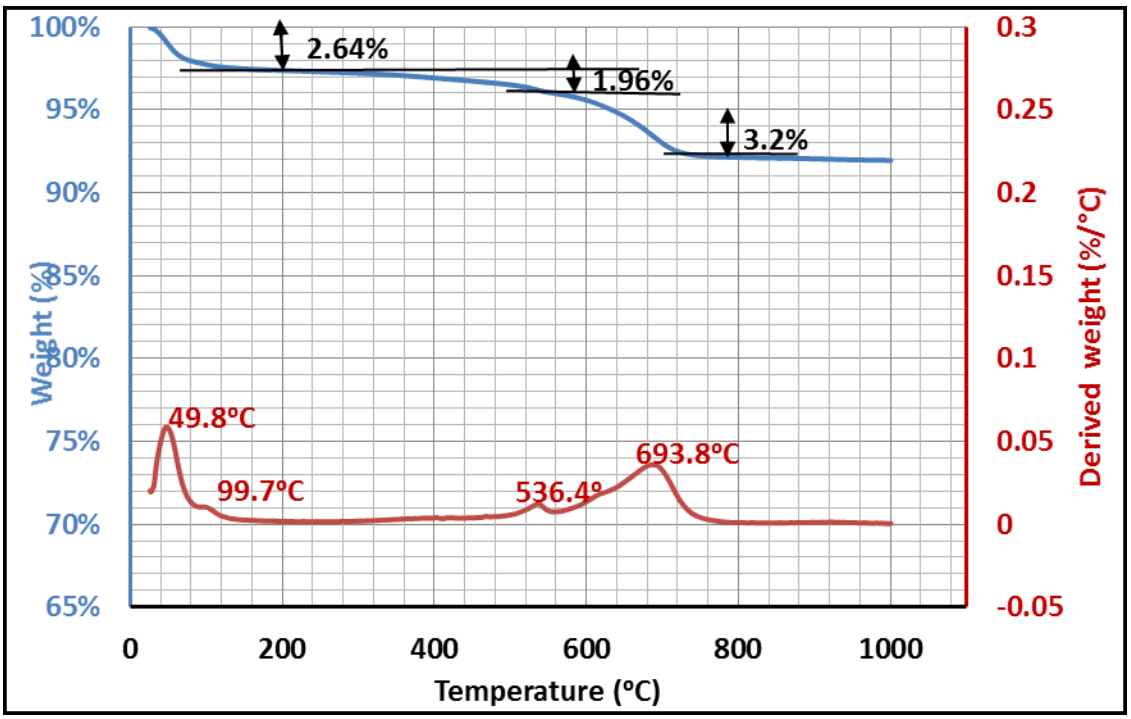
100%
95%
90%
85%
80%
75%
70%
65%
Weight (%)
2.64%
1.96%
3.2%
49.8°C
99.7°C
536.4°
693.8°C
0.3
0.25
0.2
0.15
0.1
0.05
0
-0.05
Derived weight (%/°C)
0
200
400
600
800
1000
Temperature (°C)

a) DW23

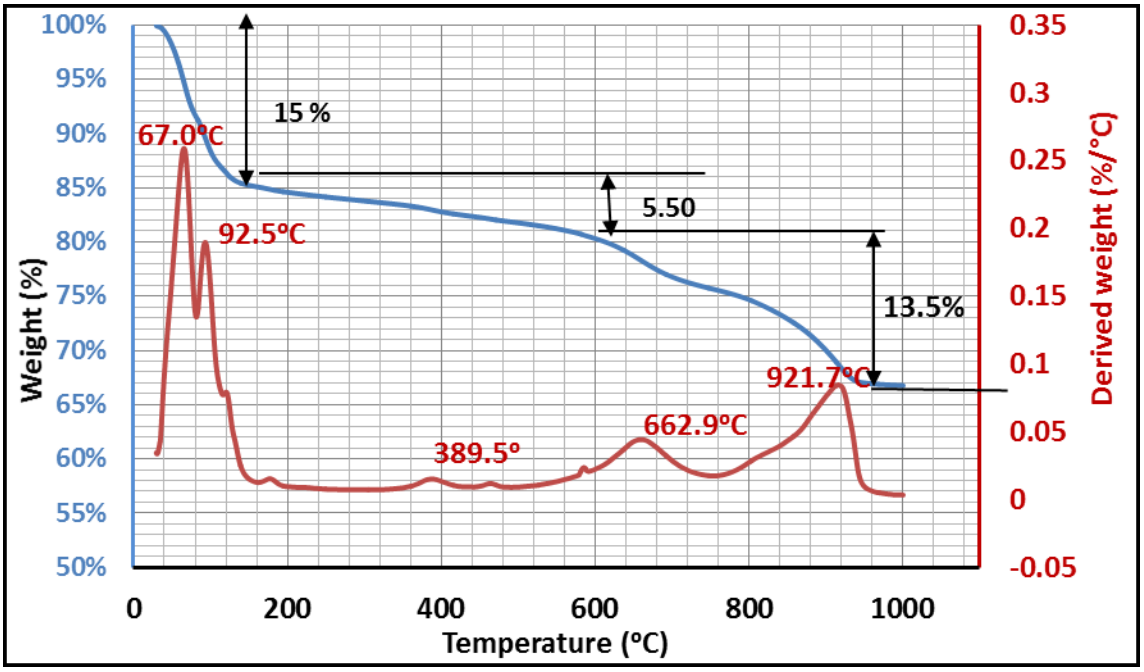
100%
95%
90%
85%
80%
75%
70%
65%
60%
55%
50%
Weight (%)
15 %
67.0°C
92.5°C
5.50
13.5%
921.7°C
662.9°C
389.5°
0.35
0.3
0.25
0.2
0.15
0.1
0.05
0
-0.05
Derived weight (%/°C)
0
200
400
600
800
1000
Temperature (°C)

b) GC23

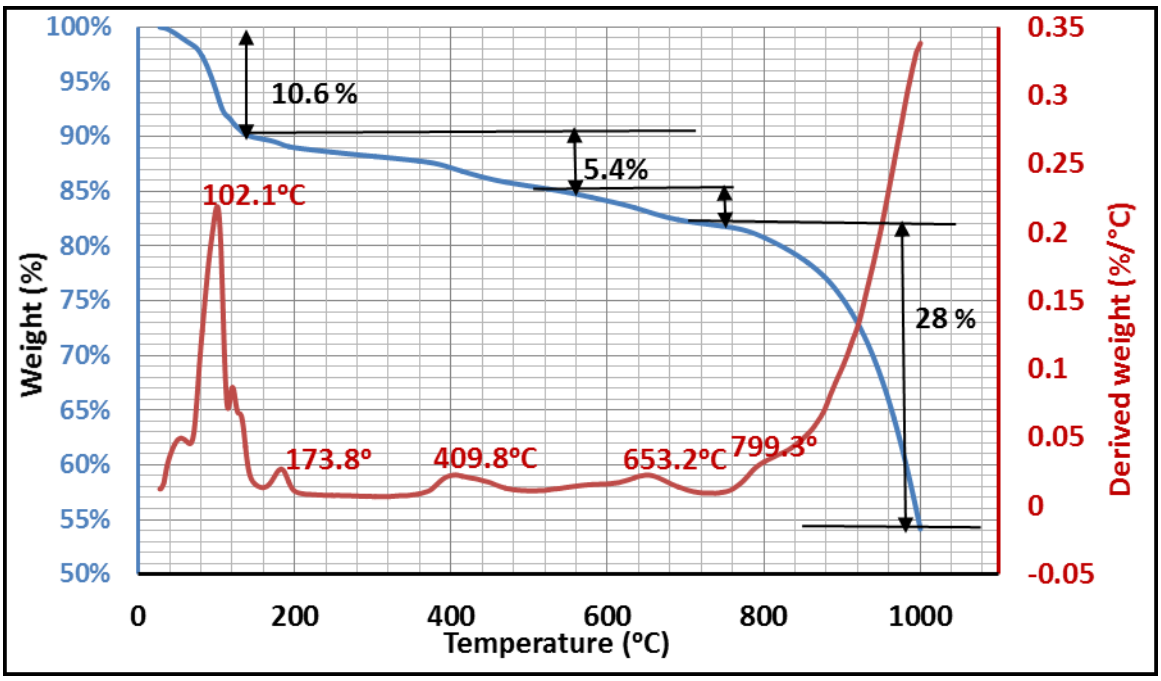

C) GC80

Figure 4.8. TGA and DTG analyses for: a) DW23, b) GC23, and c) GC80.

4.4.2.4 X-Ray Microanalysis System

The results of the EDS analysis for the chemical composition of DW23, GC23 and GC80 are illustrated in Figure 4.9 and Table 4.5. The test results demonstrate that the concentration of elemental Fe, K and Ca is increased in GC23 and GC80. However, the concentration of Al and Si is decreased in both GC23 and GC80 compared to the reference sample, DW23.

GC23 is characterized by a high increase in concentration of Fe and Ca, where Fe oxidizes to heamtite and Ca replaces Na in the smectite interlayers. GC80 shows a higher Fe content where Na-smectite has reacted with the Fe-rich solution and converted to Fe-smectite and odinite Fe-rich clay. In addition, the presence of elemental Na, Ca and Mg in GC80 has increased as well, due to the formation of salt minerals, such as halite, anorthite, and calcium magnesium chloride.

Table 4.5.Electron dispersion spectroscopy results of element weight% in the grounded samples.

Element	DW23	GC23	GC80
Na	0.78	0.77	8.06
Mg	1.50	1.66	2.43
Al	8.90	4.05	2.43
Si	26.93	11.22	5.79
K	0.56	0.76	0.78
Ca	1.44	6.70	8.59
Fe	3.04	22.76	11.86

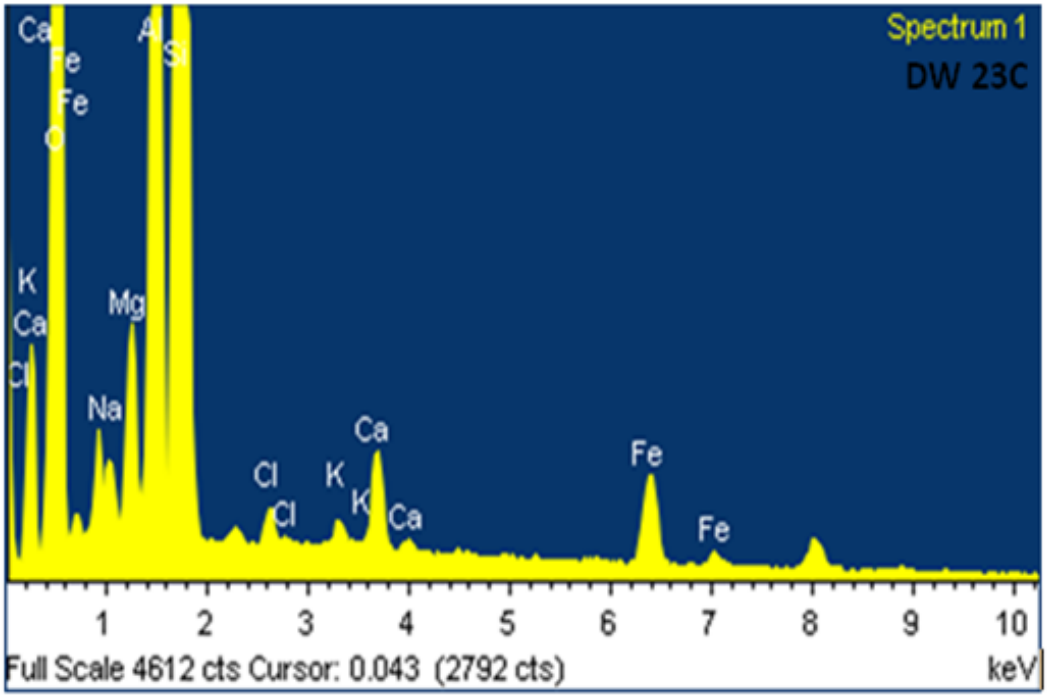

a) DW23

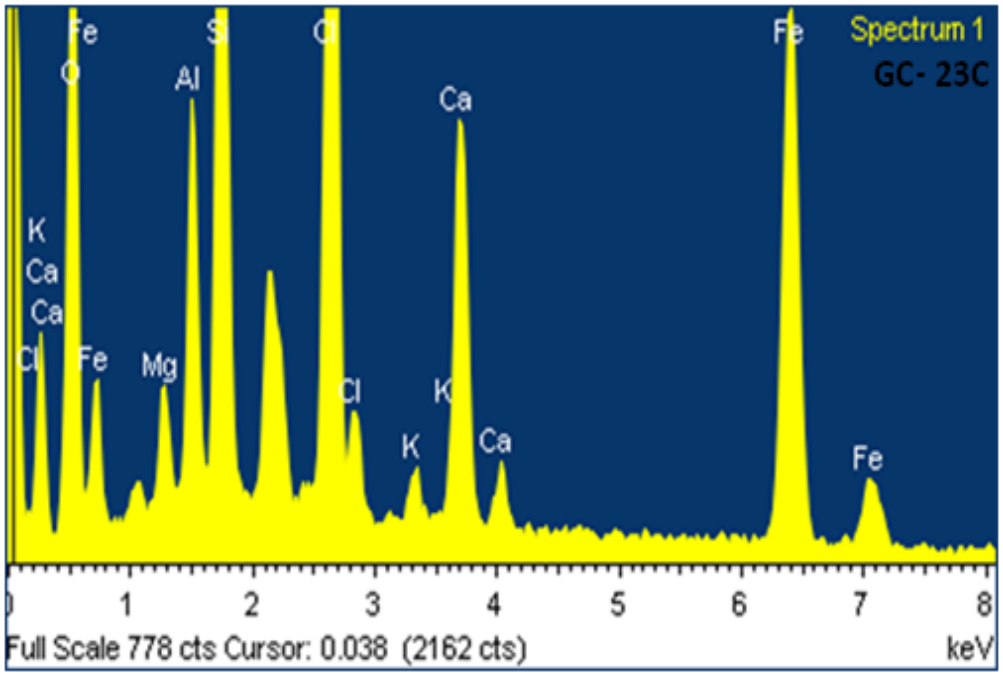

b) GC23

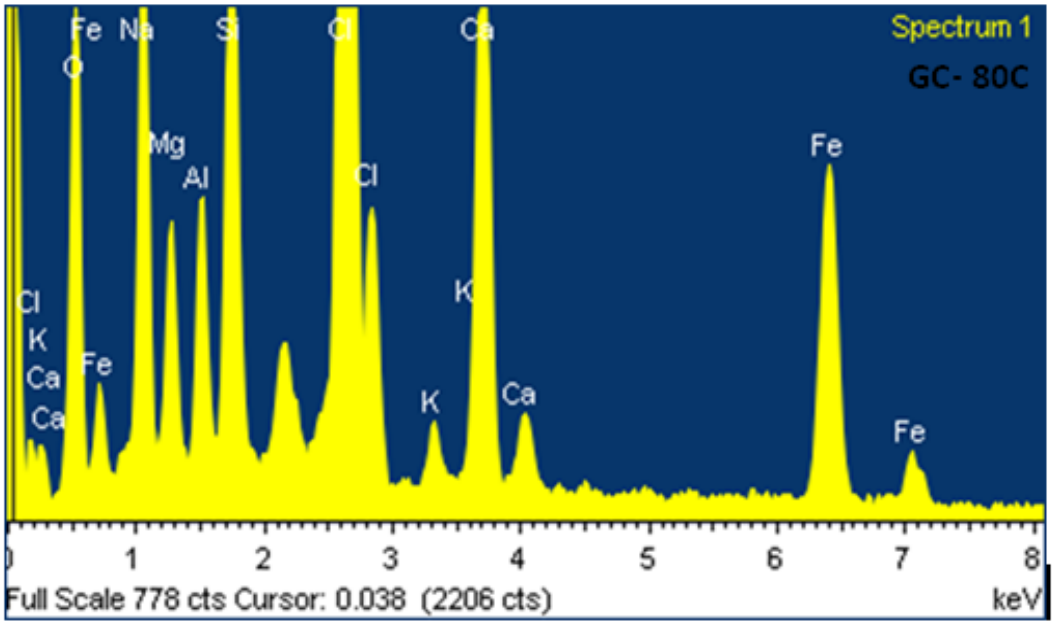

C) GC80

Figure 4.9. EDS patterns of a) DW23, b) GC23, c) GC80

4.4.3 Pore structure evolution

4.4.3.1 Surface Area and Pore Size Distribution

The results of the surface area and pore size distribution analyses for GC23 and GC80 are illustrated in Figures 4.10 and 4.11. The test results indicate that the surface area, pore size, and volume of the micro- and meso-pores of the aforementioned samples have substantially decreased compared to DW23, which is also shown in Table 4.6.

The isotherm curve for DW23 shows a hysteresis loop (Type IV) with high intensity in accordance with the International Union of Pure and Applied Chemistry (IUPAC) classification categories (Sing, 1982), while GC23 and GC80 show the same hysteresis loop (Type IV) but with lower intensity. The hysteresis loop indicates the presence of micro-pores that are less than 2 nm in diameter and mesopores of 2-50 nm in diameter (Sing, 1982). The hystersis loop (Type IV) is identified by a weak nitrogen adsorbent—adsorbate interaction and exhibited by nonporous solids (Sing, 1982).

The surface area and pore volume of GC23 are significantly decreased compared to DW23 due to the formation of coarse crystallines, such as halite with a grain size of 500 to 1000 μm (Marques et al. 2011), bischofite with a grain size less than 1000 μm (Urai, 1983), and quartz.

The incremental pore volume, cumulative pore area, and surface area for GC80 are very small compared to the reference DW23, as shown in Figure 4.11. These reductions in the surface area and pore volume of GC80 can be explained by the presence of odinite clay and coarse salt particles, such as halite, anorthite, and calcium magnesium chloride. The odinite clay has grains of a small size, but these fine particles aggregate together and form coarse particles of up to 400 μm (Bailey, 1988).

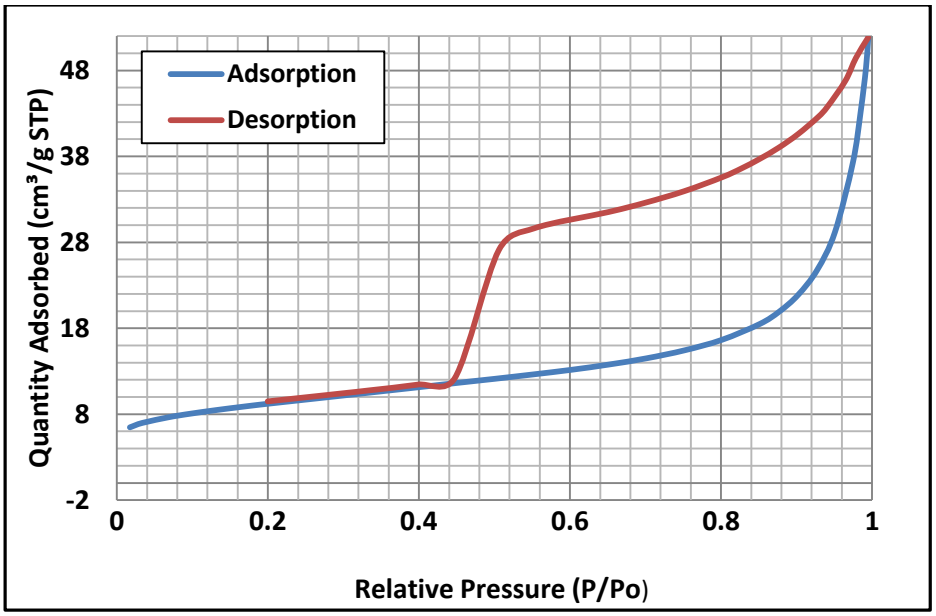
Adsorption
Desorption
Quantity Adsorbed (cm³/g STP)
48
38
28
18
8
-2
0
0.2
0.4
0.6
0.8
1
Relative Pressure (P/Po)

a) DW23

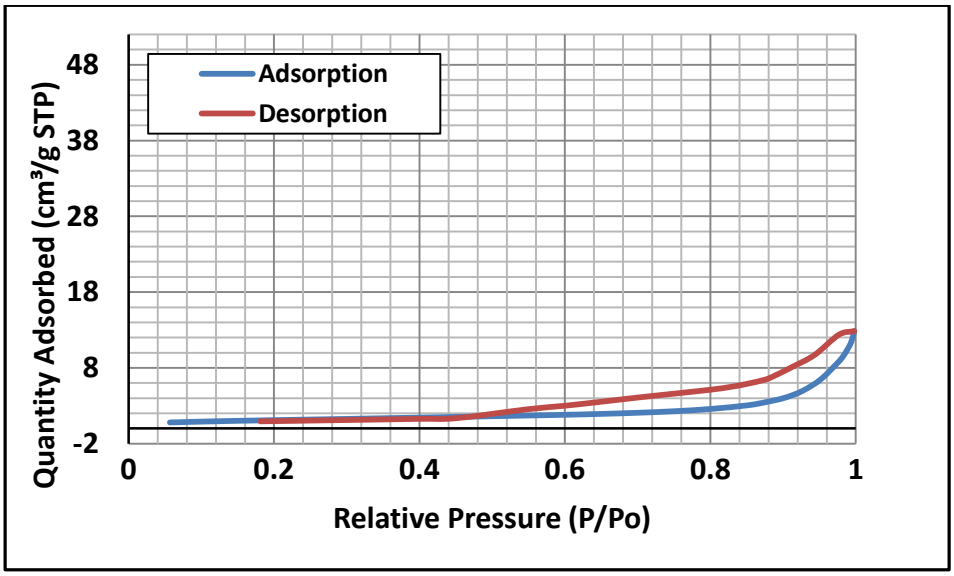
Adsorption
Desorption
Quantity Adsorbed (cm³/g STP)
48
38
28
18
8
-2
0
0.2
0.4
0.6
0.8
1
Relative Pressure (P/Po)

b) GC23

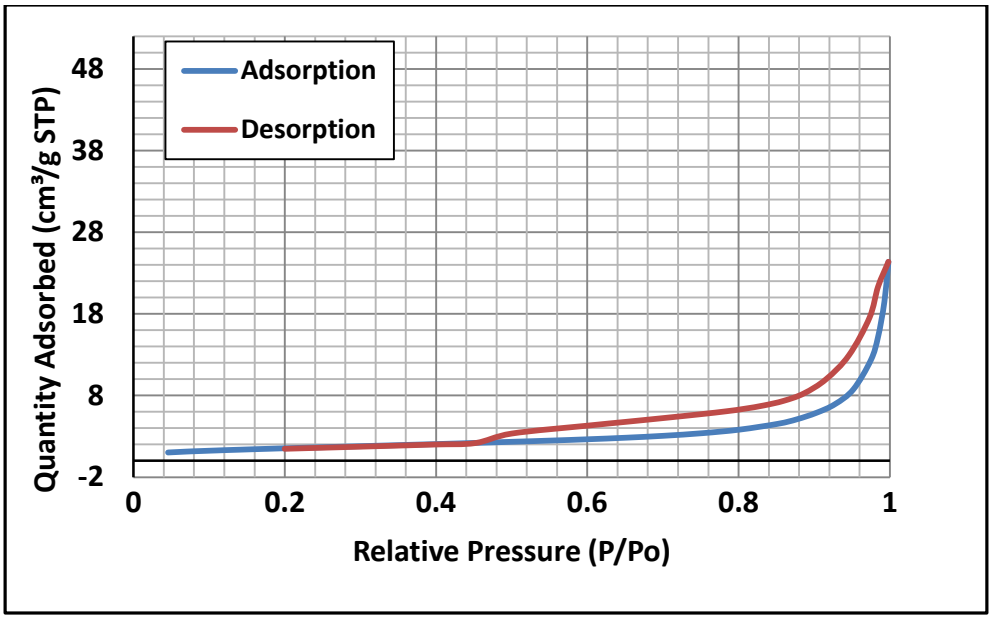

c) GC80

Figure 4.10. Adsorption–desorption isotherms of a) DW23, b) GC23, c) GC80

Table 4.6. Comparison between surface area and volume of micro- and meso-pores in DW23, GC23 and GC80.

	DW23	GC23	GC80
BET Surface area (cm²/g)	3.27E+05	4.07E+04	5.772+E4
Meso-pore volume (cm³/g)	0.054546	0.013556	0.01856
Micro-pure volume (cm³/g)	0.003087	0.000203	0.00053

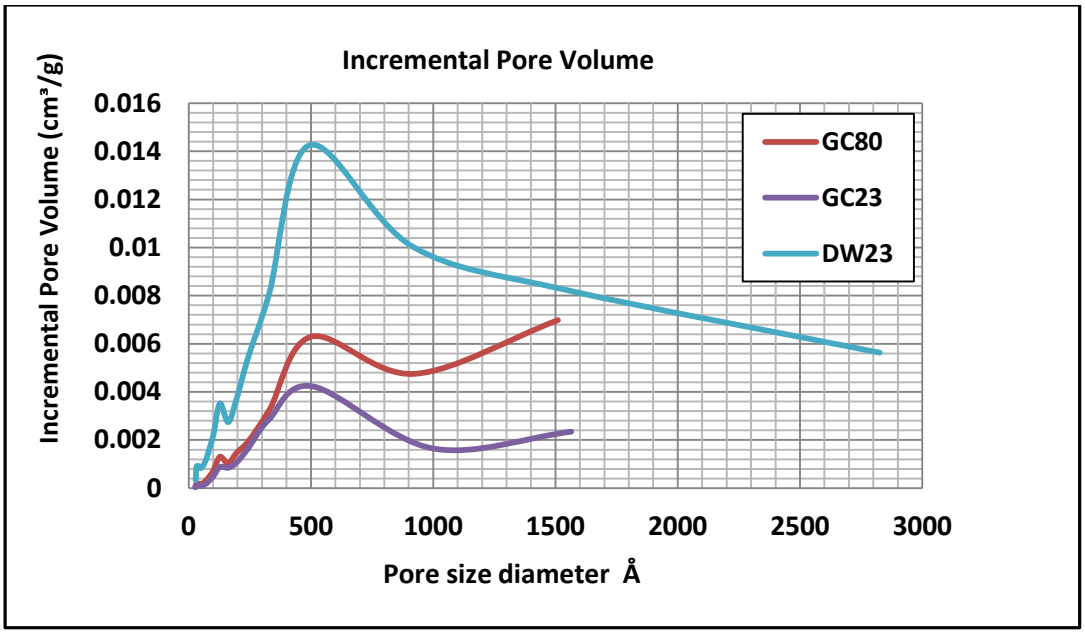

a) Incremental pore volume

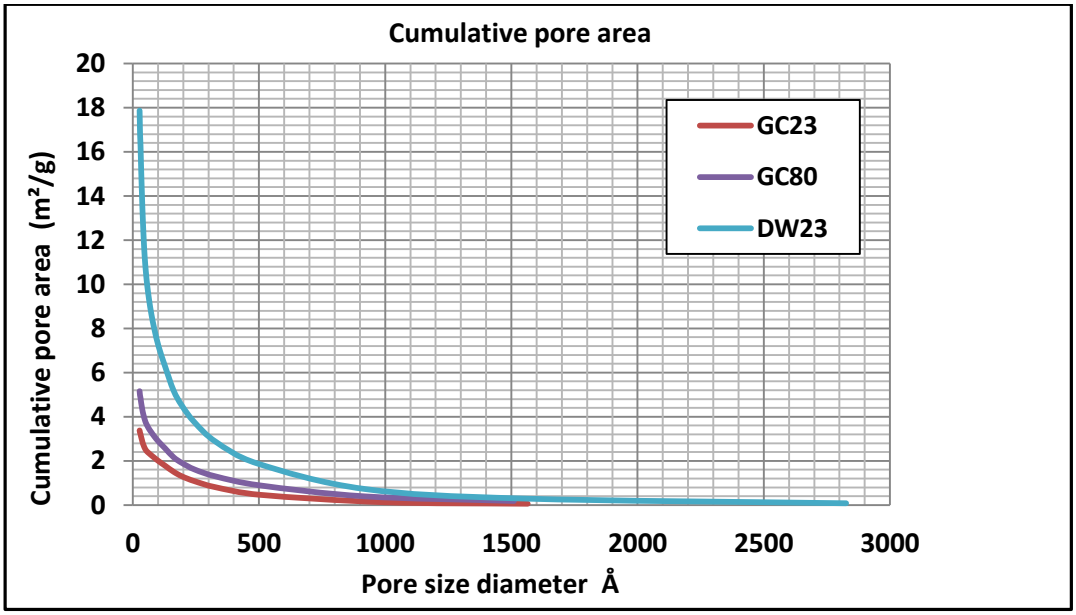

b) Cumulative pore area distribution

Figure 4.11. Comparison between BJH adsorption pore distributions for DW23, GC23 and GC80.

4.5 Conclusion

The results of the experimental tests and XRD, SEM, EDS, TGA and DTG analyses demonstrate that the treatment temperature, underground water chemistry, and corrosion product, Fe, all significantly impact the mineralogical composition, engineering properties, and nanostructure of the bentonite-sand mixture. The triple combined effect of underground water chemistry (from Guelph, Ontario), heat, and corrosion of the nuclear waste containers dramatically cause mineralogical changes which could affect the durability of EBS and the overall safety that concern humans and the environment.

The test results of the samples altered with underground water from Ontario and Fe powder at room temperature demonstrate that the Na-montmorillonite converts to a Ca-rich form that has lower swelling capacity. Fe oxidizes to hematite which gives the samples a brown reddish color. In addition, many other salt minerals, such as halite, bischofite, anorthite and quartz, are formed due to the high concentrations of salt in the underground water.

However, the sample treated at 80ºC and altered with the same water solution and Fe powder shows a lower amount of montmorillonite, and the montmorillonite present has less swelling potential. Na-smectite is found to convert to Fe-smectite and a non-swelling, Fe-rich (1:1) layer of odinite. In addition, new salt minerals, such as halite, anorthite, and calcuim magnesium chloride are formed.

4.6 References

Antao, S. and Hassan, I. (2002) Thermal analyses of sodalite, tugtupite, danalite and helvite. The Canadian Mineralogist Vol. 40. pp. 163-172.

Bailey, S.W. (1988) Odinite, a new dioctahedral-trioctahedral fe3+-rich 1:1 clay mineral. Clay Minerals. 23, 237-247.

Boudrichea, L., Calvetc, R., Hamdib, B. and Balardd,H. (2012) Surface properties evolution of attapulgite by IGC analysis as a function of thermal treatment. Colloids and Surfaces A: Physicochem. Eng. Aspects 399, 1– 10

Catling, D. and Moore, J. (2003) The nature of coarse-grained crystalline hematite and its implications for the early environment of Mars. Icarus 165, 277–300

Cheng, H., Liu, Q., Zhang, J., Yang, J. and Frost, R. (2010) Delamination of kaolinite–potassium acetate intercalates by ball-milling. Journal of Colloid and Interface Science 348, 355–359.

Craig, D.C. and Loughnan, F.C. (1964) Chemical and mineralogical transformations accompanying the weathering of basic volcanic rocks from New South Wales. Aust. J. Soil Res. 2, 218-234.

Cuadros, J. and Michalski, J.R. (2013) Investigation of Al-rich clays on Mars: Evidence for kaolinite–smectite mixed-layer versus mixture of end-member phases. Icarus 222, 296–306

Drief, A., Nieto, F., and Sanchez-Navas, A. (2001) Experimental clay-mineral formation from a subvolcanic rock by interaction with 1 m naoh solution at room temperature. Clays and Clay Minerals, VoL 49. No. I. 92-106. 2001.

Drits, V., Lindgreen, H., Salyn, A., Ylagan, R. and Mccarty, D. (1998) Semiquantitative determination of trans-vacant and cis-vacant 2:1 layers in illites and illite-smectites by thermal analysis and X-ray diffraction. American Mineralogist, Volume 83, pages 1188–1198, 1998

Dudek, T., Cuadros, J.and Huertas, J. (2007) Structure of mixed-layer kaolinite–smectite and smectite-to-kaolinite transformation mechanism from synthesis experiments. Am. Mineral. 92, 179–192

Földvári, M. (2011) Handbook of thermogravimetric system of minerals and its use in geological practice. Geological Institute of Hungary, Magyar Állami Földtani Intézet, 2011ISBN 978-963-671-288-4

GRS (2011) Fe-Bentonite Experiments and Modelling of the Interactions of Bentonites with Iron. Gesellschaft für Anlagen-und Reaktorsicherheit (GRS) mbH. GRS-295, ISBN 978-3-939355-72-4.

Guillaume, D., Neaman, A., Cathelineau, M., R. Mosser-Ruck, Peiffert, C., Abdelmoula, M., Dubessy, J., VilliE RAS, F., Baronnet, A. and Michau, N. (2003) Experimental synthesis of chlorite from smectite at 300ºc in the presence ofmetallic Fe. Clay Minerals, 38,281 –302

Hattab, A., Bagane, M., and Chlendi, M. (2013) Characterization of Tataouine's Raw and Activated Clay. Chemical Engineering & Process Technology, 4:4

Kamei, G., Oda, C., Mitsui, S., Shibata, M. and Shinozaki, T. (1999) Fe (II)-Na ion exchange at interlayers of smectite: adsorption-desorption experiments and a natural analogue. Eng. Geol. 54, 15–20.

Karathanasis, A.D. and Hajek, B.F (1983) Transformation of Smectite to Kaolinite in Naturally Acid Soil Systems: Structural and Thermodynamic Considerations. Soil Sci. Soc. Am. J., Vol.47

Lantenois, B., lanson,B., Muller,F. , Bauer,A., Jullien, A. and Plancë, A. (2005) Experimental study of smectite interaction with metal Fe at low temperature: 1. Smectite destabilization. Clays and Clay Minerals, Vol. 53, No. 6, 597-612.

Littke, R., Bayer, U., Gajewski, D. and Nelskamp, S. (2008) Dynamics of Complex Intracontinental Basins: The Central European Basin System. Springer Science & Business Media, Aug 11, 2008 - Basins (Geology)

Mackenzie, K. J. D. and Berezowski, R. M. (1984) Thermal and Mössbauer studies of iron-containing hydrous silicates. V. Berthierine. Thermochimica Acta 74 (1–3), pp. 291–312.

Marques, F.O. (2011) Microstructure and mechanical properties of halite/coarse muscovite synthetic aggregates deformed in torsion. Journal of Structural Geology, Vol. 33 April 2011, Pages 624–632

Marra, A.,Blanco, A., Fonti, S., Jurewicz, A. and Orofino, V. (2005) Fine hematite particles of Martian interest: absorption spectra and optical constants. Journal of Physics: Conference Series 6, 132–138.

Melamed, A. and Pitkanen, P. (1996) Chemical and mineralogical aspects of water-bentonite interaction in nuclear fuel disposal conditions, VTT Communities and Infrastructure.

Meunier, A. (2005) Clays. Springer-Verlag Berlin Heidenberg Germany (book)

Mitchell, J. K. and Soga, K. (1993) Fundamentals of Soil Behavior, 2nd Edition, John Wiley & Sons, Inc.

Mosser-Ruck, R., Cathelineau, M., Guillaume, D., Charpentier, D., Rousset, D., Barres, O. and Michau N. (2010) Effects of temperature, pH and iron/clay and liquid/clay ratios on oxperimental conversion of dioctahedral smectite to berthierine, chlorite, vermiculite, or saponite. Clays and Clay Minerals, Vol. 58, No. 2, 280–291.

Mouric, M. and Olives, J. (1998) transformation mechanisms and interstratification in conversion of smectite to kaolinite: a hrtem study. Clays and Clay Minerals. Vol 46, No. 5, 521-527.

Neaman, A., Guillaume, D., Pelletier, M., Villiéras, F.A., Michau, N. (2003) The evolution of textural properties of Na/Ca-bentonite following hydrothermal treatment at 80 °C and 300 °C in the presence of Fe and/or Fe oxides. Clay Miner. 38, 213–223.

Neuman, B.S. (1977): Thermal techniques. In Physical Methods in Determinative Mineralogy. Academic Press, London, U.K. (605-662).

NWMO (2007) Overview of a Carbon Steel Container Corrosion Model for a Deep Geological Repository in Sedimentary Rock. NWMO TR-2007-01

Olevsky, E. A. and Bordia, R. (2010) Advances in Sintering Science and Technology: Ceramic Transactions. John Wiley & Sons.

Osacký, M., Honty, M., Madejová, J., Bakas, T., Šucha, V. (2009) Experimental interactions of Slovak bentonites with metallic iron. Geol. Carpath. 60, 535–543.

Osacký, M., Šucha, V., Czímerová, A. and Madejová, J. (2010) Reaction of smectites with iron in a nitrogen atmosphere at 75 °C. Applied Clay Science 50, 237–244

Ouellet-Plamondona, C., Stasiakb, J., Al-Tabbaa, A. (2014) The effect of cationic, non-ionic and amphiphilic surfactants on the intercalation of bentonite. Colloids and Surfaces A: Physicochem. Eng. Aspects 444, 330– 337

Pastina, B. and Hellä, P. (2006) Expected evolution of a spent nuclear fuel repository at Olkiluoto. posiva report 2006-05. Posiva Oy, Olkiluoto, Finland

Pusch, R., and Yong, R. N. (2006) Microstructure of Smectite Clays and Engineering Performance. Book, Taylor & Francis

Quintessa (2011) Bentonite A Review of key properties, processes and issues for consideration in the UK context. QRS-1378ZG-1, Version 1.1, February.

Rivas-Sanchez, M., Alva-Valdivia, L., Arenas-Alatorre, J., Urrutia-Fucugauchi, J., Ruiz-Sandoval, M. and Ramos-Molina, M. (2006) Berthierine and chamosite hydrothermal: genetic guides in the Pena Colorada magnetite-bearing ore deposit, Mexico. Earth, Planets and Space, Vol.58 (10), pp.1389-1400

Steefel, C., Rutqvist, J., Tsang, C.F., Liu, H.H., Sonnenthal, E., Houseworth, J. and Birkholzer, J. (2010) Reactive transport and coupled THM processes in engineering barrier systems (EBS). Lawrence Berkeley national laboratory (LBNL), 09-10-2010.

Urai, J.L. (1983) Water assisted dynamic recrystallization and weakening in polycrystalline bischofite. Tectonophysics. 96, 125-157 Elsevier Science Publishers B.V. Amsterdam - Printed in the Netherlands

Wersin, P., Birgersson, M.,Olsson, S., Karnland, O. and Snellman, M. (2007) Impact of Corrosion-Derived Iron on the Bentonite Buffer Within the KBS-3H Disposal Concept the Olkiluoto Site as Case Study. Posiva 2007-11

Wilson, J., Cuadros, J., Ragnarsdottir, K., Savage, D. and Shibata, M. (2006a) The effect of iron on montmorillonite stability. (I) Background and thermodynamic considerations. Geochimica ET Cosmochimica Acta 70, 306–322

Wilson, J.,Cressey, G., Cressey, B., Cuadros , J., Ragnarsdottir, K., Savage, D. and Shibata, M. (2006) The effect of iron on montmorillonite stability.(II) Experimental investigation. Geochimica et Cosmochimica Acta 70, 323–336

Chapter 5- Conclusions and Recommendations

5.1 Conclusions

The results of the free swell and swelling pressure tests demonstrate that temperature does not have a significant impact on the swelling capacity of the studied bentonite-sand based barrier material. Furthermore, the impact of treatment temperature on the permeability of the samples is not significant as the changes in hydraulic conductivity induced by the temperature increase is less than one order of magnitude.

On the contrary, the groundwater chemistry found in Ontario (specifically in Guelph and Trenton) reduces the swelling ability of the bentonite-sand specimens by more than 90% and the hydraulic conductivity is increased by one order of magnitude compared to those of the samples treated with DW.

The coupled effect of the groundwater chemistry found in Ontario and the heat generated by nuclear waste is found to have a significant impact on the swelling capacity and hydraulic conductivity of a bentonite-sand mixture (30% to 70%, by mass). The XRD, EDS, TGA and DTG analyses have confirmed that Na-montmorillonite becomes Ca-montmorillonite and illite when treated with highly saline water solutions, (in this work, Water Solution T or G) in the presence of silica sand and accessory minerals. Therefore, the swelling capacity of the mixture is sharply reduced by 95% and the hydraulic conductivity increases more than three orders of magnitude.

Furthermore, the triple combined effect of the underground water chemistry (simulated from the water found in Guelph, Ontario), heat, and corrosion product (Fe) causes bentonite to undergo mineralogical changes. It is found that Na-smectite is converted to Fe-smectite and a non-swelling, Fe-rich (1:1) layer of odinite and newly formed salt minerals, such as halite, anorthite and calcium magnesium chloride.

Aggressiveness in the environment of a DGR for HLW, such as due to the underground water salinity, heat decay, and corrosion products, has been shown to affect the engineering and nano-structural properties of bentonite. Thus, bentonite-sand materials

lose their desirable properties as a component of an EBS as well as compromise the overall safety of DGRs.

5.2 Recommendations

Based on this study, it is evident that there are many factors that may affect the performance and durability of DGRs, including:

- that the coupled effect of highly saline underground water and heat should be taken into consideration for the design of a DGR in an environment such as that found in Ontario (Canada),
- the triple combined effects of underground water salinity, heat decay, and corrosion products should be taken into account for the design of a Canadian DGR to ensure the durability of the EBS and the overall safety of the DGR,
- taking into consideration that an increase of the bentonite ratio in a bentonite-sand mixture could increase the swelling components and may reduce the influence of the underground water, heat, and presence of Fe on the engineering and nanostructural properties of bentonite,
- in this study, the swelling and hydraulic conductivity tests are conducted at room temperature on previously cured and treated bentonite-sand specimens. It will be more accurate to study the impact of heat during the testing by running the tests on compacted samples at different temperatures, and
- to investigate the swelling capacity of the bentonite-sand mixtures, the specimens are saturated in different water solutions and the swelling strain and swelling pressure are measured with time. However, bentonite-sand barriers in DGRs will come into contact with very low permeable host rocks (10^{-9} to 10^{-11} m/s) (Pusch, 2008) and adsorb groundwater at a very slow rate. In future work, swelling tests should be conducted on specimens that have been compacted and connected with very slow flow rate water solutions from one side only to simulate actual conditions in DGRs.

5.3 References

Jensen, M., Lam, T., Luhowy, D., McLay, J., Semec, B. and Frizzell, R. (2009) Ontario power generation's proposed l&ilw deep geologic repository: an overview of geoscientific Studies. Nuclear waste management organization, geohalifax2009/GéoHalifax2009

Kursten, B., Smailos, E., Azkarate, I., Werme, L., Smart, N.R., Marx, G., Cuñado, M.A., and Santarini, G. (2004) Corrosion Evaluation of Metallic Materials for Long-Lived HLW/Spent Fuel Disposal Containers: Review of 15-20 Years of Research. EURADWASTE '04 (6th EC Conference on the Management and Disposal of Radioactive Waste) March – 1 April, Luxembourg

Pusch, R. (2008) Geological Storage of Highly Radioactive Waste. Springer-Verlag Berlin Heidelberg ISBN: 978-3-540-77332-0.

Quintessa (2011) Bentonite A Review of key properties, processes and issues for consideration in the UK context. QRS-1378ZG-1, Version 1.1, February.

RWM, Radioactive Waste Management (2003) Engineered Barrier Systems and the Safety of Deep Geological Repositories, ISBN 92-64-18498-8.

Appendixes

Appendix #1

A-1 Water solutions:

(1) Water Solution T

The total dissolved solids (TDS) in the solution = 192

The desired water content Wc = 15%

The solution density (ρl) = $\frac{565.94\ \text{g}}{500\ \text{cm}^3}$ = 1.13188 g /cm³

Solution concentration or salinity (Cm) = $\frac{\text{TDS}}{\rho\text{l}} = \frac{192}{1.13188*1000}$ = 0.1696

The liquid content (Wl) = $\frac{\text{Wc}}{1-Cm}$ = $\frac{0.15}{1-0.1696}$ = 0.1805

Therefore, 18.1% of Water Solution T by mass is added to the bentonite- sand mixture in order to prepare compacted samples with a water content of 15%.

(2) Water Solution G:

The total dissolved solids (TDS) in the solution = 300

The desired water content Wc = 15%

The solution density (ρl) = $\frac{603.32\ \text{g}}{500\ \text{cm}^3}$ = 1.2066 g /cm³

Solution concentration or salinity (Cm) = $\frac{\text{TDS}}{\rho\text{l}} = \frac{300}{1.2066*1000}$ = 0.2486

The liquid content (Wl) = $\frac{\text{Wc}}{1-Cm}$ = $\frac{0.15}{1-0.2486}$ = 0.2

Therefore, 20% of Water Solution G by mass is added to the bentonite- sand mixture in order to prepare compacted samples with a water content of 15%.

Table A.1 Water and fluid content calculations.

Parameter	Distilled water DW	Trenton Water T	Guelph Water G
TDS	0	192	300
Density (g/cm³)	1	1.13188	1.20664
Cm*	0	0.169629289	0.248624279
Wc	15%	15%	15%
Wl	15%	18.10%	20%

Cm: Solution concentration or salinity, Wc: water content and Wl: liquid content

A-2) Impact of groundwater chemistry on permeability of G23 with time

Table A.2. Changes in hydraulic conductivity values for each cycle of G23.

Cycle	Time (Sec)	K (m/s)
1	146280	8.29E-10
2	179220	5.60E-10
3	183540	6.07E-10
4	172800	6.36E-10
5	168240	6.20E-10
6	196620	5.49E-10
7	176220	5.24E-10
8	245640	5.10E-10
9	196200	5.24E-10
10	178440	5.29E-10
11	180540	6.00E-10
12	169200	5.46E-10
13	169260	5.39E-10
14	174120	5.41E-10